ASSESSMENT OF THE EFFECT OF LAND COVER/LAND CHANGES ON SURFACE RUNOFF GENERATION AND FLASH FLOOD OCCURRENCE: A CASE STUDY IN PUA WATERSHED. NOTHERN

CHAMPIKA SAMEERA MENIKPURA
May, 2017

SUPERVISORS:
Dr. D. B. P. Shrestha
Prof. Dr. V. G. Jetten

ASSESSMENT OF THE EFFECT OF LAND COVER/LAND CHANGES ON SURFACE RUNOFF GENERATION AND FLASH FLOOD OCCURRENCE: A CASE STUDY IN PUA WATERSHED, NOTHERN THAILAND

CHAMPIKA SAMEERA MENIKPURA
Enschede, The Netherlands, May, 2017

Thesis submitted to the Faculty of Geo-Information Science and Earth Observation of the University of Twente in partial fulfilment of the requirements for the degree of Master of Science in Geo-information Science and Earth Observation.
Specialization: Applied Earth Sciences - Natural Hazard, Risk and Engineering

SUPERVISORS:
Dr. D. B. P. Shrestha
Prof. Dr. V. G. Jetten

THESIS ASSESSMENT BOARD:
Dr. C. van Western (Chair)
Dr. A. Vrieling (External Examiner, Department of Natural Resources (NRS), ITC)

ABSTRACT

Many parts of the world experience frequent flash flood events in recent past. The study area Pua watershed has also been affected by 2 severe flood events in 2009 and 2011. After this 2 events, Pua watershed has experienced minor flood events also. Local people in study area have a view that flash flood frequency and magnitude have increased within recent past. The general view is that climate change and LCLU changes are responsible for this situation. The main objective of this study is to analyse effect of land cover/land use change on surface runoff generation and flash flood occurrence.

Landsat TM images and Landsat OLI images are used in preparation of LCLU maps for year 1990, 2000, 2010 and 2016. Supervised classification with maximum likelihood classifier is selected for images having training samples (2016 and 2010). Overall image classification accuracy for 2016 and 2010 images are 72.73% and 71.79% respectively. Images that do not have training samples and validation samples are classified using supervised classification with spectral angle mapper classifier.

Image classification results shows that Pua watershed has been subject to significant LCLU changes from 1990 to 2016. Dense forest cover in 1990 was 72.57% and it has been reduced to 51.27% by 2016. Dense forest cover in 1990 has changed into other LCLU types in 34% by 2016. Corn cultivation was 8.44% in 1990 and it has been increased to 26.68% by 2016. Built up/residential area which was 0.0034% in 1990 has increased to 0.0090% by 2016. The percentage of degraded forest cover has also increased. It was 9.39% in 1990 and it is 11.86 by 2016. Paddy cover has slightly decreased by 2016. It was 9.24% in 1990 and it is 9.14% by 2016. LCLU changes in Pua watershed shows that, dense forest and paddy have decreasing trend and corn, degraded forest and built up/residential area have increasing trend.

Initial catchment condition is crucial in flood occurrence. In this catchment, initial soil moisture content plays big role.

Simulation results shows only slight increase in surface runoff and flood extend. This results do not reflect effect of LCLU change on surface runoff generation and flood occurrence. This might be resulted from k_{sat} values and spatial location of LCLU changes.

Further studies are recommended to get an complete view of surface runoff generation and flood occurrence in Pua watershed.

ACKNOWLEDGEMENTS

I must express my heartfelt gratitude to two kids and wife who sacrifices their time, father's and husband's responsibilities for my studies and frequent encouragements. My acknowledgement should go to my family members – mother in law, father in law, mother, sister and other relatives who made many devotes for my studies in many ways.

I do highly appreciate supervision, guidance and critics from my supervisors, Dr. D.B.P. Shrestha and Prof. Dr. V.G. Jetten to reach the goal of MSc. thesis. Without their guidance I could not achieve this goal.

My sincere gratitude goes to Suttipat Wannaapoch and Leak Ngeang who are MSc. students of Water Resource Engineering at faculty of Engineering, Naresuan University for their great support in field work. I would express my thankfulness to Prof. Sarintip Tantanee, Dr. Weerayuth Pratoomchai, Dr. Puripus Soonthornnonda and Dr. tipwimol Taekratok for arranging field work in Pua watershed and providing lab facilities for soil sample analysis.

I should appreciate guidance and encouragements from Ir. B.G.C.M. Krol, Dr. C. Lievens, Drs. N.C. Kingma, Dr. C.J. van Westen and dr. H.M.A. van der Werff.

My special acknowledgement goes to all my classmates- students of academic year 2015-2016 ESA department for taking care of my health condition and support and encouragement in studies and thesis work. I should thank all my ITC batch mates who helped me in various ways in my studies and health issues.

Finally I must thank ITC and Netherland Fellowship Program (NFP) for giving me an opportunity to follow a MSc. degree and providing financial support for studies.

I do highly appreciate support from my all office staff members including Director General of National Building Research Organisation (NBRO), Dr. Asiri Karunawardena, Director, Landslide Research and Risk Management Division, Mr. R.M.S. Bandara and NBRO Matara district office staff who do fulfil my absence for duties.

TABLE OF CONTENTS

LIST OF FIGURES

LIST OF TABLES

1. INTRODUCTION

1.1. Introduction

The recent report of the United Nations (UN) titled "The Human Cost of Weather Related Disasters", reveals that in last 20 years from 1995 to 2015 there were 3062 major flood events which claimed approximately 157000 human lives and affected 2.3 billion people across the world. The floods accounts 43% of natural disasters within that period (UN, 2016). 2013 North Indian flood, 2011 Southeast Asian flood, 2011 Philippines flood, 2010 Pakistan flood and 2010 China flood are the most recent floods that cased most fatalities in the recent fast with numbers of 5700, 1828, 1268, 1600-2000 and 1072 respectively. Few other flood events occurred at worldwide casing significant number of fatalities are 2011 Brazil flood, 2010 Russia flood, 2010 Colombia flood, 2007 African nations flood (Sudan, Nigeria, Ghana, Kenya, Burkina Faso), 2006 Ethiopia flood and 2001 Algeria flood. These events were responsible for 894, 172, 138, 353, 705 and 827 fatalities respectively (Wikipedia, 2016). 2016 historical flood event in Louisiana, USA claimed for 8 billion US dollars economic lost ("The Weather Channel," 2016) and 2016 Southern and Northern China floods did cost for 22.73 billion US dollars economic lost (Masters & Henson, 2016). These two flood events are the most costly flood events in very recent fast. 2016 June European flood events did cost for 2.4 billion euros insured loss in Germany and 700 million – 1.4 billion euros in France (Davies R., 2016). Most significant recent flood events were caused by extreme rainfall events, monsoon rain, Typhoons and Hurricanes (Wikipedia, 2016). Observations and studies reveal that there is a significant increment in frequency, magnitude and consequences of floods and flash floods worldwide in last few decades (Blöschl et al., 2015;Zevenbergen et al., 2013;Laurens et al, 2007). UN indicates that flash floods are a major global threat nowadays (UNSIDR, 2016).

Flash flood is event of sudden or rapid rising water level of fast moving water in low lying areas along tranquil streams and creeks and normally it lasts for less than six hours. A flash flood can occur within few minutes or few hours after a high intensity rain (NOAA, 2016). Flash floods are normally generated by either high intensity rainfall, water or melt water from ice or snow flowing over ice sheets or snowfields, collapse of a natural ice/glacier lake or debris dam and manmade hydro - technical structures, such as a dams/dikes/levee (Beilicci & Beilicci, 2015). Flash floods can occur under several conditions which makes higher surface runoff when precipitation falls rapidly on saturated soil or dry soil that has poor infiltration capacity (Beilicci & Beilicci, 2015). According to the prior knowledge, rainfall intensity and duration, topography, soil properties, land cover/land use and land management are the factors that effect on rainfall induced flash floods.

1.2. Background

In 2011, Thailand experienced its worst flooding in a half a century. Flood extended from to August 2011 and January 2012 and this event inundated more than 2/3 of the country. It is ranked as forth costliest world natural disaster by 2011 and economic damage was estimated as 1440 billion Thai baths. 657 deaths and 3 people missing were reported. 13425869 people in 4039459 households were affected and 2329 houses completely damaged. 96833 houses were partially damaged. This flood event was caused by natural as well as human induced factors. Tropical monsoon rain coincided with storm events Nokten, Haitang, Nesat, Nalgae caused for 35% increment of average rainfall for that period. That was the natural cause for this event and it was magnified by human induced factors deforestation, soil erosion and encroachment of flood retention areas (GISDA, 2011). Apart from that Thailand experienced national wide large magnitude flood events in 1995, 2002, 2006, 2004, 2007, 1994, 2005, 2003 and 1996. All of this events had flood magnitude greater than 7 or equal to 7. Flood duration varied from 31 to 158 days (Gale & Saunders, 2013). Flash floods are becoming a matter for the country (ALJAZEERA, 2017). Studies show that frequency and magnitude of flash floods in Thailand in past few decades is increasing (Limsakul & Singhruck, 2016; Hilgert et al, 2015).

Pua is an administrative district of Nan province in northern Thailand. The area is affected by flash floods in recent years. According to resident in Pua, it experienced severe flash flood events in 2011 and 2009. Media reports and institutional repots also provides evident for that flash events took place in Pua (reliefweb, 2009; Climatological Center, 2011; Flood Archives, 2007).

Rainfall intensity and duration is the most important factor for flash flood occurrences in the case of rainfall induced flash floods. Terranova & Gariano, (2014) mentions that rainfalls causing flash floods are still only roughly characterized. High intensity rainfall events increase surface run off generation by decreasing soil infiltration capacity. Studies indicate that great increase in short term storms lasting less than a day which potentially leading to increase in magnitude and frequency of flash floods (Westra et al, 2014). Short duration of rainfall event and higher antecedent precipitation also increase surface runoff generation (Ziadat & Taimeh, 2013; Liu et al, 2011; Peng & Wang, 2012). Miao et al, (2016) mention that rainfall intensity is more suitable for flash flood prediction in semi-humid and semi-arid regions because excess infiltration dominates the runoff in these regions. Effects of rainfall intensity and duration on surface runoff generation depends on other related factors such as soil properties, topography, land cover/land use, land management practices and initial condition of soil, vegetation. Analysis of long term daily rainfall data would determine return periods of rainfall events causing flash floods. High temporal resolution rainfall data can be utilized in flash flood event simulation.

Topography is also significant factor in flash flood occurrence. Steep topography causes in rapid collection of surface runoff into natural water ways (Mahmood et al, 2016). Azmeri et al,(2016) reveal that flash floods are affected by topographic factors such as slope, river gradient, and stream density in Krueng Teungku watershed in Indonesia. A study shows that slope gradient effects on surface runoff generation and higher slope gradients generate higher surface runoff (El Kateb et al, 2013). The effect of surface runoff generation on topography depends on other related factors such as vegetation cover, land management practices, soil properties, rainfall intensity and duration as well.

Soil physical properties play a vital role on hydrological processes. Fraction of rainfall that is available for surface runoff depends on infiltration capacity of the soil (D. Hillel, 1980). Infiltration capacity depends on initial soil moisture content, saturated hydraulic conductivity (K_{sat}) and soil structure (Rugai, 2008). Porosity and organic content play a vital role in soil structure. Micro topography on soil surface also determines available water for surface runoff. $K_{sat,}$ initial soil moisture content and porosity are essential soil physical properties in modelling surface runoff. Bulk density is an indirect parameter to determine porosity and compaction of soil (Chaudhari et al, 2013). Accurate soil unit map and soil physical properties are crucial factor in surface runoff generation modelling.

Land cover/land use (LCLU) changes are influenced by anthropogenic activities. Studies show that LCLU changes have great impacts on surface runoff generation (Wang et al, 2014; Sajikumar & Remya, 2015; Billi et al, 2014; Wangpimool et al, 2013; Olang & Fürst, 2011). Upstream/upper catchment LCLU changes are significant in surface runoff generation (Wang et al, 2014) and that is responsible for flash floods in low lying areas. Asfaha et al, (2015) conclude that both the percentage of vegetation cover and its location in the catchments have significant effect on hydrological response in steep mountain catchments. Due to the influence of related other factors, the expected effect on surface runoff generation by LCLU changes cannot be observed direct (Sajikumar & Remya, 2015). According to the studies carried out recently it is clear that effects of LCLU changes on surface runoff generation depends on type of changes, geographical location and other related factors also. LCLU changes are believed to increment in flash flood frequency and magnitude into current situation (Billi et al, 2014; Solín et al, 2011).

1.3. Justification

Pua watershed in Nan Province, Thailand has experienced 2 severe flash flood events recently (in 2011 and 2009) and according to the information from Pua local authority office, the flood events were responsible for loss of human lives and also for damage to many houses, infrastructures and farm lands. In 2006 also, the area has experienced a severe flash flood event. According to the local people, they experience flash flood events more frequently than past and magnitude of those events are higher than earlier. They point out that certain rainfall events generated flash flood events in recent past they were either not able to produce flash floods in few decades ago or magnitudes were not much higher in few decades ago. That is the general view of elderly community in the watershed premises. Few flood/hydrological studies have been carried out within the catchment and none of these studies have considered the effect of LCLU changes in the watershed (Chuenchooklin et a., 2015;Chuenchooklin & Pangnakorn, 2015; Chuenchooklin, 2012). Chuenchooklin, (2012)clearly states that LCLU changes should be taken into account to better understanding of flood behaviour and water resources management in the catchment. Wangpimool et al, (2013) have studied 3 reforestation scenario for whole upper Nan river basin. The results shows that 2 reforestation scenarios reduce stream flow in wet season. In this study also, it has not considered effect of occurred LCLU changes on flood behaviour and surface runoff generation in the basin.
Since the watershed has experienced 3 destructive flash flood events in recent past(2006, 2009 and 2011), natural vegetation especially at upper watershed is changing into agriculture fields and general view of elderly community and lack of related studies, it is reasonable to study effect of LCLU changes on surface runoff generation and flash flood occurrence in the Pua watershed.

1.4. Problem statement

Within a 5 year time period (2006-20011), Pua watershed has experienced 3 devastating flas flood events. General view of elderly community is that flash flood frequency and magnitude has increased than few decades ago. Extreme rainfall events caused by climatic change and LCLU changes are to be believed for responsible for current flash flood situation, this has not yet been studied. Even it is not proved yet or not scientific, the statement of “certain rainfall events generated flash flood events in recent past they were either not able to produce flash floods in few decades ago or magnitudes were not much higher in few decades ago” gives a clue that rather than effect of climate there is a underlying cause/causes for current flash flood situation. It is obvious that steep – very steep slopes covered by forest is being cleared for agriculture purposes. Even 50^0-55^0 degree slopes are being using for Corn cultivation without applying any conservation measures. The relationship between LCLU change and occurrence of floods is still not clear (Deasy et al, 2014) and need to be studied for better understanding. Figure 1.3 shows the Corn cultivation on a steep slope which are adjacent to natural forest cover.

Figure 1-1 : Views of steep slopes used for Corn cultivation

Such LCLU changes are taking place in upper catchment steep slopes may contribute to higher amount of surface runoff. Forest cover plays a significant role in reducing surface runoff generation (Qin et al, 2013; Zhang et al, 2012). Not only that those surface runoff might fast accumulation into natural stream network (Dehotin et al, 2015) and causes flash flood in low lying area or lower catchment.

Identification of contribution from LCLU changes on increment of frequency and magnitude of flash flood events in Pua watershed is essential to mitigate flash flood problem in the area by implementing effective land use/land management regulations and conservations measures.

1.5. Research objectives

1.5.1. Main objective

Main objective of this study is to evaluate the effect of LCLU changes on surface runoff generation or increment in flash flood magnitude and frequency in Pua watershed.

1.5.2. Specific objectives

- To analyse and quantify LCLU changes that have taken place from 1990 to 2016
- To analyse long term rainfall data to find extreme rain events causing historical flash floods in the area
- To assess the effect of LCLU changes on surface runoff generation or flash floods

1.5.3. Research questions

- Which LCLU is responsible for producing higher surface runoff
- Which secondary data is useful for model calibration and validation
- What is the relationship between LCLU change and flash flood magnitude
- What are the other related factor for current flash flood situation

1.6 Research hypothesis

Natural vegetation such as forest cover converting into other LCLU types such as agriculture fields, settlements causes in generation of higher surface runoff and it is responsible for flash flood occurrence in low lying area/lower catchment. Hydrological models are capable of simulating surface runoff generation on LCLU types.

1.7 Thesis structure

This thesis consist of seven chapters.

Chapter 1 is composed with introduction to study under sub topics of background, justification, research problem, objectives, and hypothesis and thesis structure.

Chapter 2 contains literature review of study based on hydrological processes in a watershed paying special attention to surface runoff generation, factors effecting surface runoff generation and modelling of surface runoff.

Chapter 3 provides information of study area with a general introduction, location, climate and rainfall, land cover and land use, geology/geomorphology and soil.

Chapter 4 covers research methodology and materials used for achieve objectives. Chapter starts with general introduction. It discusses about LCLU map preparation and LCLU change detection. Long term rainfall data analysis and storm design are explained. As last part of the chapter, it discusses structure of OpenLISEM model, data base required for the model and data preparation simulations.

Chapter 5: flood simulations contains details of flood simulations under sub topics of model sensitivity analysis, model calibration, model validation and surface runoff and flood simulation.

Chapter 6 covers results and discussion under sub topics of LCLU change, design storms and surface runoff and flood simulations.

Chapter 7: conclusions and recommendations wraps up the thesis under sub topics of conclusions, recommendations and limitations.

2. LITERATURE REVIEW

The literature review is mainly based on general research objective, specific research objectives and research questions. In addition to that related topics were also concerned in literature review slightly.

2.1. Watershed hydrological process

Runoff is the fraction of precipitation, snowmelt, irrigated water that comes to uncontrolled surface streams. Runoff is classified either based on speed of appearance after the event it produces or source it generates. Based on speed of appearance, there are 2 types of runoff called direct runoff and base runoff. There are 3 types of runoff based on source named as surface runoff, storm interflow (subsurface runoff), and groundwater runoff (USGS, 2016).

Surface runoff (overland flow) is the fraction of precipitation that flow over ground surface and which enters to stream network. Overland flow can be generated based on two conditions named as infiltration excess (Hortonian flow) flow and saturation excess flow (Rumynin, 2015). Many factors effect on surface runoff generation. Few of them are rainfall intensity, rainfall amount, rainfall duration, distribution of rainfall over the catchment, direction of storm movement, soil moisture content, land use, vegetation cover, soil type, catchment shape, catchment area, elevation, topography, drainage network pattern and existing water bodies. Interception, evaporation, transpiration and infiltration are the other hydrological processes that effect on amount of water available for surface runoff. Interception is the process that deal with capturing and storing precipitation by leaves and stems of vegetation before it reaches ground. Evaporation is the process by which water changes from liquid to gas or vapour. Evaporation can take place from vegetation, ground surface and water bodies. Transpiration is the process by which soil moisture is carried through plants from roots to leaves. In a natural hydrological system much of the precipitation return back to atmosphere either by evaporation or transpiration. Within a storm event evaporation and transpiration are very limited. Infiltration is the process by which precipitation enter/absorb into soil (USGS, 2016). Soil infiltrability depends on many factors such as bulk density, porosity, particle size distribution, water-stable aggregates and organic matter content. Land utilization is the most significant factor that determine the soil infiltrability. Land use patterns such as cultivation and deforestation appear increasing bulk density of soil by the time decreasing organic matter content, water-stable aggregates and infiltration rate (Zhiwei et al, 2010). Interflow is the process of lateral movement water through unsaturated zone. This water might come to surface or enter to streams before reaching ground water. Part of infiltrated water in to soil profile moves down under gravity. This process is named as percolation and this water ultimately reaches to ground water aquifer. Base flow is the process movement of ground water to streams. This movement of water takes place through saturated zone. Figure 2.1 illustrates hydrological processes in a watershed.

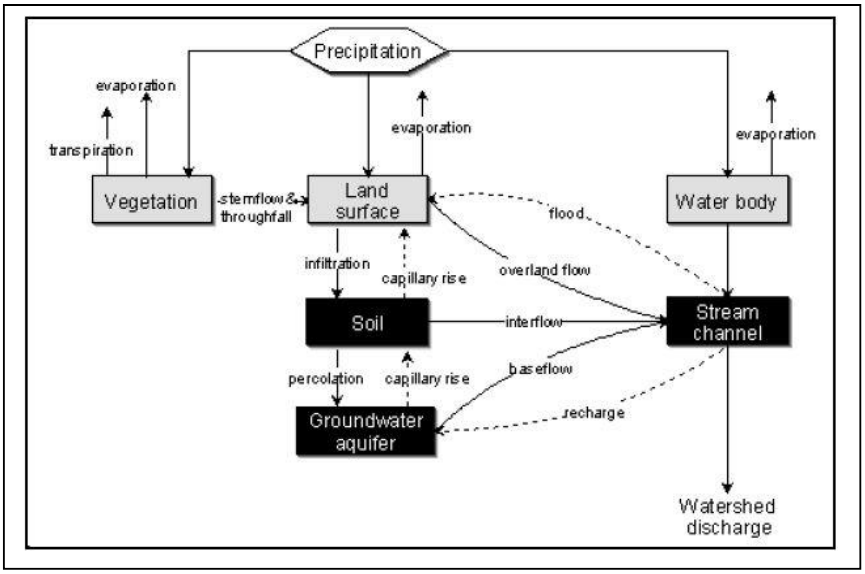

Figure 2-1: System diagram of hydrological processes at local scale in a watershed
Source: Rientjes, 2006.

2.2. Factors affecting surface runoff generation

Surface runoff is one component of hydrological cycle. Many more factors such as precipitation characteristics (depth, duration and intensity), interception, evaporation, transpiration, catchment characteristics (shape, size), topography (slope), soil properties (infiltrability, moisture content), groundwater condition and LCLU types. These factors are categorized into two groups named climatic and physiographic factors (Rugai, 2008). Climatic factors vary spatially in a catchment in conjunction with weather and climate conditions. In reality this variability is significant compared to physiographic factors. LCLU types and soil properties are the most vulnerable physiographic factors for change in time due to human interferences. Most of these factors are interrelated to each other in runoff generation and effect of single factor in generating surface runoff influence by other factor/factors.

2.2.1. Vegetation

Vegetation canopy intercepts fraction of rainfall reducing the amount of water reach to ground surface which is available for infiltration and surface runoff generation. Litter layer generated from vegetation cover also effects water availability for runoff generation. Broad leaves intercept much more amount of rainfall and broad leave litter layer capture/store higher volume of rain water compared to needle leaf vegetation. Broad leaf vegetation reduces surface runoff. Vegetation canopy properties and litter layer properties of vegetation have considerable effect on surface runoff generation (Kim et al, 2014). Bare lands responsible for generation of higher surface runoff within all types of rainfall events (Liu et al, 2016). Different type of vegetation effect in different degree in altering porosity and infiltration capacity. Reforestation improve organic matter content, porosity specially forming macro pores which increase permeability of top soil layer hence infiltration capacity is also increased. Natural forest cover shows the lower surface runoff generation (Ghimire et al., 2014). Nunes et al, (2011) showed that even afforested land cover can generate higher surface runoff than a crop land. Vegetation cover removal influence in increasing surface runoff generation in steep slopes (Xu et al., 2013). Degree of vegetation degradation in a certain vegetation type also effects on surface runoff generation and higher the degree of degradation would result in higher surface runoff generation in hill slopes (Genxu et al, 2012). Vegetation cover help in reducing the surface runoff velocity and it allows water stand on surface more time. This process helps in increased infiltration and thus reduces surface runoff (Zimmermann et al, 2006). Land use and management practices could also play a role in surface runoff generation in a particular land cover type (Peng & Wang, 2012; Ghimire et al., 2014;Marshall et al., 2014). Land cover types such as rods and skid trails generates relatively higher amount of surface runoff (Liu et al., 2016; Safari et al, 2016). Even though vegetation, LCLU in general show the same trend in surface runoff generation, its degree of effect vary from region to region.

2.2.2. Soil

Soil physical properties control surface runoff generation (Hümann et al., 2011). Caballero et al, (2012) found that physical and biological surface roughness influence on surface storage capacity affecting runoff generation. Organic matter content, texture, structure, bulk density, water retention capacity and water repellency are factors that effect on infiltration rate of a soil. Soils with high structural development and aggregation stability have higher infiltration rate (Neris et al, 2012). Degradation of soil structure causes in generation of higher amount of surface runoff (Palmer & Smith, 2013). Porosity (micro pores and macro pores) of a soil directly related to infiltration capacity. Soils with macro pores have higher infiltration rate (Sharma et al, 2013). Bulk density shows negative relationship with infiltration rate. Absolute effect of soil properties on surface runoff generation always hinder by other factors.

2.2.3. Slope

In hydrological perspective, two types of slopes have to be considered. Those are terrain slope and valley bottom (channel) slope. Terrain slope influence on timing to collect surface runoff to streams and time provide for infiltration process. Channel bottom gradient effect on channel retention capacity and velocity of flood wave. With the increment of channel bottom gradient, velocity of flood wave increases and channel retention capacity decreases (Bryndal, 2014). In general steep slopes tend to generate higher surface runoff due to the effect of gravity. El Kateb et al., (2013)studied surface runoff generation and soil erosion on different slope classes and land cover types. Results of the study shows that higher slope gradient has higher potential for surface runoff generation and soil erosion. This study carried out on land cover plots. Runoff intensity has a positive relationship with slope gradient (Huang et al, 2013). Absolute effect of slope gradient on surface runoff generation influence by other related factors such as land cover, soil properties.

022042

2.2.4. Catchment properties

The most significant catchment characteristics related to flash flood occurrence are dimension (size/area), shape, relief (slope) and hydrological condition (Zimmermann et al., 2006). In general small catchments are prone for flash floods due to experience of rainfall event by complete/whole catchment. Catchment shape is expressed by shape indexes. Catchment circularity index (C_k) is the most commonly used shape index to express the shape of a catchment. It is the ration of perimeter square to area of the catchment. Rounded/circular shape catchments tend to generate flash floods since runoff reach to outlet quickly and produce higher peak flow. Stream network density is another important catchment property in flash flood regard. Higher stream network density allows more efficient drain within a catchment. More efficient draining means that runoff get collected to streams quickly and moves down stream smoothly. This process causes in peak flow to be larger and occur faster (Bryndal, 2014). In small catchments, peak runoff is dominated by surface runoff rather than channel flow (Rugai, 2008). Absolute effect of catchment properties are also effected by other related factors.

2.2.5. Precipitation

In a rainfall event, characteristics such as rainfall depth (amount), duration and intensity are the factors which determine flash flood occurrence. It is reported that rainfall events with high rainfall depth and long duration is responsible for generation of higher amount of surface runoff (Fang et al, 2012; Liu et al, 2016). Huang et al, (2013) pointed out that surface runoff is increased with expansion of rainfall duration and time for stable surface runoff is inversely proportional to rainfall intensity. Xu et al, (2013) reported that increasing rainfall intensity is responsible for increment in surface runoff generation. Once catchment is large it does not experience homogenous rainfall. This spatial variability of rainfall event throughout a catchment is responsible for different hydrological responses of different parts of catchment.

2.3. Surface runoff models

Many types of surface runoff generation models are available. But there is no perfect model is currently available for the runoff generation simulation. Any model has its own advantages and disadvantages concerning the spatial and temporal component of the runoff generation process. By selecting proper model, realistic information on surface runoff generation and areas with diversion of normal conditions can be recognized (Beven, 2012; Solomon, 2005; Deursen, 1995).

In each and every model deal with surface runoff generation, complex runoff generation process in nature is simplified mathematically. The mathematical description of a model that simplifies factors are considered in surface runoff generation and enables to quantify the process (Beven, 2012;Rientjes, 2004). Since many factors considered in surface runoff generation have intensive spatial variation, mathematically it is impossible to capture all those variations across the space. So that average values are taken into account for variables. It means that almost all the surface runoff generation models are based on assumptions (Beven, 2012a).

All the models available for surface runoff generation can either empirical models or physical based model. There are models which are combination of empirical and physical based models (Beven, 2012a). Empirical models are based on empirical observations of runoff process rather than mathematically explainable relationship of the process. In other words, empirical models simulate empirical relations using regression equations derived from long term field observations. These models are based on regression coefficients derived from observations and there is no concern about theoretical or physical background of surface runoff process (Rientjes, 2004). The simplest runoff generation empirical models are index models. Which assumes constant rate of loss from total rainfall before producing surface runoff and that constant fraction lost from total rainfall appears as surface runoff in a catchment (Beven, 2012; Solomon, 2005). These index models are simple ways to get approximation of surface runoff (Beven, 2012a). Long term data on climate and discharge of a watershed is required to assess the accuracy of simulations. The United States soil conservation curve number method is an another simple empirical model for estimation of rainfall for surface runoff in a catchment (USDA, 1986). The ratio of actual runoff to potential runoff is equal to actual retention to potential retention is the main assumption on curve number method. This assumption does not have any physical base (Beven, 2012a). Physical based models are models which deal with physics of the under lying process and the process is expressed in a mathematical relationship (Pfeffer, 2003). These model equations are based on laws of conservation of mass, energy and momentum (Rientjes, 2004). Since that these models are complicated and data demanding (Solomon, 2005; Rientjes, 2004). Parameters of physical based model can directly be measured in the watershed field. Increase the complexity of a physical based model increases the requirements of input parameters. Since the measurement of parameters in the field or estimation of them is associated with errors, increment of input parameters influence in overall accuracy of model performance (Solomon, 2005). Complex physical based models do not essentially expand model performance. The predictions form physical based models are more close to realistic and since it is based on physics no restriction of geographical location its application. Empirical models are rather simpler models

compared to physical based models. Becoming simpler means that generalize the physical process behind it. This process generalization results in loosing spatial and temporal information of the process.
Lumped or distributed and deterministic or stochastic are the broad classification of surface runoff generation modelling approaches (Solomon, 2005; Beven, 2012). In Lumped modelling approach entire catchment is taken as a one unit and average value for all the parameters are assigned to the entire catchment. This makes loss of spatial variability of parameters over the catchment. Results obtained from such models are single values for whole catchment (Beven, 2012a). In distributed modelling approach, spatial variability of parameters over the catchment is considered. Model simulation or calculations is done based on square grid cells that can either be uniform or non-uniform. Model equations are solved for each grid cell based on parameter values assigned that cell (Rientjes, 2004). Model predictions are spatially distributed in the catchment based on spatial variability of parameters and the modelling approach allows to assess the changes over the catchment which influence for surface runoff generation (Beven, 2012a). Most of the available models use deterministic approach in surface runoff generation. These models simulates physical process of transition from precipitation to surface runoff generation. One set of values for input variables are given and model outputs are also one set of values. At each time step, it gives only one value for certain output or prediction (Beven, 2012; Solomon, 2005; Rientjes, 2004). Deterministic models are further sub divided in to 3 classes named as black box, conceptual and physical based runoff models (Rientjes, 2004). Stochastic models are also known as probabilistic models. These modules simulates chance of occurrence of hydrological variables related to surface runoff generation (Solomon, 2005). In this modelling approach, input variables and outputs are represented as in term of probability distribution function. Uncertainty associated with model prediction is acceptable due to uncertainty associated with input variables (Beven, 2012; Rientjes, 2004). Furthermore, runoff models can be classified as event based models or continues time models. As it implies by the name, event based models simulate single storm event in runoff generation. Model predictions depend on the initial conditions assigned for variables and accuracy/reliability of those initial values influences accuracy of outcomes. Continuous time runoff models take into account sequence of time stages and for each stage regulates weather or not any event that generate surface runoff. The 3 water balances in a continuous time runoff models are surface water, unsaturated zone soil moisture content and ground water. Most of the continuous models include these 3 components.
In surface runoff modelling, 2 concepts are taken into account for surface runoff generation. These concepts are infiltration excess surface runoff and saturation excess surface runoff (Huang et al, 2016). Figure 2-2 shows the surface runoff generation mechanisms could be expected in a catchment. Available runoff models are based on either one of infiltration excess concept or saturation excess concept or combination of both concepts (Huang et al., 2016). The surface runoff is a component of water budget of a catchment. Available amount of water for infiltration excess surface runoff generation is estimated by either Richards' equation, Finite Water-Content Vadose Zone Flow Method, Green and Ampt method, Philip model, Horton's equation or modified Horton equation, Kostiakov equation or Darcy's law (Tarboton, 2003; Reli et al,2016). Once rainfall intensity exceeds soil's infiltration rate and surface storage is filled up, then infiltration excess runoff take places (Miyata et al., 2010). The theory behind saturation excess runoff generation is that once soil storage capacity fulfilled by precipitation while lateral flow and percolation are taking place, additional precipitation becomes runoff (Dodrico & Porporato, 2006; Johnson et al., 2003). Surface runoff flow/propagation and flood is modeled based on either Kinematic wave theory, Diffusive wave theory or Dynamic wave theory (Singh, 1996; Mujumdar, 2001; Miller, 1984;Beven, 2012b). Kinematic wave and Diffusive wave theories are simplified formats of dynamic wave theory. Surface runoff routing is based on principles of continuity (conservation of mass) and momentum (Mujumdar, 2001). Dynamic wave defines motion under influence of mass and force in contrast Kinematic wave defines motion without considering influence of mass and force (US Army Corps Of Engineers, 1993). When inertial and pressure forces are

not significant for movement of wave, Kinematic wave dominates flow. Flow of Kinematic wave theory is not accelerated considerable amount and flow remains almost uniform along the channel (US Army Corps Of Engineers, 1993). Kinematic flows are uniform unsteady flows. Visible surface wave cannot be clear and flood wave passage is observed on banks as uniform rise and fall of water surface. Dynamic wave rule long wave movements in shallow water. It resembles to large flood wave in a broad rivers. Diffuse wave theory considers hydro-statistic gradient. Diffuse wave enables evaluate effects of gravity and friction on boundary conditions of up-stream to down-stream (US Army Corps Of Engineers, 1993). In general, flood flows are led by Kinematic wave (US Army Corps Of Engineers, 1993).

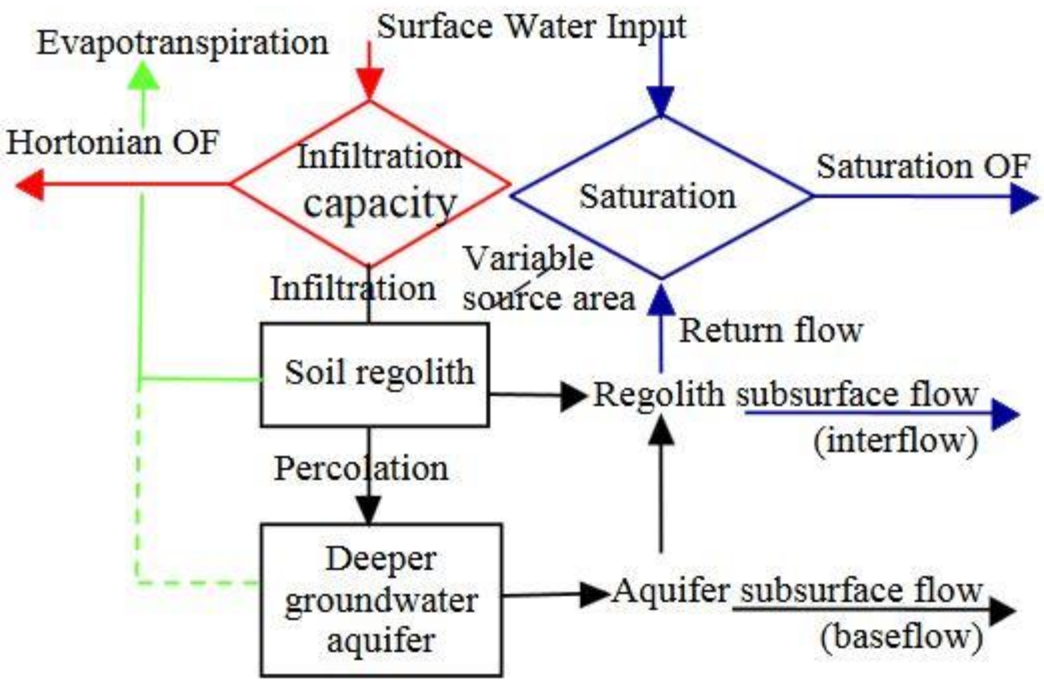

Figure 2-2: Surface Runoff generation mechanisms
Source: Tarboton, 2003

Now a days a large number of surface runoff models are available. Those models are belong to above mention categories. They are based on different concepts/theories related to hydrology.
Selection of a model should be primarily based on objective/objectives of the study and secondary it should take into account availability of data, time and financial component.

3. STUDY AREA

3.1. General description

Study area is located in Pua administrative district of Nan province in Thailand. Pua district is composed with 12 sub-districts and 107 administrative villages. Extend of district is 657.363 km^2. According to the 2015 statistics, population is 64813 with a density of 99 people per square kilometer ("Population statistics 2015," 2016). A part of Thailand's largest national park, Doi Phu Kha National Park and 1,980 m high Doi Phu Kha peak in the Luang Prabang range itself are within Pua District.

3.2. Location

The study area, Pua watershed is situated in Pua district of Nan province at northeastern part of Thailand. Geographical extend of Pua watershed is in between North latitudes $19^0\ 7^/\ 13.73^{//}$ and $19^0\ 20^/\ 56.29^{//}$ and East longitudes $100^0\ 50^/\ 5.1^{//}$ and $101^0\ 7^/\ 53.9^{//}$. Pua watershed is a small catchment of Upper Nan River basin and it's extend is 405.655 km^2. The watershed has 3 main rivers/stream named as Pua, Khwang Khun and Yo. Maximum length across the catchment in East-west direction is approximately 30.5 km and maximum length across the catchment in North-south direction is approximately 25.5 km. A larger part of the watershed is covered by Doi Phu Kha National Park. Fig. 3.1 shows the location of Pua watershed in Thailand.

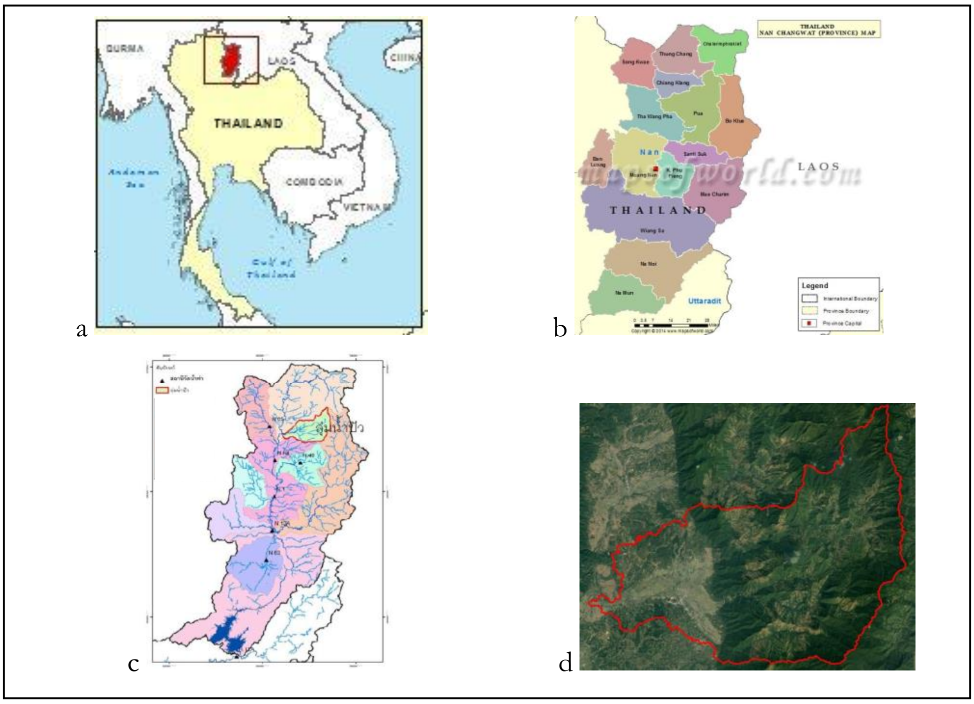

Figure 3-1: Location of study area – Pua watershed
a: Location of Nan province in Thailand b: Pua district in Nan Province
c: Pua watershed in Upper Nan River basin d: Extend of Pua watershed
Source: www.mapsofworld.com, Google Earth, Journal of Water Resource and Hydraulic Engineering Jul. 2015, Vol. 4, Iss. 3, PP 293-302

3.3. Climate

Pua watershed belongs to tropical climate zone and it is influenced by Northeastern and Southwestern monsoons (Solomon, 2005; Gale & Saunders, 2013). Southwestern monsoon starts at late April and continuous up to October. Northeastern monsoon starts at December and continues till early March. Dry and cool winter, hot spring and wet hot summer are the 3 distinct seasons within the region (Solomon, 2005). In southwestern monsoon, it experiences much cooler temperatures in the day time and night remains warmer. Annual mean temperature of the area is 32^0 C. In general month of April area experiences highest temperature reaching to 36^0 C during the hot summer. December is the coldest month and temperature may reach to 14^0 C. Study area receives average annual rainfall of 1304 mm (based on rainfall data from Pua rain gauge (28042), 1921 to 2015). Annual rainfall may vary from 708 mm (in 1921) to 1828 mm (in 2004). Maximum monthly average rainfall is 301 mm August. Average number of rainy days within a year is 70 days. Online weather service states that average annual rainfall in Pua is 1315 mm and average rainy days within a year is 147. Figure 3.2 shows the average high, average low temperature distribution and precipitation, average number of rainy days within a year on monthly basis. This graphs are based on data from 2000 to 2012.

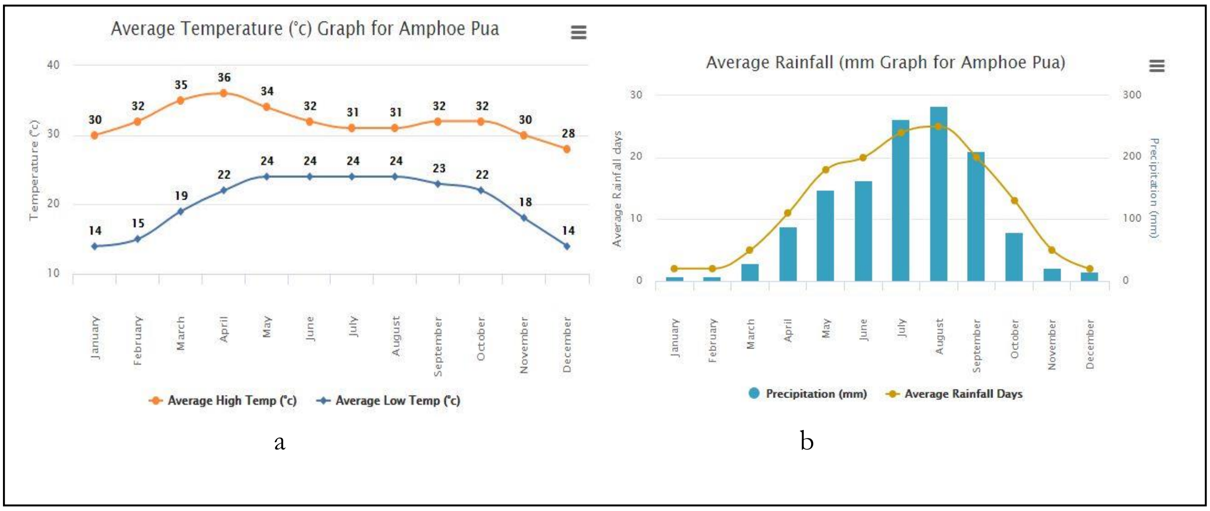

Figure 3-2: Average temperature, precipitation and average rainy days data of study area

a: Average high and average low temperature distribution

b: Precipitation and average rainy days distribution

Source: https://www.worldweatheronline.com/amphoe-pua-weather-averages/nan/th.aspx

3.4. Land cover and land use

Economy of the district is mainly based on agriculture. Rice and maize cultivation are major crops. Maize cultivation has made sever environmental problems in the area. It expands to steep hilly areas and leading to deforestation. The condition is worst since farmers do not apply any conservation measures in farming practices. Main land cover types are tropical rain forest (deciduous forest), paddy fields, maize/corn cultivation, degraded forest/bamboo/teak/shrubs and built up/residential area. Tropical rain forest/deciduous forest is the predominant land cover type in the upper catchment. Paddy fields are situated within lower catchment. Maize fields can be observed in steep slopes associated with forest of upper catchment, moderately steep slopes associated with degraded forests and flat-gentle slopes in lower catchment. Degraded forests are common at lower catchment and foot slopes at boundary of lower-upper catchment. Built up/residential areas predominant in the lower catchment. Few settlements can be found at foot slopes at lower-upper watershed boundary and steep slopes associated with forests. Figure 3.3 represents settlements situated on steep slopes within rain forests. Most of the built up/residential areas have high building density. Even at remote villages, it can be observed that houses are located close to each other. Built up areas are associated with major road network. Most of the residential areas also lined with road network. According to the census data 2015, number of buildings is 15140 ("Population statistics 2015," 2016). Upland crops mixed with vegetables and cash crop, orchard and fruit trees and water bodies are minor land cover classes (Chuenchooklin & Pangnakorn, 2015). According to OpenStreet map, the study area consist with different type of access/roads. Those are footway, paths, primary roads, primary link roads, residential roads, secondary roads, secondary link roads, service roads, steps, tertiary roads and tracks. Higher road density can be observed at built up areas and residential areas. Access are limited to hilly and forest areas. Primary roads at built up areas are as wide as 30 m and most of the tracks are accessible by vehicles having average with of 3 m. Hemwan, (2013) emphasizes that agricultural land use practices of hill tribe communities have changed from nature-based subsistence agriculture such as long-fallow cultivation to commercial intensive land use such as short-fallow cultivation or annual cropping. There is clear evidence that natural vegetation cover is changed into agriculture fields. This situation is more prominent in upper catchment. As farmers do not apply any soil conservation measures in cultivation, intense soil erosion features in steep crop lands and sedimentation in low lying area could be observed in fieldwork.

Figure 3-3: Dense settlements on steep slopes within rain forests
Source: Google Earth Images

3.5. Geology and Geomorphology

Pua watershed consists of lithological units belonging to 6 different time scales (Department of Mineral Resources, 2016). Jurassic, Triassic, Jurassic-Cretaceous, Permian-Triassic, Miocene-Pliocene and Quaternary are the geological time eras of existing rocks originated. Figure 3.4 elaborates distribution of those lithological units within the watershed. Upper catchment consist with lithological units belonging to Jurassic, Jurassic-Cretaceous, Permian-Triassic and Triassic eras. Lower catchment is composed with lithological units originated in Quaternary and Triassic eras. Jurassic era lithological units belongs to Phu Krodung formation and Khorat group. Siltstone, sandstone, claystone and conglomerate are rocks of that lithological unit. Triassic era lithological is composed with shale, chert and limestone. Jurassic-Cretaceous era lithological units belong to Phra Wihan formation and Khorat group. It consists with siltstone, claystone, intercalcated conglomeratic sandstone and quartzitic sandstone. Sandstone, tuffaceous sandstone, argillaceous limestone, meta-rhyolitic tuff, mete-andesitic tuff, shale, chert and onclitic limestone are Permian-Triassic era rocks. Miocene-Pliocene era lithological units belong to Mae Moh group and it consist siltstone, claystone, calcareous claystone, mudstone, ligneous claystone, conglomerate, sandstone, limestone and carbonaceous shale. Quaternary era lithological units are fluvial deposits containing gravel, sand, silt and clay (Department of Mineral Resources, Thailand, 2016; Solomon, 2005). Upper catchment is composed with steep-very steep slopes having V shaped valleys. Flood plains, river terraces, foot slopes and dissected hills or hill ranges. Foot slopes is associated with boundary of upper-lower catchment. Dissected hills or hill ranges are low elevated and they are situated in lower catchment with flood plains and river terraces. Elevation from mean sea level within the catchment varies 200 m to 1915 m.

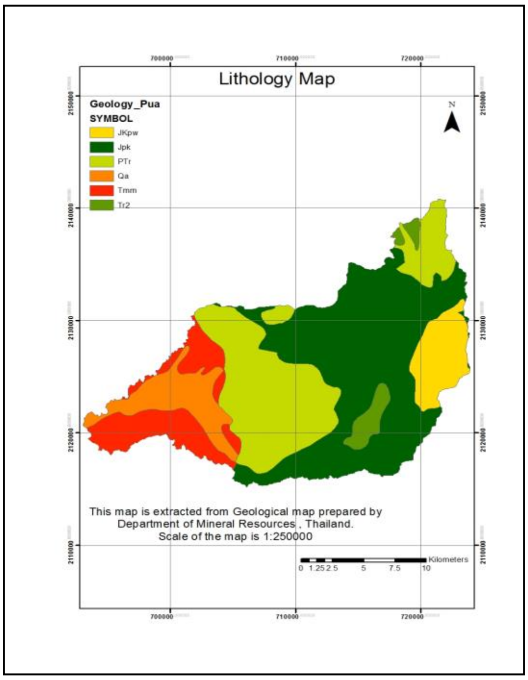

Figure 3-4: Lithological units based on formation time era
Source: Department of Mineral Resources, Thailand

3.6. Soil

Laboratory analysis of soil samples reveals that soil texture classes within the study area varies from sandy clay loam to clay. Lower catchment flood plains consist with silty clay and river terraces contain with sandy clay. Foot slopes associated with boundary of lower-upper catchment covers with sandy clay loam. Dissected hills or low elevated hill ranges situated in lower catchment consists with loam. Hilly areas of upper catchment is mostly covered with clay loam. Other soil types, silty clay loam, sandy loam and clay are observed in upper catchment hilly areas.

4. MATERIALS AND METHODOLOGY

This chapter contains the materials used in the study and scientific methodologies applied in the study to achieve the specific objectives and to answer the research questions.

4.1. Introduction

The main objective of this is study is to analyse the effect of LCLU changes on surface runoff generation and flash flood occurrence in lower catchment. General outline of the study is as follows. As first step of the study, LCLU maps of study area belongs to different times are to be generated using satellite images. LCLU changes within the catchment during last few decades is to be analysed as the second step. Available long term rainfall data is to be analysed to evaluate return periods of flood events. Intensity duration frequency curves (IDF) are to be used for generation of storms relevant to different return periods. Available high temporal resolution rainfall data and design storms are to be used in surface runoff generation simulations. Sensitivity of the model to input parameters is to be analysed. With the aid of measured and recorded data, model calibration and validation is to be conducted. Effect of LCLU changes on surface runoff generation is to be assessed through model simulation by means of rainfall events belong to different return periods. The materials used and methodology/methodologies applied in the each step is described in details under following subtopics. The figure 4-1 given below summarizes major steps of this study.

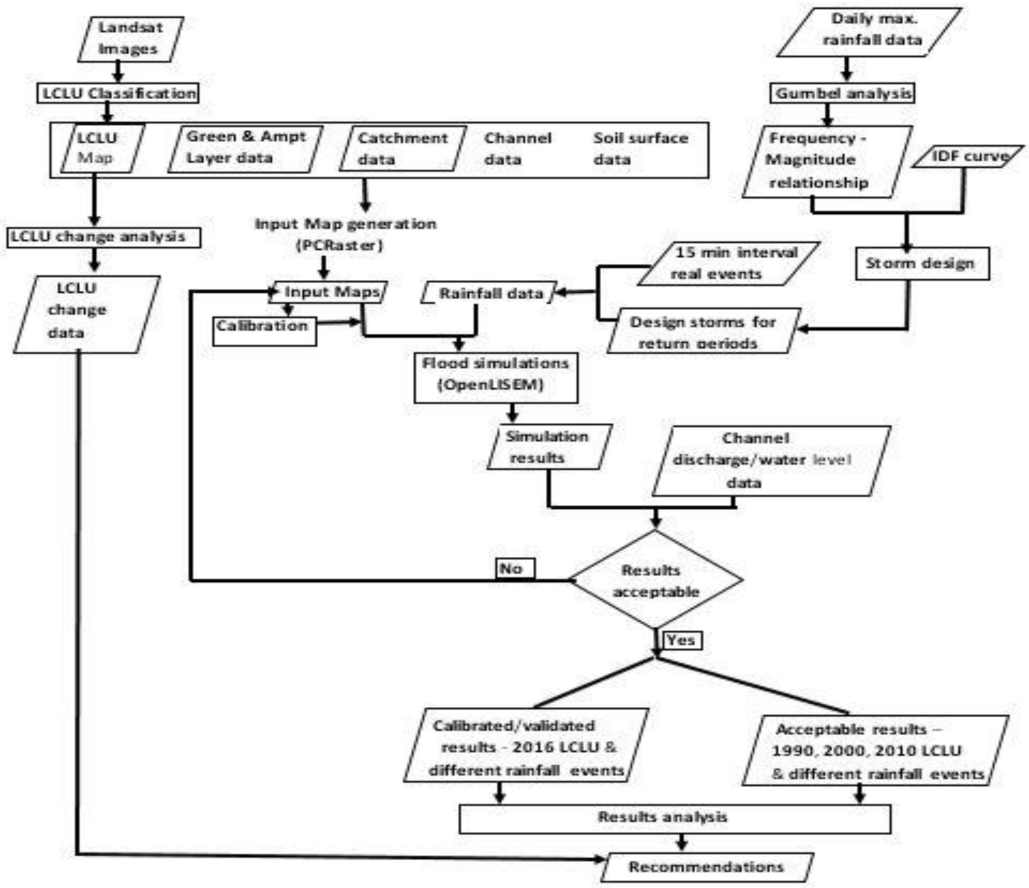

Figure 4-1: Flow chart of methodologies applied in this study

4.2. LCLU map preperation and LCLU change analysis

4.2.1 Materials

Landsat images are used to preparation of LCLU maps of different time periods of study area. Landsat4, Landsat5 Thematic Mapper (TM) images and Landsat8 Operational Land Imager (OLI) were used for LCLU map preparation. Landsat images were downloaded from United States Geological Survey (USGS) Earth Explorer website (http://earthexplorer.usgs.gov/). Table 4.2 shows the detail information about the used Landsat images. Landsat images were selected for LCLU map preparation because of its spatial resolution (medium spatial resolution) is good enough for LCLU mapping (Gong et al., 2013) of this study, its long term (from 1972) availability and its free accessibility. Scene cloud cover represents percentage of image that is covered by clouds. Image quality is the composite image quality for the scene or errors encountered in archiving process and/or visible artifacts in data that can be identified in visual inspection. Best is 9 and worst is 0 (USGS, 2015).

174 mm rainfall event was recorded in study area on 2016.08.14. Landsat images available for 2016 August have scene cloud cover 47-74%. All the available Landsat images from mid-May 2016 to September 2016 have scene cloud cover more than 20%. Close image having less than 10% cloud cover is 2016.05.05 image. Nan province rice and corn cultivation depend on rainy season (mid May- September). For the time period of March- mid May, paddy and corn fields are not planted and still remain after harvesting of previous plantation – fallow (CGIAR, 2012; Hauser, 2014). Since two major crops have same status of crop cycle and images have less cloud cover, Landsat images from March to mid-May are selected.

Table 4-1: Specifications of Landsat images used for LCLU classification

Sensor	Acquisition Date	Entity ID/ Meta Data file	Spatial resolution /m	Path/ Raw	Data Type	Image Quality	Scene Cloud Cover %
Landsat8 OLI	2016.05.05	LC81300472016126LGN00 LC81300472016126LGN00_MTL	30	130 047	L1T	9	0.17
Landsat5 TM	2010.05.05	LT51300472010125BKT01 LT05_L1TP_130047_20100505_20161015_01_T1_MTL	30	130 047	L1TP	7	1
Landsat5 TM	2000.03.06	LT51300472000066BKT00 LT51300472000066BKT00_MTL	30	130 047	TM L1T	9	0.01
Landsat5 TM	1990.04.12	LT51300471990102BKT00 LT51300471990102BKT00_MTL	30	130 047	TM L1T	9	0

ENVI 5.3 (64-bit) and ERDAS IMAGINE 2015 are the software were used in image classification.

4.2.2 Image Classification for LCLU map preparation

Selection of proper image enhancement technique increases image quality (Hossain et al., 2015) and image preprocessing is vital in extraction of accurate information from images (Badreldin & Goossens, 2014).

Radiometric correction of the Landsat images were implemented in ENVI 5.3 using extinction of radiometric calibration. Meta data file of the image is the input for execution of this operation. Then atmospheric correction for the image was done using Quick Atmospheric Correction (QUAC) extension. This operation is also based on Meta data file of the image. Pre-processed images were exported into ERDAS IMAGINE format (img). For image classification process, images were visualised/displayed in Natural Color Composite (NCC). Band 1, band 2 and band 3 of Landsat5 TM images displayed in blue, green and red guns provides NCC. Landsat8 OLI band 1, band 2 and band 3 displayed in blue, green and red guns provides NCC. The advantage of using natural color composite is that objects in the image resembles colors in nature. Contrast stretching techniques comes under radiometric enhancement were applied to better visualization of images. A nonlinear linear stretching called Logarithmic stretching was applied to OLI image and TM images were subjected to Gaussian stretching.

Preprocessed images were classified into LCLU classes in ERDAS IMAGINE 2015 Remote Sensing software. Based on the field observations and characteristics of vegetation types, 5 LCLU classes were identified: forest, paddy fields, corn, degraded forest and built up/residential areas. Degraded forest class consist degraded forest, bamboo, teak, shrubs and orchards. In this LCLU class tree density and ground cover fraction is more or less similar as observed. Maximum Likelihood classifier is broadly used in remote sensing data based LCLU classification and it is based on second-order statics of Gaussian probability density function model for each class. Normal distribution of each class in every band of image is the assumption behind this classifier (Mei et al., 2016). LCLU classification done based on Landsat images using supervised classification and "Maximum Likelihood" parametric rule have shown reliable results with higher overall accuracy and kappa statistics in many parts of the world (Ghebrezgabher et al., 2016; Mei et al., 2016; Rawat et al., 2013; Sisodia et al., 2014). So that all Landsat images: 2016, 2010, 2000 and 1990 images were classified using "supervised classification" method and parametric rule used was "Maximum Likelihood". Signature files for image classification were built using spectral characteristics of training samples.

Training samples for different LCLU types of 2016 image were collected during the fieldwork by using a handheld GPS receiver (Garmin eTrex 30x). In addition to that training sample locations were also extracted from recent Google Earth image. Due to inaccessibility and unavailability of proper transportation media, representative samples of LCLU were collected as much as possible. Total number of training sample points for 2016 May image is 84. Number of training samples for forest, paddy fields, corn, degraded forest and built up/residential areas are 10, 8, 8, 11 and 7 respectively. Validation/test samples were also collected in same manner, their numbers for the corresponding LCLU classes are 11, 6, 7, 8 and 10 respectively.

Training samples and validation/test samples for 2010 image were extracted from 2010 Google Earth image. 2016 Landsat image and 2010 Landsat image were visually analyzed and identified areas with same tone (color), texture, pattern and location/association (Lillesand et al., 2008). LCLU types for selected locations were assigned based on the Google Earth image. Field experience was also incorporated to LCLU type assignment to Google Earth image. 121 total training samples for the image was distributed among LCLU classes' forest, paddy fields, corn, degraded forest and built up/residential areas as 27,21,31,32 and 11 correspondingly. Number of validation/test samples for LCLU classes in same sequence are 10, 8, 8, 7 and 6 respectively.

Training samples and validation/test samples for 2000 image were extracted from 2000 Google Earth image. Selection of training and validation/test samples and assignment of LCLU types for selected locations were made as same as procedure followed for 2010 image. The signature file was based on 50 training samples. LCLU classes' forest, paddy fields, corn, degraded forest and built up/residential areas included 15, 10, 10, 8 and 7 training samples respectively. Number of validation/test samples for LCLU classes in same sequence are 10, 8, 7, 11 and 7 respectively.

Training samples and validation/test samples for 1990 image were extracted from 1990 Google Earth image. The same procedure followed for 2010 and 2000 images was applied for 1990 image to select training and validation/test samples and LCLU type assignment for selected locations. The signature file was based on 50 training samples. LCLU classes' forest, paddy fields, corn, degraded forest and built up/residential areas included 12, 12, 9, 10 and 7 training samples respectively. Number of validation/test samples for LCLU classes in same sequence are 10, 8, 7, 11 and 5 respectively.

3*3 Majority filter was applied to classified images to remove isolated pixels/pixel clusters (salt-and-paper appearance) within a certain LCLU class (Canty, 2014). Majority filtering is available in ERDAS Imagine software under Raster, Thematic, Neighborhood operation. Figure 4-2 shows LCLU maps of year 1990, 2000, 2010 and 2016 respectively.

Image classification accuracy assessment was carried out for smoothen images of 2016, 2010, 2000 and 1990 by applying 3*3 Majority filter. The operation Accuracy Assessment under Supervised Classification in ERDAS Imagine software was utilized for this function. It is based on LCLU types of validation points and that of classified image. Accuracy of classified image is evaluated on Producers accuracy, Users accuracy and KAPPA statistics.

4.2.1. LCLU change detection

There are many change detection techniques available. Image differencing, vegetative index differencing and post classification comparison are the most commonly using change detection techniques (El-Hattab, 2016; Lu et al., 2004). Post classification comparison techniques was used to assess LCLU changes within the study area from 1990 to 2016. This techniques selected since it provides qualitative and quantitative information on changes. In other words, it gives change location, change amount and change type based on number of pixels sharing within the class and number of pixels converted to other classes (El-Hattab, 2016; Yu et al., 2015; Mas, 1999). Cross tabulation technique, Union Matrix operation available in ERDAS IMAGINE was utilized change detection analysis.

4.3. Rainfall data analysis and Storm design

4.3.1. Material

Sub office of Thai meteorological department at Thu Wang Pha provided daily rainfall data of Pua rain gauge (rain gauge reference 28042) from 1921 to 2014. A rainfall data analysis report published in 2001 for upper north part of Thailand compiled by Thai meteorological department was also used. This report includes rainfall depth data and Intensity-Duration-Frequency (IDF) curves of different return periods for 24 hours. The closest rain gauge to study area is approximately 42 km southwards. Appendix 02 shows rainfall data and IDF curve for the closest rain gauge mentioned in the report. The IDF curve has been generated on rainfall data belongs to periods of 1964-1983 and 1986-1993. The rainfall data from rain gauge

28042 and information from the report were the materials used rainfall data analysis and storm design. In addition to that 15 minutes rainfall data from an automated rain gauge belongs to Water Resource department of Nan was also incorporated into flood simulations. 15 minutes rainfall data is available for December 2012-September 2016. This 15 minute interval rainfall data consist with 2 large rainfall events. First rainfall event occurred on 2014.08.29 and its duration was 435 minutes. Total rainfall of that event was 115.5 mm. The second storm started on 2016.08.14 and ended on 2016.08.16. It lasted for 1515 minutes and rainfall amount was 174 mm.

4.3.2. Daily maximum rainfall data analysis

Daily rainfall (amount) data is available for Pua rain gauge from 1921 to 2014. Since Thailand's water year starts form April, rainfall data is recorded from April to March. All daily rainfall data was rearranged to January to December. For year 1950 and 2008, daily rainfall data is not available. For another 9 years, daily rainfall data is missing for a month or a few months. Years without any daily rainfall data were ignored. Daily maximum rainfall for particular year was extracted. For the 9 years with missing data, daily maximum rainfall figures were collected from only available data. Gumbel distribution of extreme values methodology was utilized in rainfall data analysis to establish a relationship between daily maximum rainfalls and return periods. In total 93 daily maximum rainfall figures were sorted ascending order and ranked from smallest to highest value. Left probability (P_{left}), Right probability (P_{right}), Return period (RP) and Plotting position of rainfall data distribution were calculated using following equations 4.1, 4.2, 4.3 and 4.4 correspondingly (Shrestha & Jetten, 2016).

$P_{Left} = R/ (N+1)$	.........4.1
$P_{Right} = 1-((R/ (N+1))$	.........4.2
$PR = 1/P_{Right}$	.........4.3
Ploting Position (PP) = $-\ln(-\ln (P_{Left}))$	.........4.4
Where R = Rank (Order)	N = Number of records

Figure 4.3 (a) below shows the plot of return periods against daily maximum rainfall. Linear trend line of plot shows relationship by equation of y = 0.218x – 16.631 with R^2 (R-squared) 0.458. Linear trend line does show poor fit between 2 parameters. Exponential trend line of return periods and daily maximum rainfall denotes by equation of $y = 0.2068e^{0.0255x}$ with R^2 value of 0.9541. Even though Exponential trend line has good fit with higher R^2 value, extreme high rainfall values are significantly faraway from trend line. Since it is power of rainfall to base of e, slight difference in rainfall effects on return period significantly. To overcome this matter and fit the data set to a linear trend line with a higher R^2 value, -ln (-ln (LP)) was plot against daily maximum rainfall figures. Figure 4.3 (b) represent the graph of this plot. Extreme rainfall figures are much closer to trend line rather than above mentioned 2 methods. The relationship between 2 parameters show by equation of y = 0.0339x - 2.8314 with R^2 value of 0.9845. The equation y = 0.0339x – 2.8314 was utilized in return period estimation of rainfall depth of storms belong to return periods 10,25,50 and 100 years.

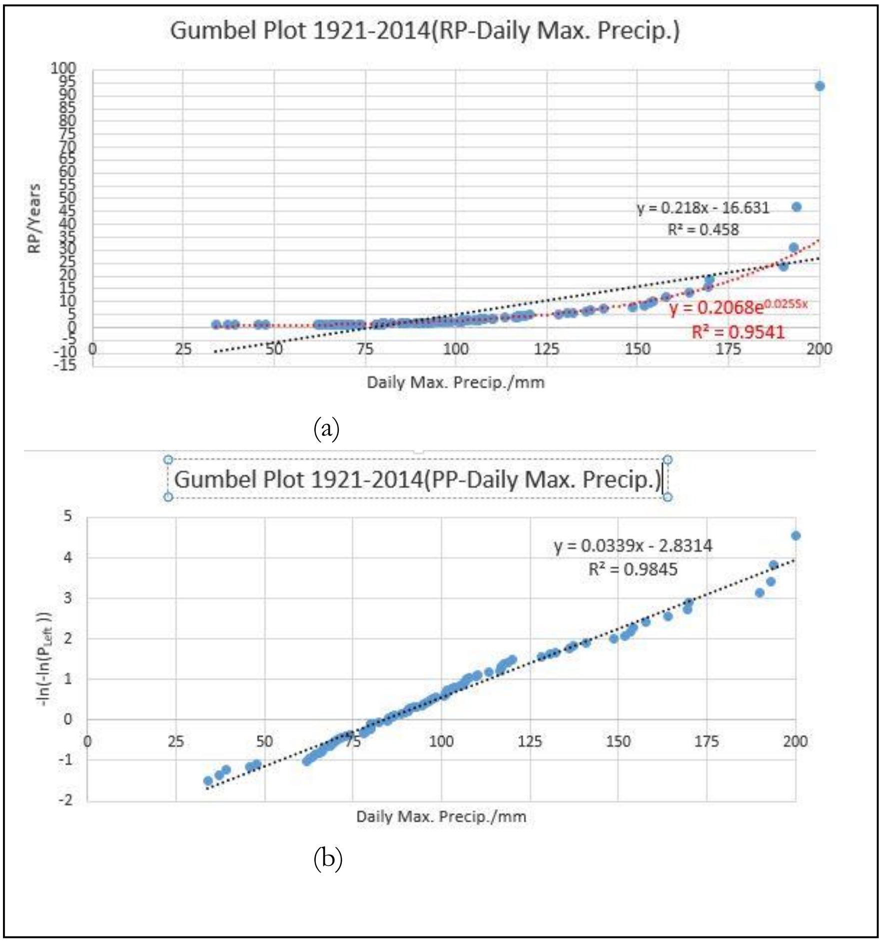

Figure 4-2: Gumbel plot of Pua rain gauge for 1921-2014
(a) RP vs Daily Max. Precipitation (b) PP vs Daily Max. Precipitation

4.3.3. Storm design for different return periods

The rainfall data analysis report 2001 of Thai meteorological department for upper north part of Thailand contains rainfall depth and intensity values at 15, 30, 45, 60, 120, 180, 360, 720 and 1440 minutes time intervals and for return periods of 2,5,10,25,50,100,200, 500 and 1000 years for the closest rain gauge to study area. Power trend lines were fitted for rainfall intensity against time intervals for the return periods of 10, 25, 50 and 100 years. Table 4-2 denotes tend line equation and R^2 for relevant return periods.

Table 4-2: Power trend line Equations and R^2 values for different return periods

RP/Years	Power Trend line Equation	R^2
10	$y = y = 1200.1x^{-0.735}$	0.9673
25	$y = 1450.4x^{-0.701}$	0.9603
50	$y = 1321.9x^{-0.669}$	0.9777
100	$y = 1420.5x^{-0.662}$	0.9750

Source: Page no 18 of a rainfall data analysis report for upper north part of Thailand compiled by Thai Meteorological department in 2001.

With basis of fitted trend line, rainfall intensities were calculated for 15 minute intervals up to 1440 minutes which is equal to 24 hours. Then rainfall for each time step were calculated based on intensity. Next step was calculation of incremental rainfall depth. After that incremental rainfall was calculated. Summation of incremental rainfall was compared with rainfall figures related to Gumbel analysis. For all 4 return periods, the summation of incremental rainfall were smaller than the rainfall values achieved by Gumbel analysis. To make tally with Gumbel analysis values, incremental rainfall values were multiplied by a factor larger than 1. These multiplied incremental rainfall values were used for calculation of rainfall intensities at time steps. Alternative Block Method was used to generate design storms (Chow et al., 1988;Hsu et al., 2000). This is a frequently used method in storm design in many fields such as hydrology, engineering and water resource management. Figure 6-5 shows 24 hours design storms for return periods of 10, 25,50 and 100 years. Rainfall amount for rain storms of return periods 10, 25, 50 and 100 years are 151.5 mm, 178.5 mm, 199 mm and 219.5 mm respectively.

4.4. Data preperation for Flood simulations

4.4.1. Introduction

OpenLISEM is the model selected for surface runoff and flood simulations. It is a physically based distributed model for surface runoff, flood and soil erosion simulations. It is an event based hydrological model working on surface water balance. Since it is an event based model, it does not take in to account evapotranspiration and ground water flow in simulations (Westen & Jetten, 2015). The model estimates surface runoff by Green and Ampt infiltration theory for each pixel and it is routed to stream network based on kinematic wave theory. Water in stream network is also routed by kinematic wave. When streams overflow the overflowing water is distributed based on St Vanent theory (Westen & Jetten, 2015). It has been utilized in many parts of the world belongs to different climatic conditions (Westen & Victor, 2015; Baartman et al., 2012) and has given good results. Even though OpenLISEM was developed for small to medium size catchments, theoretically it can be applied for any size (small, medium, large) catchments and technically there is no limit on catchment size (Baartman et al., 2012). Since OpenLISEM has not yet been applied to the catchment, it has no limit on catchment size, it does not consider ground water (Data/information regarding ground water was not able to find) flow, have experience with the model and it is capable to address research objectives and questions, OpenLISEM was selected for runoff and flood simulations in Pua watershed.

4.4.2. OpenLISEM model

OpenLISEM is an event based hydrologic model. The model processes several functions related to hydrological cycle. Those processes are interception, infiltration, surface storage, overland flow, channel flow, flooding from channels, discharge, splash detachment, flow detachment, sediment transport and sediment discharge (Jetten, 2013). Figure 4-4 denotes the hydrological processes that are processed by OpenLISEM.

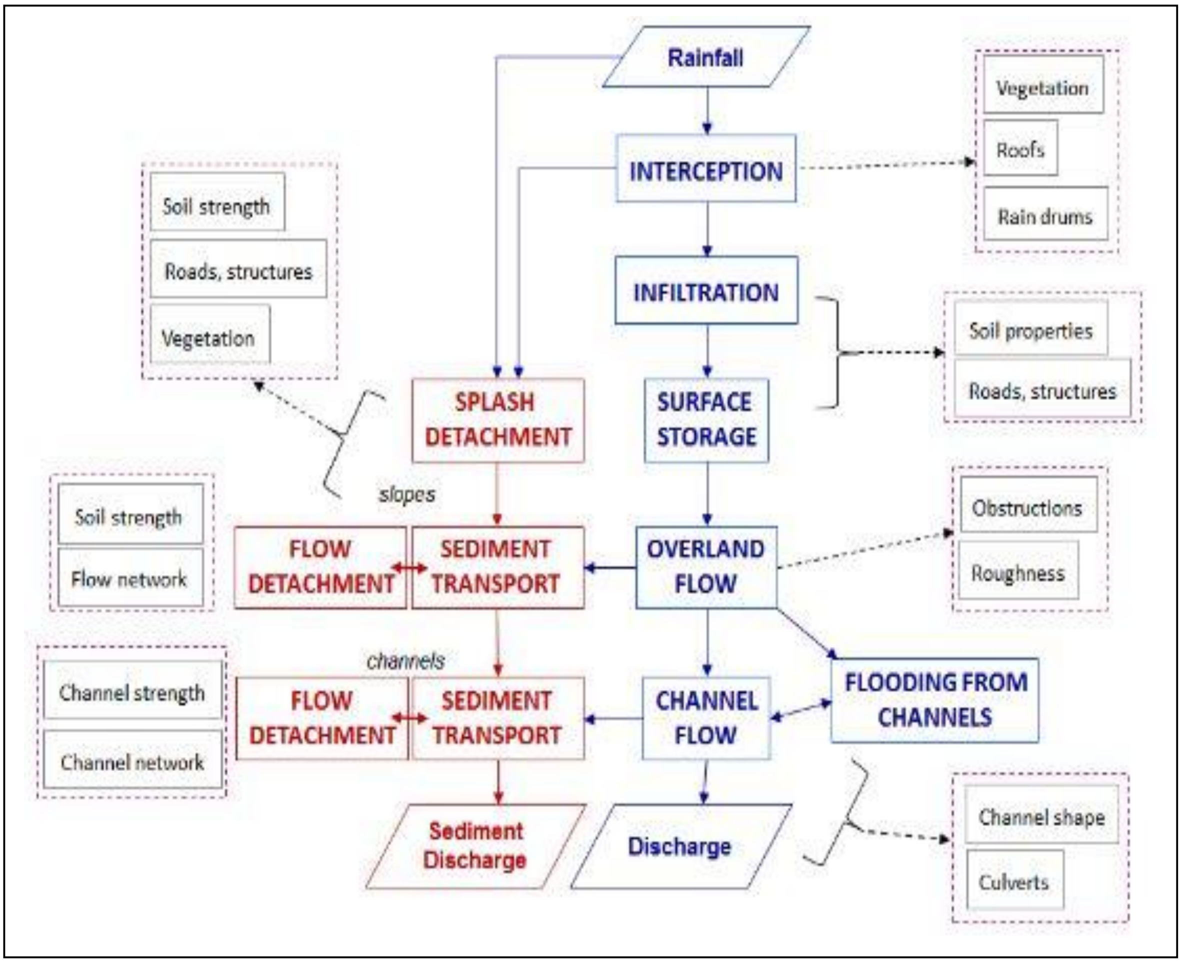

Figure 4-3: Basic structure of OpenLISEM
Source: Jetten, 2013 (http://blogs.itc.nl/lisem/basic-theory/)

Interception is calculated for vegetation. Canopy is considered as fixed storage and it is filled up with rainfall. Once storage is filled up, it starts overflow. The actual canopy interception (Cs) at a given instant is calculated based on maximum canopy storage (Smax) and cumulative rainfall (Pcum). Equation 4.5 given below is used for interception calculations. The maximum canopy storage can be either defined by user as a input map or by a derivative of a Leaf Area Index (LAI) based on empirical equations available in literature (Jetten, 2013).

$$Cs = Smax*(1-\exp(-k*Pcum/Smax)) \qquad \text{.........4.5}$$

Where k is a parameter related to canopy openness and it depend on LAI (Jetten, 2013).

There is no sufficient studies have been done on roof/building interception. Normally, roof/building interception is set to a general value. Based on available literature, roof/building was set to 1 mm (Lull & Sopper, 1986).

2 categories of infiltration mechanisms are incorporated in the model. First one is a simple 1 or 2 soil layers vertical water flow of simplified Darcy law denotes by Green and Ampt model, Smith & Parlange model or simple K_{sat} subtraction. This mechanism assumes that 1 or 2 soil layers are homogeneous and wetting front is parallel to soil surface. Gravity and suction at wetting front are the driving forces for infiltration. Green & Ampt model and Smith & Parlange model calculates infiltration rate based on equation 4.6 given below (Jetten, 2013).

$$f = -k_{sat} * (dh/dz + 1) \qquad \ldots\ldots\ldots.4.6$$

Where f – infiltration rate (mm/h)
k_{sat} – saturated hydraulic conductivity (mm/h)
dh – sum of pressure by water layer at surface and matric suction at wetting front (mm)
dz – infiltration depth (mm)

Second one is a full multilayered soil water balance model named SWATRE (Soil Water Balance for Terrestrial Ecosystems) model based on Richards equation. This mechanism calculates infiltration based on soil water capacity which depends on hydraulic conductivity, pressure potential, volumetric water content and gravitational potential (Jetten, 2013). It calculates surplus infiltration by subtracting actual infiltration from potential infiltration at each time step. It is possible to set lower boundary of soil profile as “open” or “closed”. Impermeable lower boundary option prevents percolation from lower boundary of soil profile to ground water.

Surface storage is the unmovable water content which is retained by micro relief of terrain characterized Random Roughness (standard deviation of surface elevation in small scale-RR). Surface storage is determined using Maximum Depression Storage (MDS). MDS is calculated based on digital elevation model (DEM) at 1m^2 scale. OpenLISEM allows to take place surface runoff before it reaches to MDS. This is due to runoff at micro scale is a spatial phenomenon of ponds that fill up and overflow into each other. Because of this mechanism, water at edges of pixels moves downstream (Jetten, 2013).

When water at surface reaches to surface storage, water starts to flow downhill. It is routed downhill with a kinematic wave function or diffuse wave function over a predefined flow network called Local Drainage Direction (LDD). LISEM adds rainfall minus interception to water layer on the surface and infiltration is subtracted from that. The new water height at each pixel is used to calculate velocity and discharge over each pixel. A 4 point finite-difference solution of the kinematic wave is used together with Manning’s equation to route distributed overland flow (Jetten, 2013).

Separate kinematic wave is solved for pixels with channels. A channel receives only part of overland flow depending on the velocity of overland flow. Water height at channel pixels is used to calculate velocity and discharge over channel pixels. A 4 point finite-difference solution of the separate kinematic wave is used together with Manning’s equation to route distributed overland flow (Jetten, 2013).

Once channels overflow, flood water is distributed over flood zone using full St. Vanent equation for shallow water flow (Jetten, 2013). Figure 4-6 given below shows processes of overland flow, channel flow and flooding from channels and routing mechanisms of the processes.

The discharge calculated per pixel based on Chow et al. ,(1988) is routed downhill towards catchment outlet with kinematic wave function over LDD (Jetten, 2013).

OpenLISEM simulates splash detachment as a function of soil aggregate stability, rainfall kinetic energy and depth of surface water layer (Jetten, 2013).

Flow detachment is simulated as a function of energy carries by water flow and it assumes that it is independent of material carried by water flow. Soil detachment takes place only if sediment concentration is less than transport capacity of water flow (Jetten, 2013).

Sediment transport depends on transport capacity of overland flow and channel flow. Transport capacity is simulated as a function of unit stream power. Sediments in water flow is transported among pixels based on kinematic wave (Jetten, 2013).

Sediment discharge relates to sediment detachment, sediment transport and sediment deposition. Net effect of these processes is sediment discharge. Sediment discharge is a suspension in discharge at outlet. Sediment deposition takes place only if sediment concentration exceed transport capacity (Jetten, 2013).

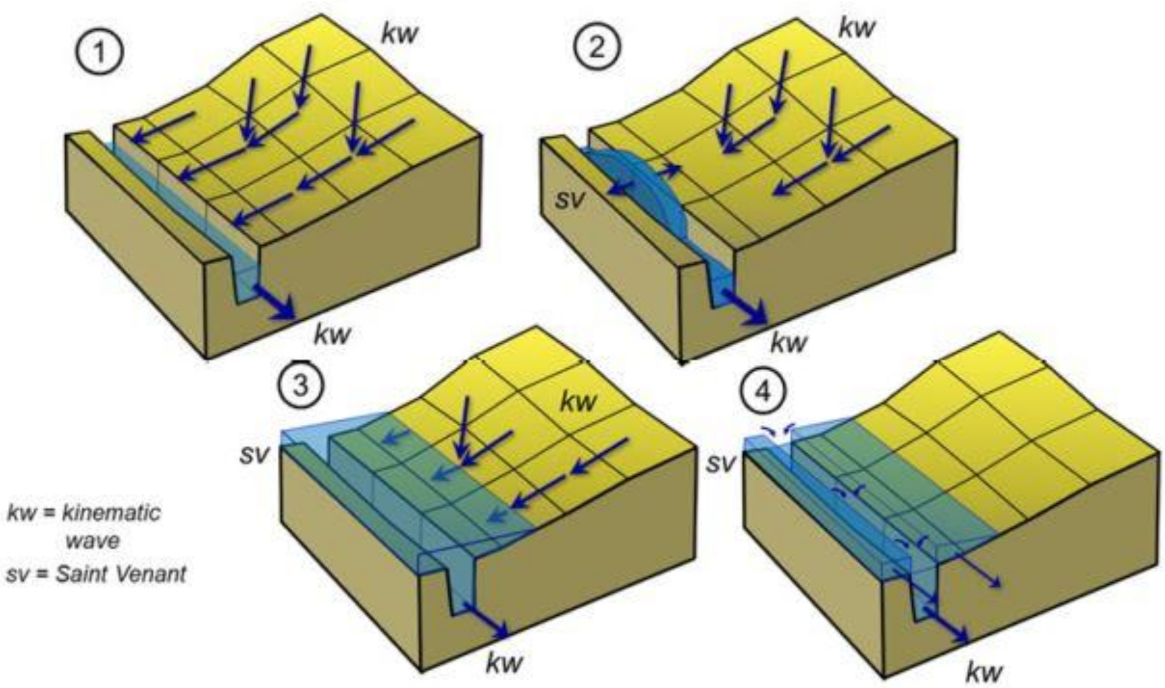

Figure 4-4: Overland flow, channel flow and flooding from channels routing mechanisms
1) Schematic representation of flow processes from 1D kinematic wave runoff and channel flow
2) to overflow of channels
3) spreading out of water from the channels outward using 2D full Saint-Venant equations
4) flowing back into the channel when water levels drop, most likely the runoff has stopped by now
Source: Westen & Jetten, 2015

4.4.3. OpenLISEM database

OpenLISEM requires minimum 24 input maps depending on the input options available at interface (Jetten, 2013). Infiltration options, channel simulations may require additional maps. All required input maps can be derived from Digital elevation model (DEM), land use map, soil map and map of impermeable layers. OpenLISEM input maps can be structured into 6 classes as catchment maps, vegetation maps, soil surface maps, infiltration related maps, erosion/deposition related maps and channel maps (Jetten, 2013). All input maps of OpenLISEM are raster format and they are generated in PCRaster GIS software. All the output maps are also in PCRaster format. Table 4-3 given below denotes the required maps for OpenLISEM.

Since this study does not focus on soil erosion process, erosion/deposition related maps are not going to be generated. These maps are aggregate stability map, cohesion of bare soil map, additional cohesion by roots and D50 values of soil map.

Table 4-3: Details of input maps of OpenLISEM

Catchment maps				
Map name	Content	Type	Unit	Range
LDD	Local drain direction	ldd	-	1-9
Mask50m	Catchment boundary	boolean	-	1
id	Area covered by rain gauge	nominal	-	1
grad	Slope gradient (sine of slope angle)	scalar	-	0<grad=<1
outpoints	Location of outlet and measurements of discharge/water levels	nominal	-	0-2
Vegetation maps				
lai	Leaf area index	scalar	-	0-12
per	Fraction of soil covered by vegetation	scalar	-	0-1
ch	Vegetation height	scalar	m	0-30
Soil surface maps				
n	Manning's n	scalar	-	0.001-0.5
rr	Random roughness	scalar	cm	0.5-20
stonefrc	Fraction covered with stone	scalar	-	0-1
crustfrc	Fraction cover with crust	scalar	-	0-1
roadwidt	Width of impermeable roads	scalar	m	0-12
Infiltration related maps- Green and Ampt 1 layer				
ksat1	Saturated hydraulic conductivity	scalar	mm/h	0-1000
thetas1	Saturated volumetric soil moisture	scalar	-	0-1
thetai1	Initial volumetric soil moisture content	scalar	-	0-1
psi1	Soil water tension at wetting front	scalar	cm	0-1000
soildepth	Soil depth	scalar	mm	0-1000
Erosion/deposition related maps				
aggrstab	Aggregate stability	scalar	-	0.0001-200;-1
coh	Cohesion of bare soil	scalar	kPa	coh+cohadd>=0.196
cohadd	Additional cohesion by roots	scalar	kPa	coh+cohadd>=0.196
D50	D50 value of the soil	scalar	µm	25-300
Channel maps				
lddchan	Local drain direction of channel network	ldd	-	1-9
changrad	Channel gradient	scalar	-	0.0001-106
chanman	Manning's n for the channels	scalar	-	0.001-0.6
chancoh	Cohesion of the channel bed	scalar	kPa	>0.196
chanwidt	Width of channel	scalar	m	0-cell width
chanside	Channel cross section shape	scalar	-	0-10

Source: Jetten, 2013

4.4.4. OpenLISEM database preparation

4.4.4.1 DEM modification

5m spatial resolution DEM derived from ortho-photos by land development department of Thailand (LDD) is available. This DEM does not cover northeast part of Pua watershed. The DEM contains elevation values with 3 decimal points and its accuracy is 2m. Pua watershed is covered by 2 files of ASTER GDEM version2 and 30m is DEM resolution. These files are named as ASTGTM2_N19E100_dem and ASTGTM2_N19E101_dem. ASTER 30m resolution DEM's elevation values are rounded up to nearest 1m value and its overall accuracy is 17m.

5m DEM was resampled to 30m resolution using bilinear resample technique. It determines new value of a pixel based on weighted distance average of four nearest cells. This technique is proper for continues data. It makes smooth of data and wont result data values outside of exiting range (Esri, 2016). Resampling was performed using ArcGIS 10.5. Missing values at northeast part of resampled DEM were replaced by elevation values of ASTER 30m DEM. This operation was done using raster calculator in ArcGIS 10.5.

4.4.4.2 Catchment maps

Local Drainage Direction (LDD) map was created in PCRaster GIS software based on DEM. PCRaster command lddcreate was used in this operation and DEM was modified by subtracting elevation by 2m along channel mask, by subtracting elevation by 10m at main outlet and by adding 2 times elevation of barriers. Subtraction of elevation along channel mask by 2 m was done to make sure that channel network generated based on DEM compatible with channel network. Elevation at outlet was subtracted by 10 m to make sure that catchment outlet generated from DEM make comparable to catchment outlet. 2 times of barrier elevation was added to DEM to prevent channel network going through barriers.

Catchment boundary map was generated using ArcGIS 10.3 software. Operation watershed under hydrology which comes with spatial analysis tool was used in this purpose. The DEM and outlet of catchment were inputs for the operation.

ID map contains only one rain gauge and it assumes that whole catchment receives uniform rainfall. The rain gauge having long term daily rainfall data is situated at lower catchment. The rain gauge with 15 minute interval rainfall data is also located at lower catchment and it is situated at a location 3.5 km northeast to daily rainfall station. Due to unavailability of rain gauges at different terrain units of the catchment, orographic effect on rainfall distribution was not considered.

Grad map was compiled based on DEM. It is maximum value of either slope gradient or minimum slope. It should be greater than 0.

Outlet and outpoint maps were generated using GPS points collected in the field. Outlet is the point where Pua river gets connected to Nan river. Outpoint is the place where discharge and water level data are measured. This place is 40 m upstream to Pua weir. Points were converted to raster format of 30m pixel size using feature to raster operation available in ArcGIS. Outlet and outpoint maps were generated to record simulation results (discharge, water level, sediment discharge and pesticide concentration). The model records simulation results at this points.

4.4.4.3 Vegetation maps

The map of fraction of soil covered by vegetation (per.map) was generated based on normalized difference vegetation index (NDVI) map. Formula 4.7 given below was used to generate map of fraction of soil covered by vegetation.

coverc = 1 – exp (-2*NDVI.map)/(1.5-NDVI.map) ………4.7

where

coverc - fraction of soil covered by vegetation

NDVI – normalized difference vegetation index

Leaf area index (LAI) map is compiled based on map of fraction of soil covered by vegetation. The formula 4.8 was used to compile lai map.

lai = ln (1-coverc)/-0.4 ………4.8

Maximum canopy storage (Smax) map was prepared using empirical formulas developed based on LAI for vegetation types. The formula used for forest and degraded forest is shown by 4.9. Formula 4.10 was used to calculate Smax for corn and paddy fields.

Smax = 0.935+0.498*lai-0.00575*(lai * lai) ………4.9

Smax = 0.7856 * lai ………4.10

Appendix 3 shows PCRaster script used for input map generation. Which is compiled by Prof. Victor Jetten on 1 December 2013.

Appendix 5 presents random roughness and Manning's values assigned for different LCLU types in study area.

4.4.4.4 Soil surface maps

Manning's n map was prepared based on LCLU types and values were assigned to LCLU types based on literature (Chow et al., 1988).

Random roughness map (rr.map) is the standard deviation of surface elevation in small scale. Random roughness values for LCLU were extracted from literature (Renard et al., 1997).

Roadwidt maps consist width of impermeable roads. Road layer of study area was downloaded from OpenStreet maps. Since impermeable roads only are considered primary, secondary, tertiary and residential roads extracted from OpenStreet road layer. Width of the road categories were measured from GoogleEarth images. Primary, secondary, tertiary and residential roads were assigned 12m, 8m, 4m and 3m as width respectively.

4.4.4.5 Soil texture, soil physical property analysis and Infiltration related - Green and Ampt 1st layer maps

Soil samples were collected during the fieldwork to analyse the required soil parameters for flash flood model simulation. 24 undisturbed and disturbed soil samples were collected. Saturated hydraulic conductivity (K_{sat}), porosity, organic matter content, initial soil moisture content and soil texture classes are to be analysed using collected soil samples.

K_{sat} (saturated hydraulic conductivity) map, thetas1 (saturated volumetric soil moisture content) map and thetai1 (initial volumetric soil moisture content) map were prepared based on analytical results of soil samples. Average value of measured/calculated K_{sat}, thetas1 and thetai1values were assigned to LCLU types of forest, paddy, corn, degraded forest and built up/residential area.

Water suction/tension at wetting front (psi1) values for soil texture classes were extracted from literature (Hillel et al., 1998).

Soil depth map was prepared measured soil thickness values in the field and interpreted geomorphological units.

4.4.4.5.1. Sampling technique

Soil physical properties have an influence by LCLU and slope (Tsui, 2004)Zinke, 1962). It was planned to apply judgmental sample technique for soil sample collection (Carter & Gregorich, 2014). Based on soil map of study area, representative soil samples from all possible combinations of LCLU type and terrain units were to be collected. Due to unavailability of soil map, finally representative soil samples from combination of different LCLU types and terrain units were collected. Because of inaccessibility and unavailability of suitable transportation media, collection of soil samples well distributed within the catchment was not able to be done. Altogether 24 undisturbed and 24 disturbed soil samples were collected. Appendix 4 shows locations of soil samples collected for texture analysis and physical properties determination.

At a selected location, top layer of tree debris/decomposed materials was completely removed and then steel sampling ring (diameter 5 cm and height 5 cm) was vertically aligned on the soil surface. Using the soil sampler, the ring was driven to the soil subsurface gradually until ring get completed by soil. While sampling special attention was paid to drive the ring vertically into soil layer and not to make any disturbance to the sample. The sample ring was carefully taken out from soil layer removing soils surrounded it. Then sample was labeled and sealed with lids. This undisturbed soil sample is to be used for saturated hydraulic conductivity, porosity and initial soil moisture content analysis. A disturbed soil sample (from dig out soil) from the same location was collected to a plastic sampling bag. The disturbed samples are to be used for analyze organic matter content and soil texture classes.

4.4.4.5.2. K_{sat} determination

A piece nylon cloths was attached to upper edge of the ring and measured the weight of soil sample - W1 (soil + ring + nylon). After that soil samples were put in a water bath keeping nylon piece as bottom support and water level was about 1 cm from the ring bottom. Samples were kept for 24 hours in the water bath to get saturated. K_{sat} values were measured under constant head method (D. Hillel, 1998) using simple field equipment set up shown in figure: 4-7.

Saturated soil sample was established in the setup and provide a constant hydraulic head. After establishment of constant head, the time for drain a 1 cm^3 was measured. Measurements were carried out until 3 consecutive value record for draining a 1 cm^3 of water through the sample. Then the sample was removed from the set up and place in an oven under 105^0 C for 24 hours. This step was done to remove water within pore spaces of soil sample. This Weight of dry sample - W2 was measured. As the final step, weight of cleaned ring – W3 was measured.

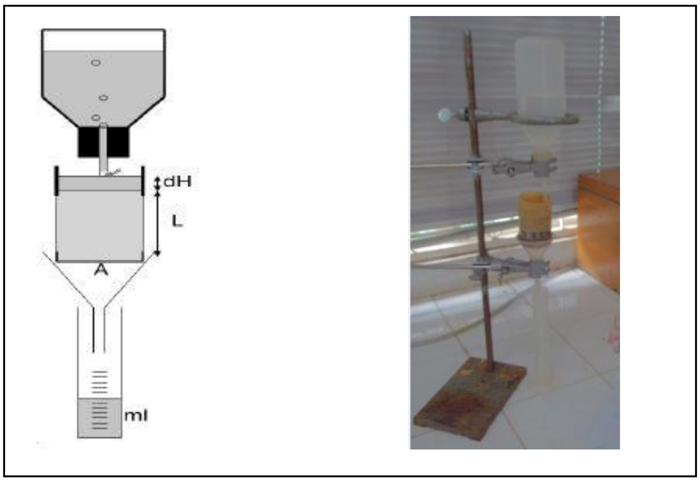

Figure 4-5: Set up of simple field instrument for K_{sat} measurements
Source: Rugai, (2008). ITC MSc. Thesis, 2008

The Darcy's Law is the theory behind calculation of K_{sat} of a soil under constant hydraulic head. The equation 4.11 was used to calculate K_{sat}.

$$K = \frac{V*L}{A*t*h} \quad \text{………………… (4.11)}$$

Where,
K= permeability coefficient or k-factor
V= water volume collected in measuring cylinder
L= length of soil sample
A= cross-section surface of soil sample
t= length of time lapse
h= hydraulic head

22 undisturbed soil samples were analyzed for K_{sat} measurements in the field. Table 4-4 shows the measured K_{sat} values. Undisturbed soil sample no 6 and 15 were set up on instrument shown in figure 4-7 for days. Even though those 2 samples did not give any measurable water volume passed through them.

4.4.4.5.3 Bulk density, soil moisture content and porosity calculation

The general equations available in soil science were used to calculate bulk density, initial soil moisture content and porosity. Required weight/mass values for calculation of those parameters measured based on the same samples used for K_{sat} value analysis. Table 4-4 shows the calculated bulk density, initial soil moisture content and porosity for 22 samples.

Bulk density (dry) of soils samples were calculated using equation 4.12.

$$P_b = \frac{\text{mass of dry soil (W2-W3)}}{\text{Volume of soil as whole}} \quad \text{…………………… (4.12)}$$

Initial soil moisture content was calculated using equation 4.13.

$$U\% = \frac{\text{mass of water (W1-W2)}}{\text{mass of soil (W1-W3)}} * 100 \qquad \text{......................} \ (4.13)$$

W1-W2 represents mass of soil including moisture content

Porosity was calculated using equation 4.14.

$$\varphi\% = 100 - \frac{P_b}{\text{Particle density}} * 100 \qquad \text{......................} \ (4.14)$$

4.4.4.5.4 Soil texture analysis

Disturbed soil samples were used for texture analysis. Procedure mentioned in ITC GeoScience Lab manual for particle size analysis was followed for texture analysis (Van Reeuwijk, 2002). As first step, soils sample was separated into fine fraction and large fraction using 2 mm sieve. 20 g from fine fraction was separated and mixed with 30% H_2O_2 15 ml and 15 ml distilled water to decompose organic matter content. The solution was kept overnight stand. Then it was put on a water bath at 80^0 C until it gives clear supernatant and H_2O_2 was also added time to time looking at the clearness of the supernatant. After decomposition of all the organic matter associated with soil sample, sample was taken off from water bath and demi water was added till volume of 300 ml. Then it was placed on a hot plate and boiled for an hour to remove remaining H_2O_2. After removal of H_2O_2, the solution in beaker was allowed to cool in a slight angle. Beaker was kept until it gives clear supernatant and then supernatant was siphon off. The suspension in the beaker was mixed with 20 ml of 4% Sodium Hexametaphosphate and it was completely to 1 l polythene bottles. The solution was made to 400 ml using demi water and ti was shaken overnight in a mechanical shaker. The overnight shaken suspension was passed through 50 micro sieve and suspension was collected 1000 ml measuring cylinder. The remaining on the sieve was well washed and what was passed through the sieve was collected to the measuring cylinder. The remaining on the 50 micron sieve was completely transferred to crucibles and was dried overnight in an oven at 105^0 C. Oven dried sample was sieved 10 minutes (mechanical sieving) using 1000, 500, 250, 100 and 50 micron sieve set. Different sand fractions remained on the sieves was measured using a scale. The remaining of sieve set bottom was transferred to the measuring cylinder with suspension. The suspension in the measuring cylinder was made to 1 L using demi water. Pipette analysis was utilized in determination of silt and clay fractions. 20 ml fractions from properly suspended materials in the cylinder were extracted at 1 minute, 5 minute and 5.5 hours. Extracted fractions were dried in an oven overnight at 105^0 C and mass of extracted fraction was measured. Sand, silt and clay fractions were calculated based on procedure of lab manual. Figure 4-8 shows few steps of particle size analysis procedure. Table 4 - 4 denotes texture analysis results for 14 samples.

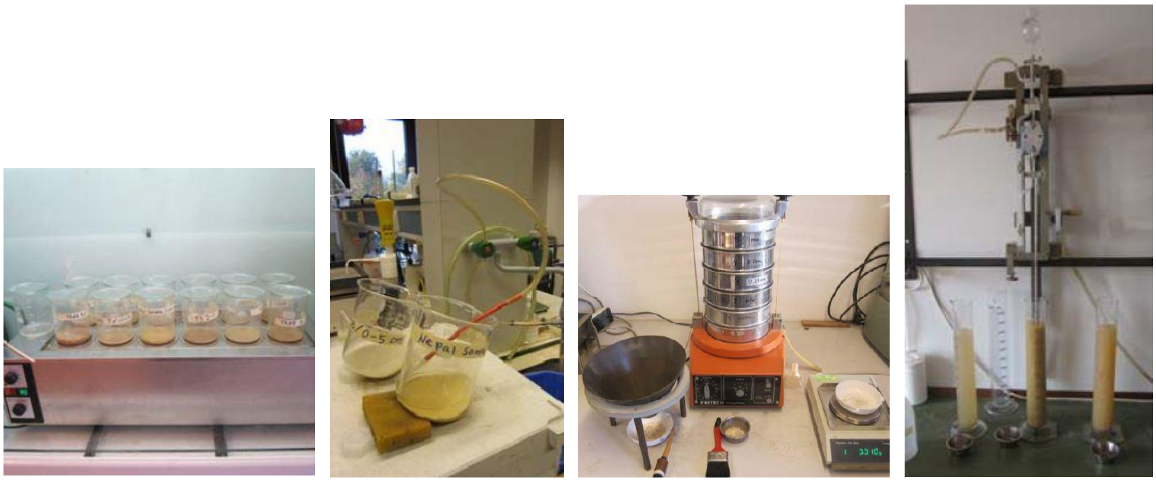

Figure 4-6: Few procedures followed in soil texture analysis

It took more than 10 days to decompose organic matter content of soil samples. And rest of the steps in texture analysis is also much time more time consuming procedures. Due to time constrain, all the soil samples could not be analyzed for texture.

Interpolation of soil texture data within the catchment was done based on geomorphological units. Geomorphology/topography might be considered as main controlling factor of soil formation/development (Cantón et al., 2003).Since soil samples were not able to be collected from covering the entire catchment, geomorphological unit based soil texture interpolation was utilized. Google Earth image of study area was downloaded and geo-reference in ArcGIS using 4 ground control points well distributed on the image. Road intersections were selected as ground control points. The geo-referenced image was exported into "img" image format. Operations available in ILWIS 3.4 were utilized in preparation of Stereo-pair for 3D visualization. The image was imported to ILWIS using via GDAL option and it was resampled to 5 m gird cell size using nearest neighbour technique. The resampled Google Earth image's domain was assigned as image and a color composite (RGB) was compiled. The operation StereoPair from DTM under Image processing was used to create stereo images. Color composite image from Google Earth and 5 m DEM were inputs for this operation. Geomorphological unit interpretation was carried out using Anaglyph. It was done by separating colors of color composite of Google Earth image into grey scale, then making a stereo-pair from DTM and visualization as anaglyph. Red and Green glasses were used to visualize the anaglyph.

Geomorphological units were delineated based on features associated with their origin (Damen & Krol, 2015).4 mechanisms could be identified as geomorphological terrain unit origins in the study area. They are fluvial, denudational, structural and structural-denudatonal. Flood plains, river terraces, mountain range with steep slopes, foot slopes and low elevated hillocks/cluster of hillocks with moderately steep slopes are the geomorphological units that could be identified by image interpretation as mentioned above.

Soil texture classes were assigned to geomorphological units. Certain geomorphological unit was given a soil texture class with majority value (texture class) if the unit contains more than one texture class. Soil texture classes of flood plains and river terraces are silty clay and sandy clay respectively. Mountain ranges with steep slopes have soil texture class of clay loam. Foot slopes consist with soil texture class of sandy clay loam. Soil texture class of low elevated hillocks/cluster of hillocks with moderately steep slopes is loam.

Thickness of surface soil layer was measured in the field. At 18 locations, soil layer thickness was measured. Open earth cuts and soil pits were the locations where measurements were made. Soil thickness values were also assigned to geomorphological units. Flood plains and river terraces are having soil thickness of 1500 mm. Mountain ranges with steep slopes have soil thickness of 400 mm. Soil thickness of foot slopes is 1000 mm and that of low elevated hillocks/cluster of hillocks with moderately steep slopes is 750 mm.

4.4.4.5.5 Organic matter content

Combustion method was utilized in soil organic matter content analysis. A half gram of fine fraction of soil was measured to a porcelain crucible and it was put in a muffle furnace at 650^0 C overnight (Pleijsier, 1986). Crucible was allowed to cool and mass of the burnet crucible was measured. For organic matter analysis process, 4 decimal digit scalar was used. 4 specimens from a certain soil sample were burnet to assess the organic matter content. Table 4-4 shows the results of organic matter analysis.

Table 4-4: Soil bulk density, initial moil moisture content, porosity, k_{sat} and organic matter content analysis results

Sam. No	LC	$P_{b/}$ (g/ cm^3)	φ%	U%	Ksat-mm/h	OM%	Texture
12	Forest	1.35	49.31	14.08	140	9.65	–
3	Rubber	1.53	42.30	8.41	60	5.52	–
20	Forest	1.34	49.57	11.60	153	12.41	Clay loam
10	Corn	1.56	41.26	4.16	36	7.55	–
15	Forest	–	–	–	–	7.57	Sandy clay loam
7	Corn	1.43	46.08	6.68	77	3.48	Silty clay loam
19	Corn	1.56	41.36	3.27	113	12.50	–
9	Forest	1.40	47.35	12.42	16	9.36	Loam
13	Corn	1.50	43.55	6.61	94	8.76	Silty clay loam
17	Paddy	1.23	53.89	17.42	2	2.89	–
5	Forest	1.21	54.66	14.33	150	18.11	–
1	Forest	1.37	48.44	14.73	90	13.73	–
21	Bamboo	1.41	47.02	11.50	102	5.47	Sandy clay loam
4	Teek	1.54	42.11	7.92	111	6.10	–
16	Forest	1.37	48.50	19.22	148	9.47	Loam
14	Forest	1.15	56.76	18.79	37	15.63	Clay
18	Forest	1.13	57.57	15.56	225	15.07	Sandy loam
22	Paddy	1.16	56.49	15.85	10	5.80	–
11	Corn	1.45	45.45	7.46	32	7.74	Clay loam
6	Teek	–	–	–	–	4.85	Clay loam
23	Paddy	1.13	57.45	14.20	15	4.29	Clay loam
8	Shrub	1.44	45.85	13.46	49	4.19	–
2	Corn	1.46	45.14	6.67	117	7.73	Silty clay
24	Paddy	1.25	52.92	13.80	11	3.35	Sandy clay

Since that soil samples were collected from close to soil surface, this might be a reason for higher organic matter content. According to available literature, soils of north-eastern part of Thailand contains relatively higher amount of organic matter content. Organic matter content links with flood regime. In lower flood regime, organic matter content is 13.1+/-4.9. It is 6.7+/-2.4 and 3.9+/-2.2 for middle flood regime and upper flood regime respectively (Seng et al., 2004).

4.4.4.6 Channel maps

Map of local drain direction of channel network – lddchan.map was prepared based on DEM, channel mask and main outlet. Elevation values along channel mask was extracted and then elevation at main outlet was subtracted by 10. This resulted elevation map was used to generate local drain direction of channel network.

Channel slope map- changrad.map was compiled based on DEM values along channel mask. It is maximum value of either slope gradient of channel mask or minimum slope. It should be greater than 0.

Manning's n for the channels was assigned based on literature. It was assigned to 0.05 (Chow, 1959).

Cohesion of the channel bed was assigned as 8 based on available literature.

Width of channel - chanwidt.map was created using equation of "max (2.0, min (celllength ()*0.95, accuflux (lddchan, cellarea)/3.22e4)**(1.18)))". According to the equation, minimum channel width is 2 m. In reality there are streams which are wider than pixel size 30m. When streams having higher order is assigned width more than pixel size, it introduces significant mass balance error.

Model OpenLISEM is not capable of dealing with complex channel cross section. It can make simulations either rectangular or trapezoid shapes. Channel cross section shape – chanside.map was assigned as rectangular. So that channel side angle is 0.

Appendix 5 shows assigned channel parameters values.

4.4.4.7 Modelling effect of paddy fields

In reality paddy fields are surrounded by small bunds in all directions. Because of these bunds paddy fields acts as retention ponds. So that paddy fields capture and store significant amount of water. This water is not available for overland flow until paddy fields fills upto certain level of bunds or upto bund level. Once paddy fields become one of either situation, it starts overflow from paddy to paddy. Since paddy fields consists with soil types having low k_{sat} values, model shows quick/instant overland flow in paddy fields. In reality this overland flow is stagnated in paddy fields itself for certain period of time. This process occurs in paddy fields was modeled using alternative procedure. The fraction of rainfall pour down to paddy fields were let to be stored in top soil layer. Thickness of surface soil layer made thinner to control amount of water enter to it and it was set to 100 mm. To store rain water in surface soil layer quickly, k_{sat} value was increased to a very large value and it was assigned as 100000 mm/h. This will allow rain water to infiltrate rapidly. To increase water storing capacity of surface soil layer of paddy fields, porosity and initial soil moisture content were also altered. Porosity was increased to 95%. Paddy fields were set to completely dry by assigning initial soil moisture content to 0. This alternative techniques allows preventing quick overland flow and allow water to pond in paddy fields.

5. FLOOD SIMULATIONS

This chapter mainly focus on flood simulations. Sensitivity analysis, model calibration, model validation and flood simulations on different LCLU maps and different rainfall events are discussed in this chapter.

5.1. Model sensitivity analysis

In literature and previous studies, it is mentioned that OpenLISEM model is highly sensitive to saturated hydraulic conductivity (k_{sat}) and initial moisture content (thetai) (De Roo & Jetten, 1999; Hessel et al., 2003). Sensitivity analysis was carried out with a view to quantify catchment response for few selected parameters. Model sensitivity analysis was done by either increasing or decreasing k_{sat} and thetai values in certain percentages respectively. The rainfall event took place on 29 August 2014 was used for model sensitivity analysis. It is a 115.5 mm rainfall event with duration of 505 minutes. This event has return period of 3 years. This rainfall event was selected to overcome simulation time constraint. Model was allowed to run for 1440 minutes in sensitivity analysis process.2016 database was used for sensitivity analysis. In addition to that, model's sensitivity to porosity (thetas) was also analysed. Appendix 6 shows the results of original database and that of changed values of k_{sat}, thetai and thetas.

Reduction of k_{sat} vlues should increase total discharge. This is due to lowering k_{sat} causes reduction of infiltration. That increses surface runoff and as consequence increase total discharge also. Increment of discharege may cause in flood . Increment of k_{sat} has negative effect on total discharge and flooding. This is due to decrease of surface runoff as aresult of increment of infiltration.

Initial soil moisture content effect on volume of water that can be infiitrated in to soil profile. If initial soil moisture content higher amount of water that can be infiltrated reduces. This results in incresing surface runoff. So that increment of initial soil moisture content has effect of incresing surface runoff and may cause flooding.

The soil samples are collected from close to soil surface after removing tree debris on soil surface and then removing 1-2 cm of top soil. So that soil contains higher amount of organic matter. It could be observed macropores in many sample locations. These macro pores might be resulted from higher organic matter content and animals live in top soil layer. Macropores allow quick infiltration and percolation of water. It provides much more space water to get stored in soil (Pearce et al., 1986). Slight change in porosity effects on available storage space in soil profile significantly. Model calculates available storage space by (porosity-initial soil moisture content)*infiltration depth. If porosity is reduced by 10%, available storage space is reduced by more than a half (0.6). So reduction of porosity reduces storage space and consequently decreases infiltration. It results in increasing surface runoff. As a consequence flooding might be take place. Increment of porosity by 10% results in increasing available storage space by more than 1.5. This causes in increasing infiltration and decreasing surface runoff significantly. Model sensitivity for porosity is not directly related to porosity. Model's sensitivity for porosity is actually due to fact of "porosity – initial soil moisture content".

.

5.2. Model calibration

Model calibration was performed by only increasing initial soil moisture content. 2 times of field measured initial soil moisture content was able to provide simulated discharge close to measured one. Either discharge data or water level data is not measured at outlet of Pua watershed. Measured discharge data and water level data are available only at Pua weir location. The measurement point is situated close to boundary of hilly terrain and low lying area of the catchment. Figure 5-1 shows the location of outlet and measurement point- Pua weir. This data set covers time period from 2010 to September 2016. According to staff members of Pua sub office of Royal Irrigation Department of Thailand, discharge and water level data are measured at 8.00 am every day. Since discharge and water level data are measured once in a day, calibration had to be done on comparing measured values at 8.00 am and simulated values belongs to 8.00 am of the day or days. If rain event had started after 8.00 am of the day, it had to be considered measured values of following day. For a reliable calibration, it was attempted to calibrate model for 2-3 measurements of 8.00 am.

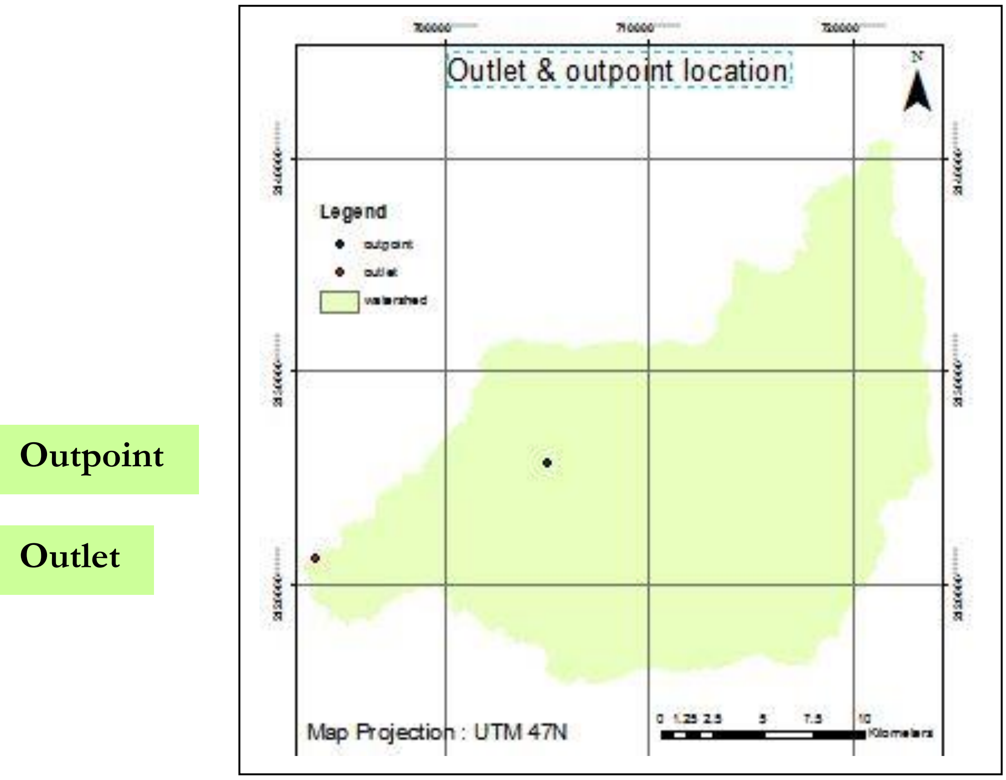

Figure 5-1: Location of outlet and discharge measurement point

15 minute interval rainfall data is available from 2012 December to 2016 September. There are large data gaps within this dataset. Data is missing from 2014 January to 2014 June and from 2015 August to 2016 June. Even within a rainfall event, it could be observed missing values for time steps. Department of Water resources in Nan expressed that missing values are due to malfunctioning of automated rain gauge or failures of mobile network. Within available data, there are 2 rainfall events having rainfall depth more than 100 mm. First event occurred on 2014.08.29 and its rainfall depth is 115.5 mm. This rainfall event started at 00:30 am and ended at 7:45 am. Its duration was 505 minutes. Second rainfall event took place on 2016.08.14 and 2016.08.15. The event started at 9:45 am of 2016.08.14 and ended up at 11:00 am of 2016.08.15. Event duration was 1515 minutes and rainfall depth was 174 mm. Since this rainfall event occurred during two days – 25 hours and 15 minutes, it is impossible to calculate return period for this rain event.

Model calibration was performed on 2016 database and measurements related to 174 mm rainfall event were compared with simulations. Model was simulated for 4500 minutes. Since available hydrological data is daily basis, Model calibration could be done for a single value. So that model was run for longer time with a view to calibrate model for following days. Simulation time step was set to 30 seconds since pixel size of database is 30m. Measured discharge and water level values of 15, 16 and 17 August 2016 were compared with simulation values at minutes 1235, 2675 and 4115. Figure 5-3 shows the hydrograph for base data set and model calibration data set at 115.5 mm rainfall event. These 3 minute values correspond to measured values at 8:00 am of 3 days. Appendix7 shows discharge and water level values for original database and that for 2 times thetai. The table includes difference between simulations and measurements. Appendix7 includes difference between measurements and simulations. Since sufficient discharge measurements are not available, it is not possible to calibrate the model for peak discharge time.

By assigning initial soil moisture content to 2 times of measured values in the field, simulated discharge value could be made close to August 15 measured discharge value. The simulated value is 1.88 m^3 higher than measured value and the percentage of difference compared to measured value is only 1.95. But simulated discharge values of August 16 and August 17 are very low compared to measured values. The difference between simulated and measured values are -11.08 m^3 and -10.39 m^3 for August 16 and 17. The percentage of difference compared to measured discharges are -71.12 and -90.27 for 2 dates respectively. OpenLISEM model calibration for large catchments has short comes because of spatial variability of ksat values within catchment (Baartman et al., 2012). OpenLISEM is an event base model and it is not capable of simulation for longer timescales (Baartman et al., 2012). August 16 and August 17 correspondent simulation values for measured values are simulated after 2675 minutes and 4115 minutes after rainfall event started respectively. This might be the reason for simulations giving deviated values from measurements of discharge.

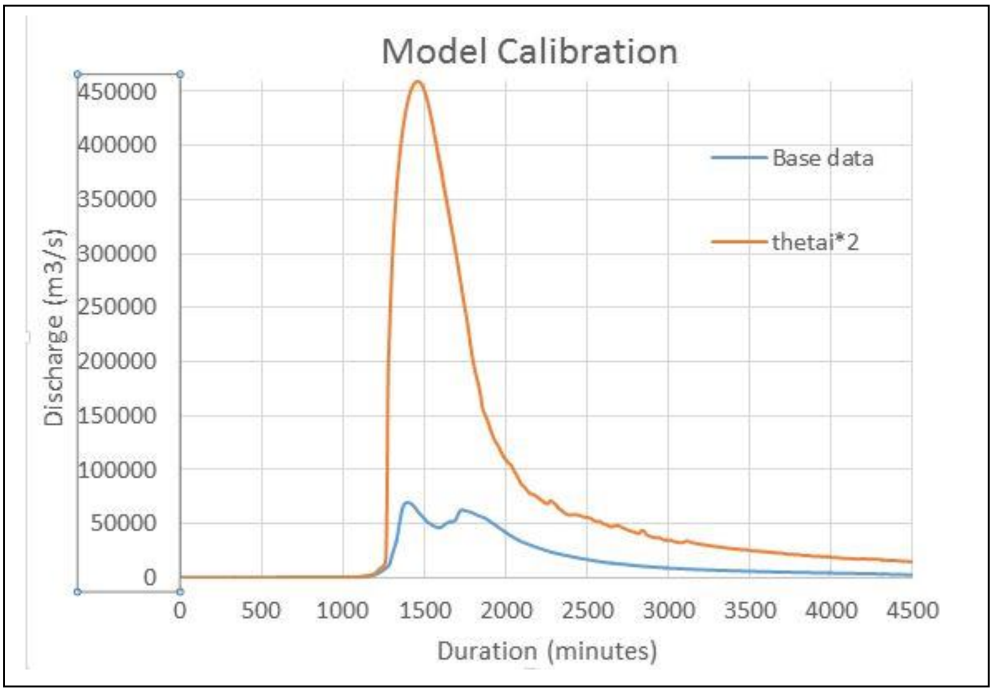

Figure 5-2: Hydrograph for Base data set and calibrated parameter-thetai*2

Channel water level simulations are far away from measured values. The Pua weir is situated 40m downstream to where water level is measured. Measured water levels encounter the water level of water stagnated by weir. Weir height is 3.7m. So that the measured water level consists two portions and it is addition of existing water level due to weir and water level of river flow. There is no data or information to separate these two parts. Data or information for introduce base flow to model simulations cloud not be found. So that component of base flow has to be skipped for simulations. Due to above 2 factors, river water level data could not be utilized in model calibration in this situation.

It is not possible to be done model calibration for peak discharge since sufficient discharge data – high temporal resolution discharge data is not available.

5.3. Model validation

For the purpose of model validation, 2016 database with calibrated parameters was selected. Rainfall event on 2014.08.29 was used for model validation. Measured discharge and water level values were compared with that of simulated values at 8:00 am. Flood simulation for model validation was allowed to run for 1440 minutes. Simulation values at 450th minutes corresponds to 8:00 am measurements. Figure 5-3 presents the hydrograph of model validation rainfall event at outpoint2. Due to lack of measurements, model validation for peak discharge time was not able to be performed. Appendix8 shows results of model validation by means of discharge and water level values.

In validation simulation, simulated discharge value is 2.64 m^3 lower than that of measured one. Percentage of defference between simulation and measurement compared to measured value is -14.35. Validation of model by discharge measurement provides acceptable results. Simulated water level far deviates from measured value. Percentage of difference between simulated and measured water level compared to measured water level is -88.92. Model validation using water level measurement is not possible due above mention facts in model calibration section.

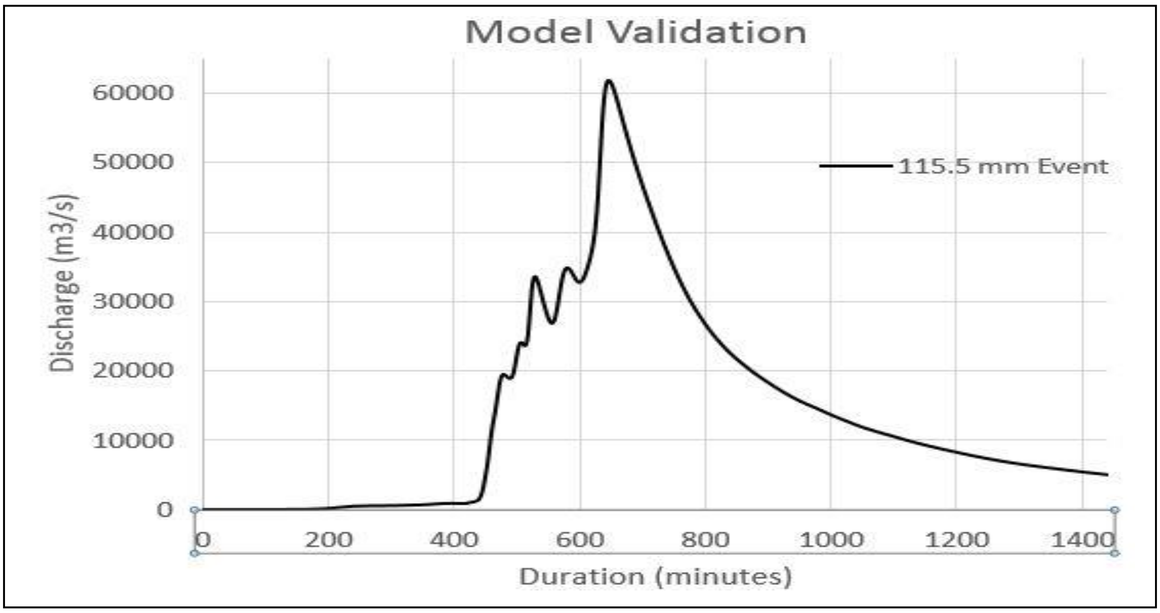

Figure 5-3: Hydrograph for model validation

5.4. Surface runoff and Flood simulations

Based on availability of required input data, runoff generation and flood simulations could be run for year 1990, 2000, 2010 and 2016. The general objective of this study is to analyse effect of LCLU change on surface runoff generation and flood occurrence. These different years were selected to evaluate surface runoff generation and flood occurrence on LCLU of particular years. LCLU map and its derivatives are the only dynamic inputs for different years. All other input maps are same for every year. Simulation for different years can provide evidence for effect of LCLU on surface runoff generation and flood occurrence and how does LCLU change effect on it.

Watershed has it's extend of 442 square kilometres. Since watershed is relatively large, all input maps were generated in spatial resolution of 30m. Maps with fine resolution in OpenLISEM database (smaller pixels) increases simulation time significantly (Rugai, 2008). DEM resolution and DEM quality are critical factors on hydrological modelling. Even 5m resolution DEM is available, due to catchment size and computation time, coarse resolution database has to be used in simulation. Resampling of DEM to a coarse resolution effect in DEM quality. It may makes slopes flatten and shortened flow path length. This short comes introduce errors in direct runoff generation (Vieux, 1993; Shih, 2014). Due to this fact ASTER DEM'm resolution is kept as same and final DEM was compiled as mentioned in section 4.4.4.1 of chapter 4.

One objective of the study is to evaluate effect of LCLU change on surface runoff generation and flash flood occurrence. To achieve this objective, LCLU maps for year 1990, 2000, 2010 and 2016 which is one of major base map for runoff generation simulation were generated. The LCLU maps were produced by Landsat image classification. LCLU map preparation is described in section 4.2.2 of chapter 4. Parameter values saturated hydraulic conductivity, porosity, initial soil moisture content, random roughness and manning's n are assigned to LCLU units. Appendix5 shows assigned parameter values.

Values of suction at wetting front are assigned to soil texture map compiled based on geomorphological unit map.

Two real rainfall events having higher rainfall depth and high temporal resolution rainfall depth data are available. These 2 events are used for model calibration and model validation. Model calibration was done for rainfall event having 174 mm and duration of 1515 minutes. Calibration simulation was run for 4500 minutes. Rainfall event having 115.5 mm rainfall depth was used for model validation. Simulation ran for 1440 minutes. The rainfall event with 174 mm has duration of 25 hours and 15 minutes. Table 5-1 presents information about those 2 rainfall events.

Table 5-1: Information of 2 rainfall events having higher rainfall depth and high temporal data

Event	Start date & time	End date & time	Duration/min	Rainfall depth/mm	Return period/years
Calibration	2016.08.14 09:45	2016.08.15 11:00	1515	174	-
Validation	2014.08.29 00:30	2014.08.29 07:45	505	115.5	3

Pua local authority and residents in low lying are confirmed that houses/buildings were not flooded by this event. But they told that paddy and agriculture fields in low lands were subjected to minor floods for short time period. Data collected regarding flood extend and flood depth by means of interviewing local people are contradiction to each other.

Design storms could be used in runoff generation and flood simulations. Storms of different return periods imply severity of flood event when return period increase. Daily annual maximum series of rainfall depth data of Pua rain gauge provides relationship between return period and rainfall depth (Chow et al., 1988). Table 5-2 shows rainfall depth for different return periods.

Table 5-2: Rainfall depth for different return periods

Return period/years	10	25	50	100
Rainfall depth	151.5	178.5	199	219.5

IDF curves for 24 hours duration are available for rain gauge located at 42 km down south to study area. Based on available IDF curves for 24 hours, storms were designed for return periods of 10, 25, 50 and 100 years. Rainfall depth of each storm is calculated and compared with rainfall depth values given by Gumbel analysis. If two rainfall depth values are not equal, design storms rainfall depth is multiplied by a certain factor to make them comparable to each other. Storm design is discussed in section 4.3.3 of chapter 4.

OpenLISEM considered that channel width is less than pixel resolution (Hessel, 2005). In reality it could be observed streams having with more than 30m at certain parts of lower catchment. If stream width is increased more than pixel resolution, it introduce mass balance error. So that stream width is assign less than pixel resolution.

Hessel (2005) states that selection of simulation time step depends on pixel resolution. When time step is smaller, simulation results are better. On the other hand smaller time steps increases computation time also. Considering all these factors, simulation time step is set to 30 seconds.

Calibrated model with 2 times of initial soil moisture content is simulated on LCLU maps of 1990, 2000, 2010 and 2016 considering real rainfall event of 174 mm and design storms for return periods of 10, 25, 50 and 100 years. This is done with a view to evaluate effect of LCLU change on surface runoff generation and flooding and to evaluate response/behavior of LCLU types on different type of rain storm.

6. RESULTS AND DISCUSSION

This chapter provides results of LCLU changes, results of runoff and flood simulations and discusses effect of LCLU changes on runoff generation and flood occurrence.

6.1. LCLU classification

Major LCLU types in the study area are forest, paddy, corn, degraded forest and built up/residential area. LCLU maps belong to year 1990, 2000, 2010 and 2016 are shown in figure 6-1.

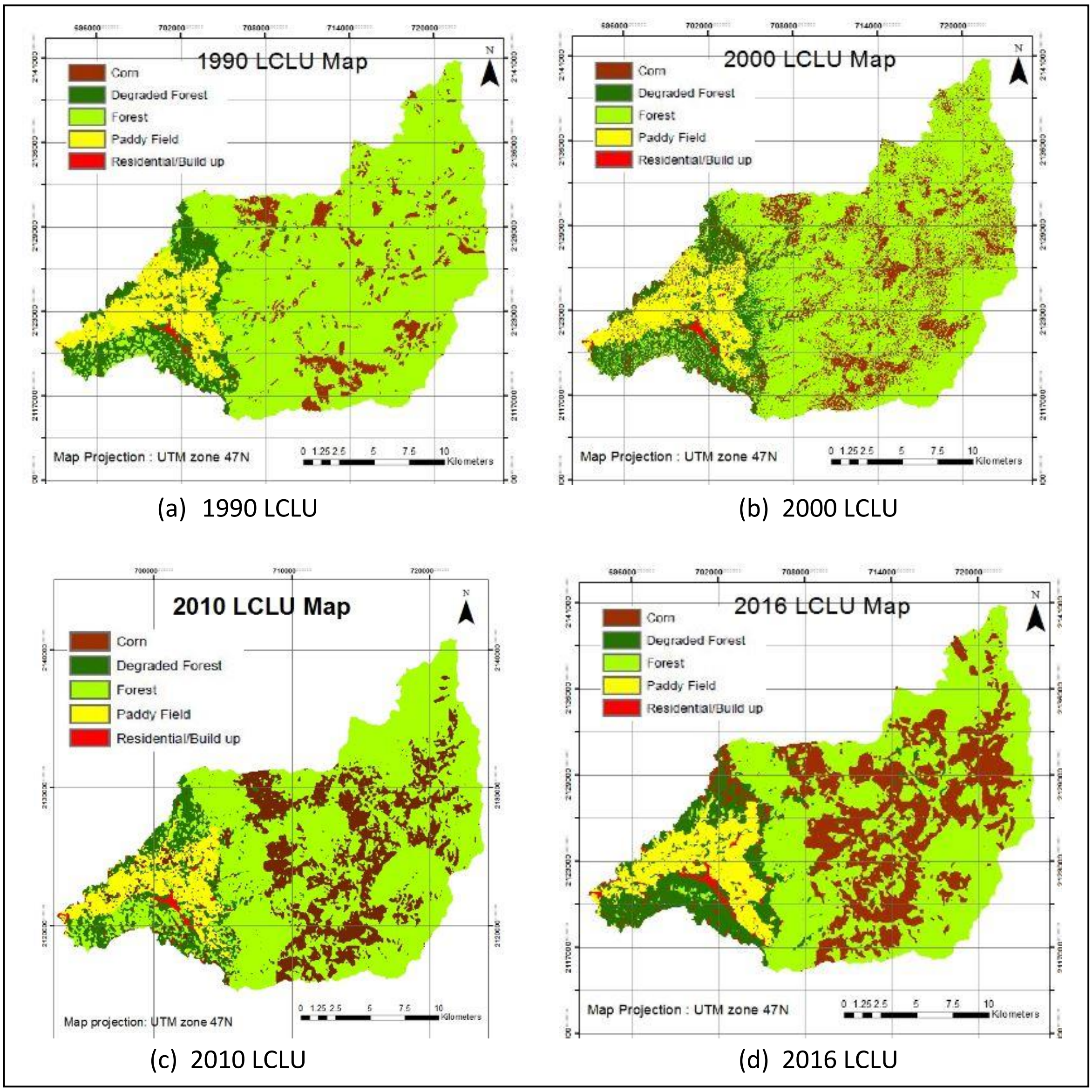

Figure 6-1: LCLU maps for year 1990, 2000, 2010 and 2016.

LCLU classification is performed using supervised classification method and parametric rule used is "Maximum Likelihood Classifier". Overall classification accuracy of 2016, 2010, 2000 and 1990 images are 72.73%, 71.79%, 72.09% and 70.73%. Appendix 1 shows accuracy the accuracy assessment report of Landsat images 2016, 2010, 2000 and 2010.

Table 6-1 displays area in km² belong to each LCLU types in year 1990, 2000, 2010 and 2016.

Table 6-1: Extend of LCLU types in different years

Year	LCLU type/km²				
	Forest(1)	Paddy(2)	Corn(3)	Degraded forest(4)	Built up/residential area(5)
1990	293.76	37.41	34.16	38.00	1.39
2000	254.47	33.80	72.83	41.88	2.05
2010	252.54	29.91	85.77	33.24	2.55
2016	207.56	36.98	108.66	48.00	3.65

LCLU classification results show that dense forest cover exists on hill slopes. Corn cultivation is prominent in hill slopes and it expands in to adjacent slopes. Built up/residential areas are situated in lower catchment. Degraded forest are prominent in lower catchment and dense forest boundaries and hill slope corn cultivations are frequently associated with degraded forests.

6.2. LCLU change

It can be observed that forest cover has gradually decreased from 1990 to 2016. Both corn and built up/residential area have increased gradually within same period. Table 6-1 provides evidence for these changes. Figure 6-1 denotes the areas that have not changed and have changed their LCLU type from 1990 to 2016. Forest cover has reduced by 86.20 km² from 1990 to 2016.For the time period of 6 years from 2010 to 2016, forest cover has reduced by 44.98 km². For time period of 1990 to 2016, corn cover has increased by 74.50km². It could be observed 38.67 km² increment in corn cultivation from 1990 to 2000. For total time frame, built up/residential area has expanded by 2.26 km². Largest expansion of built up/residential area has taken place from 2010 to 2016. It is 1.1 km². Paddy has decreasing trend till 2010 and from there upto 2016 it has increasing trend. For entire time period, paddy has decreased by 0.43 km2. Degraded forest does not have regular change trend throughout time period. From 1990 to 2016, degraded forest has decreased by 10 km². When it is consider the area of LCLU that been subjected to changes, forest, corn and degraded forest have highest values in sequence.

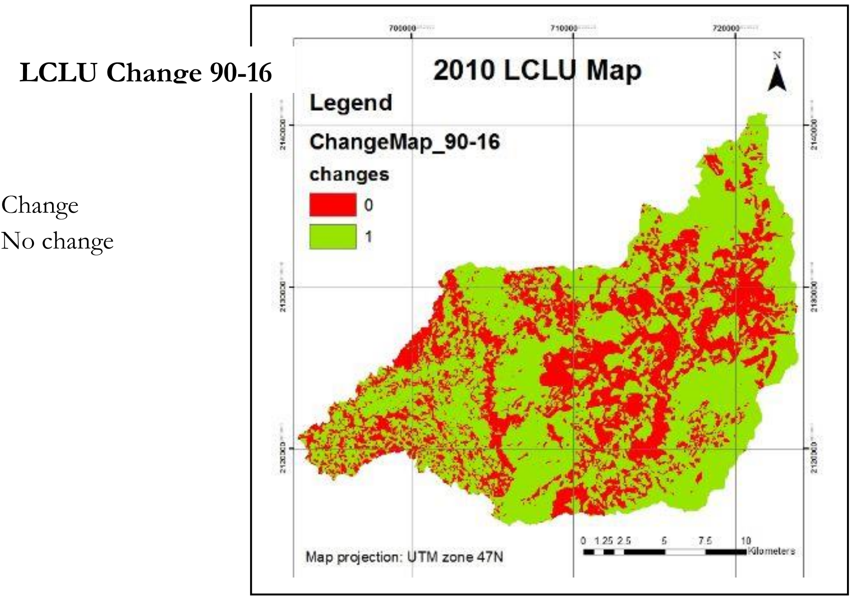

Figure 6-2: Changed and unchanged areas of LCLU 1990-2016

Figure 6-3 given below denotes extend of forest, corn and built up/residential area, degraded forest and paddy in 1990 and 2016.

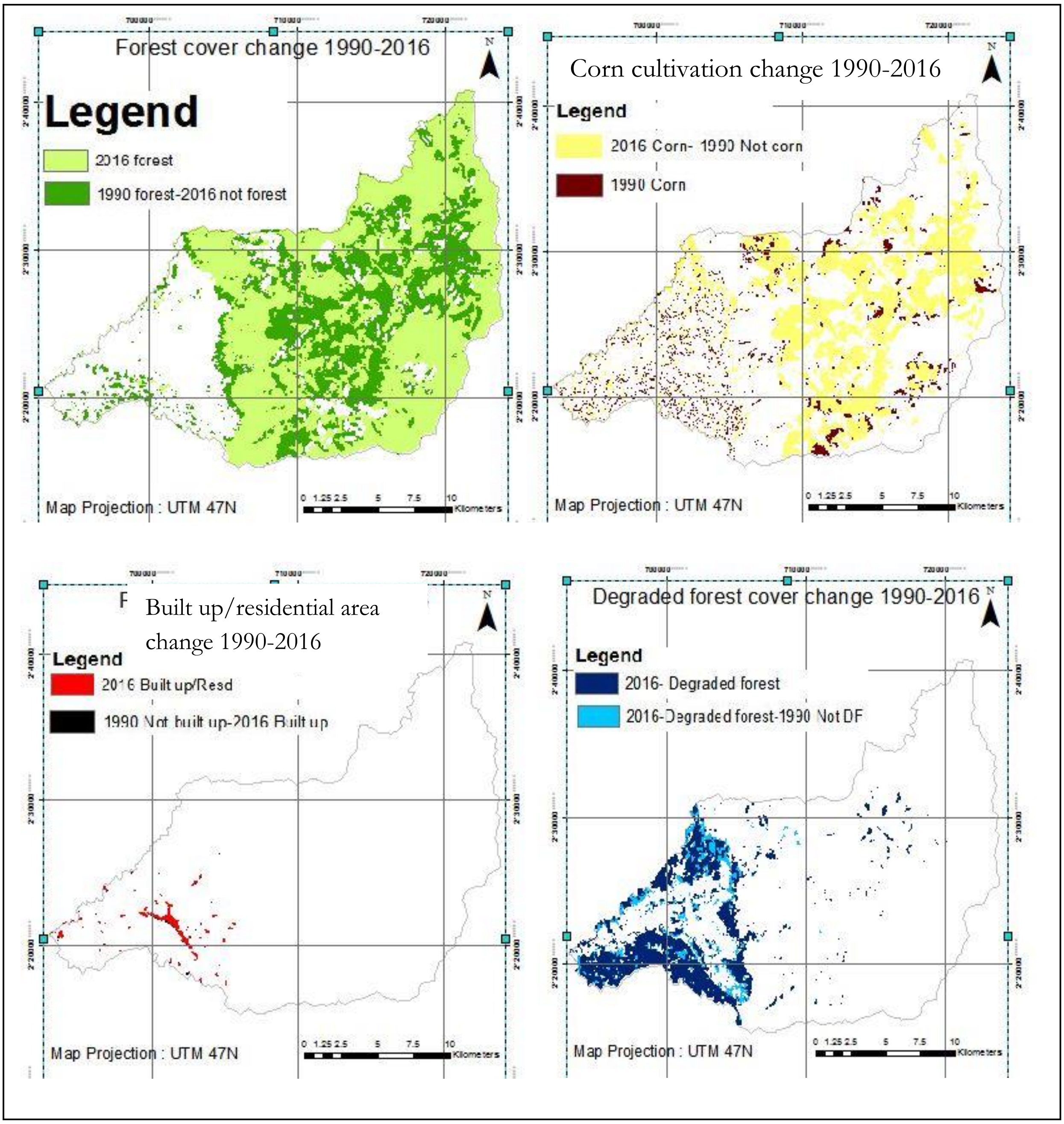

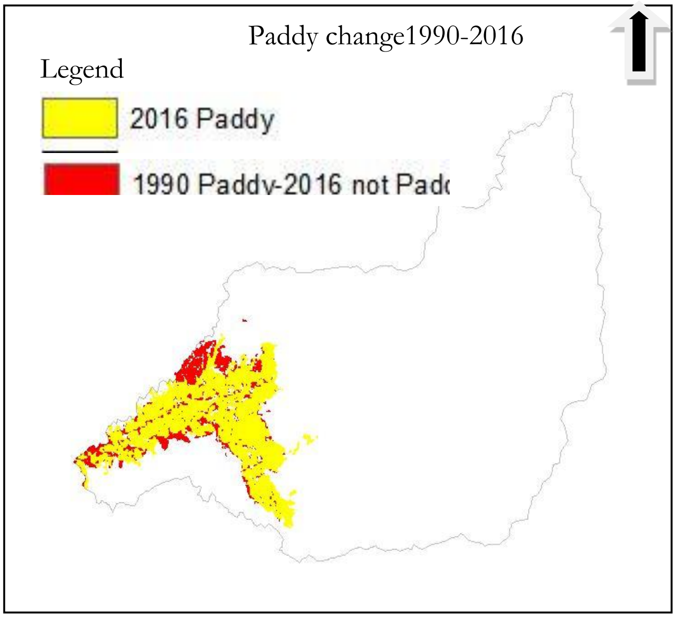

Figure 6-3: Forest, corn and built up/residential area, degraded forest and paddy extend in 1990 and 2016

Major LCLU changes from 1990 to 2016 is as follows. 100.99 km² covered by forest in 1990 have converted to other LCLU types of paddy, corn, degraded forest and built up/residential areas. Among that extend 84.79 km² were changed into corn and 14.85 km² were became to degraded forest by 2016. 8.81 km² of paddy fields have converted to other LCLU types (forest, corn, degraded forest and built up/residential area). Among these changes, paddy fields to degraded forest and paddy to build up/residential area are quite significant and area changed are 7.02 km² and 1.37 km² respectively.12.57 km² and 1.51 km² which were corn in 1990 were converted into forest and degraded forest by 2016 respectively. 6.69 km² and 4.01 km² which had land cover degraded forest have changed their land cover to paddy and corn correspondingly. Table 6-2 given below shows complete details of LCLU changes during period of 1990-2016.

Table 6-2: Change matrix for LCLU 1990-2016

		2016 LCLU/km²						
		Forest	Paddy	Corn	Degraded forest	Built up/ Residential	Total area	Loss
1990 LCLU/km²	Forest	192.63	1.18	84.79	14.85	0.17	293.62	100.99
	Paddy	0.32	28.6	0.1	7.02	1.37	37.41	8.81
	Corn	12.57	0.29	19.74	1.51	0.02	34.13	14.39
	Degraded forest	1.8	6.69	4.01	24.24	1.22	37.96	13.72
	Built up/ Residential	0	0.23	0	0.28	0.88	1.39	0.51
	Total area	207.32	36.99	108.64	47.9	3.66		
	Gain	14.69	8.39	88.9	23.66	2.78		

Appendix 9shows change matrix for 1990-2000, 2000-2010 and 2010-2016. Appendix10 shows few major LCLU change map for time periods of 1990-2000, 2000-2010 and 2010-2016. Change matrixes and change maps gives complete and detail view of LCLU changes within time periods.

Hemwan, (2013) clearly mentions that hill tribe people live in Doi Phu Kha national park area that is upper catchment of Pua watershed have changed their land use patterns in both traditional and recent periods specially in agricultural land use. Hill tribe people deviates from their traditional agricultural land use pattern of nature-based subsistence agriculture such that long-fallow cultivation investing low coast. They are adapting commercial intensive agriculture land use pattern such as short-fallow cultivation or annual crop. Support and guidance form from both government and non-government organizations, introduction of commercial agriculture, high population growth and expansion transport medias effect on this agricultural land use pattern change (Hemwan, 2013). Table 6-2 shows percentage that a certain LCLU type has changed to other LCLU types within given time periods.

Significant forest cover reduction may be due to local people are getting used to commercial intensive agriculture. Due to shortage of suitable land for agriculture, people tend to move to forests. And people know that soil under forest cover is fertile. Major crop that affect forest cover is corn cultivation. Local people use paddy fields also for corn cultivation. It could be observed that paddy fields close to urban areas are been filled for construction purposes. This might be reasons for decrement of paddy field extend from 1990 to 2010. It can be observed expansion of rice paddy from 2010. This might be a result of Thai government new policies to provide stable market price and crop insurance for cultivation (Welcher, 2017). Corn cultivation expands in hill slopes tremendously. This is resulted from facts mention in previous chapter. Forest degradation might be resulted from commercial intensive agriculture expand in to forest cover. Decrement of degraded forest cover from 2000 to 2010 might be a result of reforestation program implemented by government based on 1998 reforestation act (Ongprasert, 2014).

6.3. Design storms

Storms are designed for 10, 25, 50and 100 years return periods. Storm duration is 24 hours. The methodology used for storm design is explained in section 4.3.3 in detail. Rainfall depth for 10, 25, 50 and 100 years return periods are 151.5 mm, 178.5 mm, 199 mm and 219.5 mm respectively . IDF curves for 24 hour duration for A. Muang rain gauge is used for storm design. IDF curve rain gauge location is shown in Figure 6-4. This location is 42 km away from the southern boundary of study area. Design storms are represented in Figure 6-5.

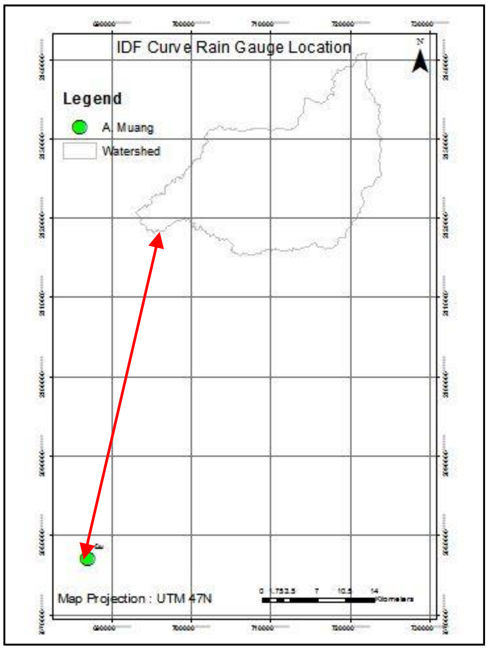

Figure 6-4: Location of IDF curve rain gauge

Pua watershed's elevation from mean sea level ranges from 205m to 1932m. Pua rain gauge and automated rain gauge are situated at lower catchment. Elevation of locations of those 2 rain gauges falls into 236m-249m range. Majority of the catchment consists with steep hill slopes. Due to this topographic undulation there should be a spatial variability of rainfall within the catchment (Grimm et al., 2007; Konrad II, 1996). There is no sufficient rain gauges covering different topographic/terrain units to analyse the orographic effect on rainfall distribution. Because of this reason, rainfall has to be assumed uniform or identical within whole catchment. This would be effected on surface runoff simulations.

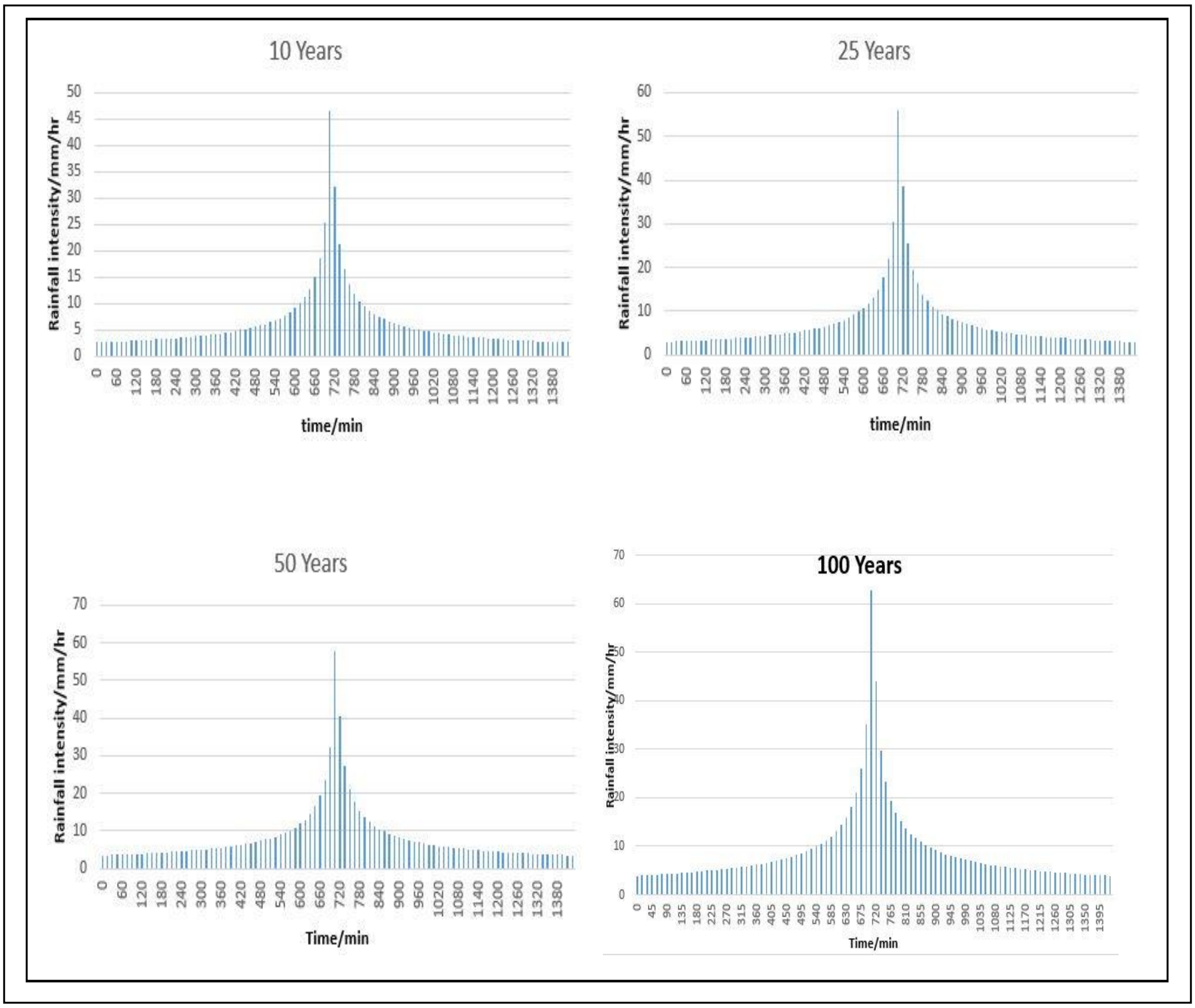

Figure 6-5: Design storms for 10, 25, 50 and 100 year return periods

6.4. Model sensitivity analysis

Reduction of k_{sat} by 10% and 20% rsults in increasing total discharge by 1.9% and 4.8% coresspondingly (Kabeja, 2016). It also increases flood volume by 14.28% and 33.33% respectively. Increment of k_{sat} has negative effect on total discharge and flood volume. Increment of k_{sat} by 10% and 20% rsults in decresing total discharge by 1.4% and 2.5% respectively. It also decreases flood volume by 4.76% and 9.52% coresspondingly. Increment of total discharge with reduction of k_{sat} has higher trend than decrement of total discharge with increment of k_{sat}. Decrement of initial soil moisture content by 10% and 20% result in decreasing total discharge by 0.4% and 0.8% seperately. Increment of initial soil moisture content by 10% and 20% result in increasing total discharge by 0.6% and 1.3% respectively. Increment or recuction of initial soil moisture content by either 10% or 20% do not effect on flood volume. Increment of total discharge with increment of initial soil moisture content has higher trend than decrement of total discharge with decrement of initial soil moisture content. With change of k_{sat} and initial soil moisture content by above mention percentages, flooede area deos not have any effect.

Reduction of porosity by 10% result in increasing total discharge by 50%. It increases flood volume and flood area significantly. Reduction of porosity by 10% increases flood volume by 58.05 times and flood area by 4 times respectively. Increment of porosity by 10% reduces total discharge by 58%. It prevents flooding also. Model sensitivity for porosity is not directly related to poroisity. Model's shown sensitivity for porosity is actually due to fact of "porosity – initial soil moisture content". Figure 6-6 shows hydrographs for model sensitivity analysis. First figure presents discharge for different k_{sat} compared to base data set. Second figure shows discharge for different initial soil moisture contents compared to base data. Third figure shows discharge for different porosities compared to base data.

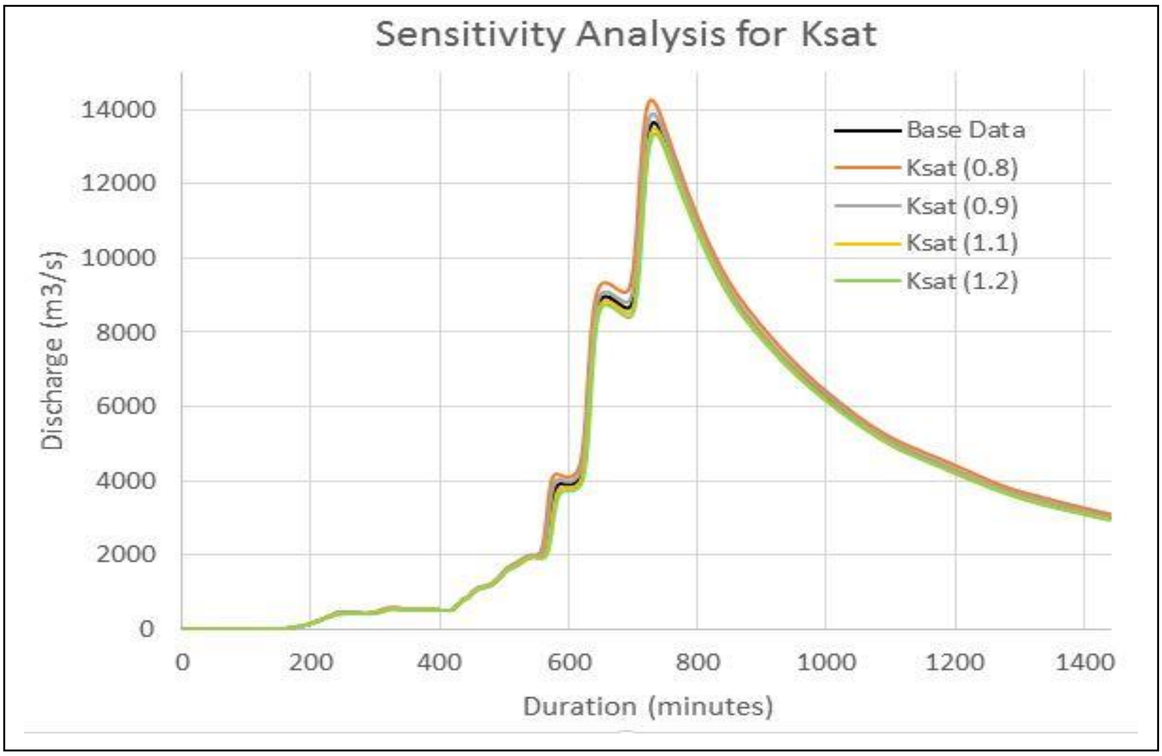

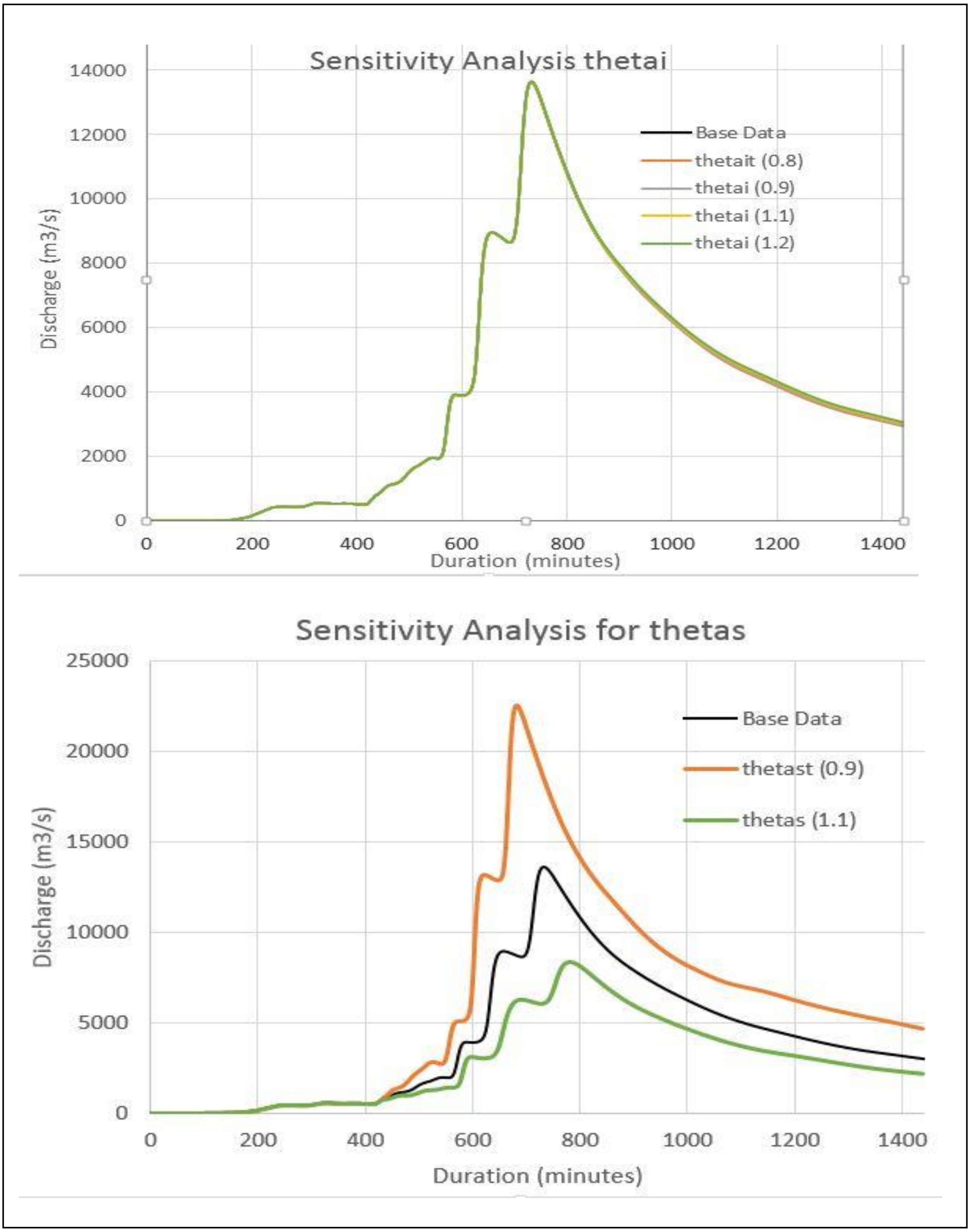

Figure 6-6: Model sensitivity analysis results for different k_{sat}, initial soil moisture content and porosity values

6.5. Surface runoff and Flood simulations

This section covers results of surface runoff generation and flood simulations for different years' LCLU and different storm events. 2016 LCLU map is used as base line map to compare simulation results with other years concern.

6.5.1. Surface runoff generation and flood behaviour on 2016 LCLU map

As first step, 174 mm real rainfall event on 14 and 15 August 2016 is simulated on 2016 LCLU map. It is done to see response of LCLU on surface runoff generation and flood occurrence. Then design storms for return period 10, 25, 50 and 100 are considered for simulations. Objective of this simulations is to observe catchment's response on different return period rainfall events.

174 mm rainfall event results in total discharge of 18322439 $m^{3.}$ 16650558 m^3 and 20960100 m^2 are maximum level flood volume and maximum level flood area respectively. Peak discharge and time for peak discharge at outlet are 441486 l/s and 1462.5 minutes correspondingly. Peak discharge and time for peak discharge at outpoint are 235441.9 l/s and 1304 minutes correspondingly. Appendix11 gives total values of each simulated parameters related to surface runoff and flooding. Flood has occurred at low lying areas. It is clear that paddy fields along stream network effected by flooding. Instead of that valley bottoms associated with stream network at upper catchment is also flooded at few locations. Figure 6-7 maximum flood level values and highest flood level is 7.33 m in this incident. Highest flood levels which is more than 3 m can be observed at certain locations along stream network.

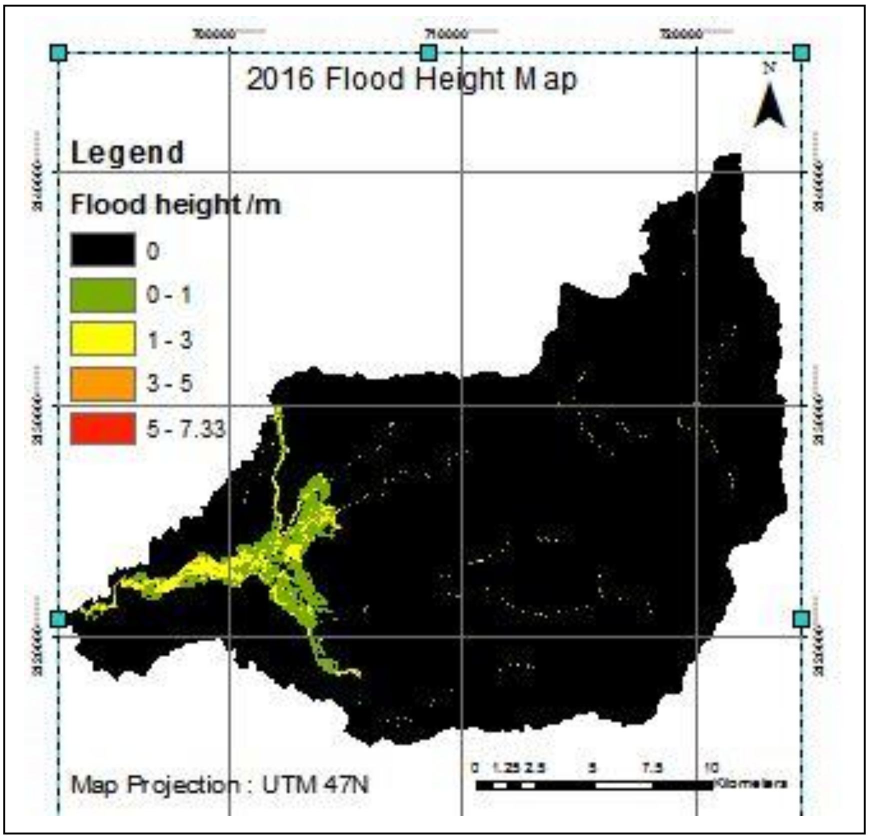

Figure 6-7: 2016 max. Flood level map for 174mm rainfall event

Figure 6-8 shows flood duration map. Highest flood duration is 3399 minutes (56 hours and 39 minutes) in this incident. Low lying areas in lower catchment has flood duration range from 12 to 57 hours. Valley bottoms at upper catchment also have higher flood duration time range from 48 to 57 hours.

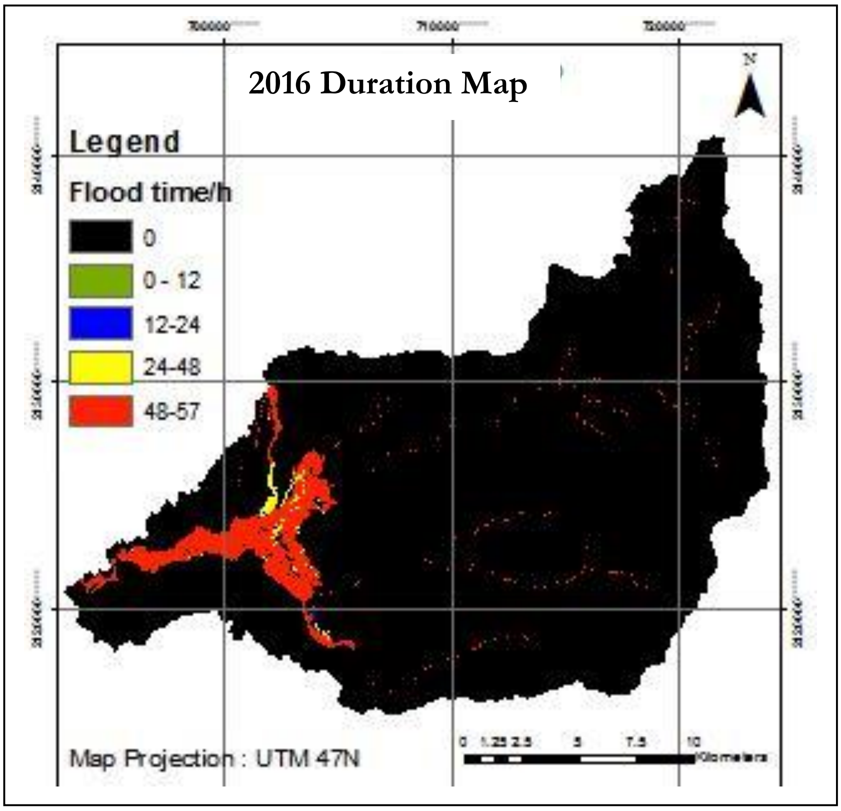

Figure 6-8: 2016 Flood duration map for 174mm rainfall event

Infiltration map provides indirect evidence on surface runoff generation. Since surface storage is relatively very less amount, the rainfall amount does not infiltrate becomes surface runoff. Forest cover shows highest infiltration values range from 75 to 116 mm. It means that forest cover generates lower surface runoff. Paddy fields also shows higher infiltration range from 75 to 100 mm. This is an artificial values caused by assignment of very higher k_{sat} values for paddies. Corn cultivation and degraded forest shows least infiltration values range from 16 to 25 mm. In other words, corn cultivation and degraded forest generates highest surface runoff. Figure 6-9 shows infiltration map for 174 mm rainfall event.

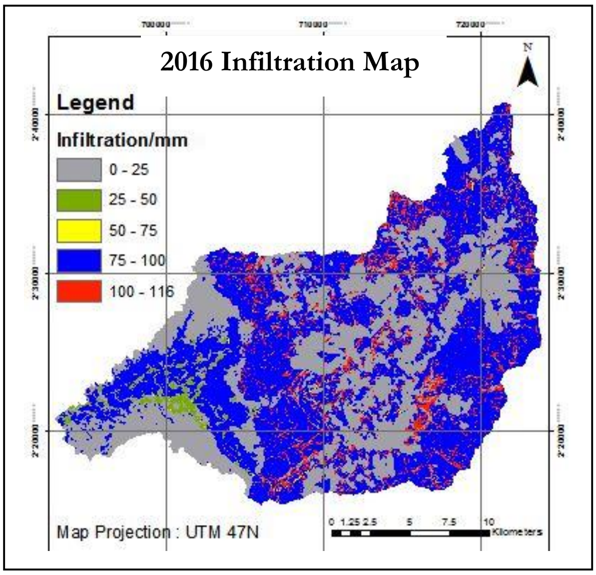

Figure 6-9: 2016 Infiltration map for 174mm rainfall event

Simulation results of few related parameters for 174 mm event and design storms of 10, 25, 50 and 100 years return periods show correlation with rainfall depth. Table 6-3 shows simulation results for these events.

Table 6-3: Simulation results for few hydrological parameters in 174 mm and different return period events for 2016.

Event	Tot dis./ mm	Tot infil. /mm	Wat. in Overland flow/mm	Water in chan. /mm	Tot. dis./m^3	Peak dis./ precip. %	Max. flood vol./m^3	Max flood area /m^2
174 mm	45.28	116.22	6.926	0.8706	18322438	26.02	16650558	20960100
10 Year 151.5 mm	25.02	116.02	3.700	1.5683	10142967	16.66	3652327	9590400
25 Year 178.5 mm	42.33	117.85	10.286	1.9988	17128116	23.87	10354476	16181100
50 Year 199 mm	54.43	118.06	16.490	2.2159	22025404	27.59	16377732	20853000
100 Year 219.5 mm	66.42	118.40	23.590	2.6648	26874461	30.39	23434943	24465600

All parameters: total discharge, total infiltration, water in overland flow, water in channel flow, maximum flood volume and maximum flood area have increasing trend with return period increment. Total infiltration increases in slightly. Infiltration increases with rainfall depth and intensity as a result of surface ponding (Dunne et al., 1991). 100 year return period infiltration has increased by factor of 1.0205 compared to 10 year return period event. Water in overland flow has increased by factor of 6.375 by 100 year return period event. Total discharge, maximum flood volume and maximum flood area have increased by factors of 2.649, 6.416 and 2.551 by 100 year return period event respectively. Figure 6-10 given blow shows flood level and flood duration maps of rainfall events of 10 year and 100 year return periods.

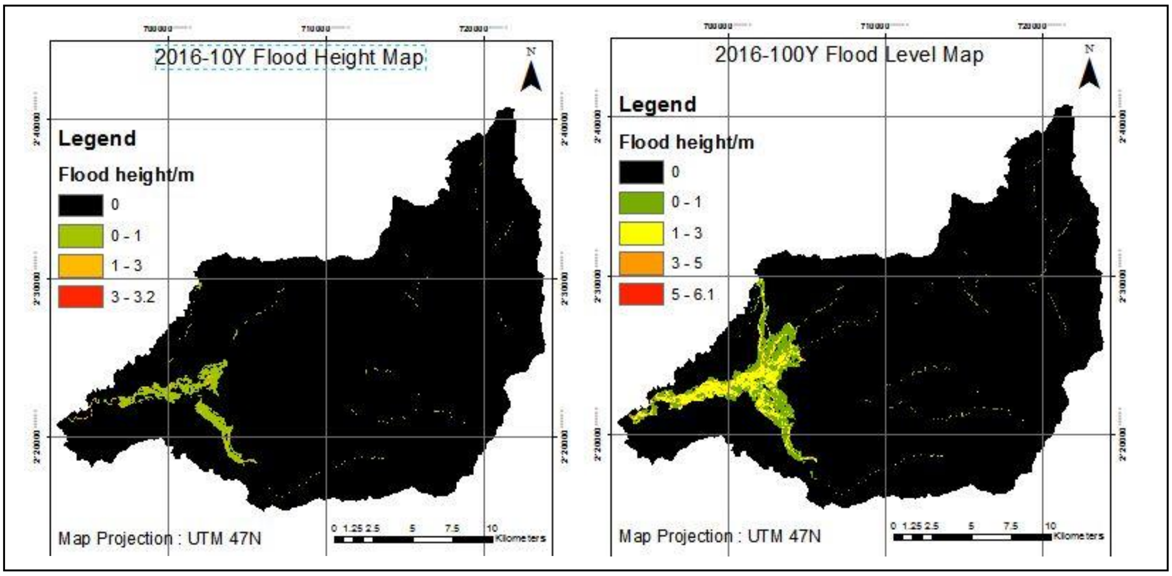

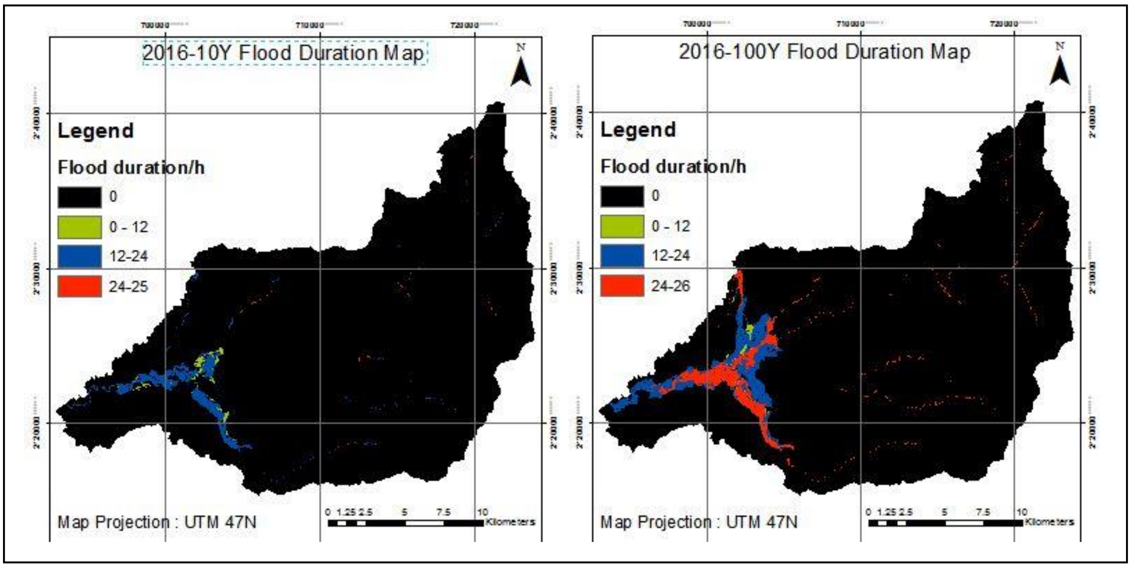

Figure 6-10: Flood height and flood duration maps for 10Y and 100Y return period events of 2016

Figure 6-11 given below shows that hydrograph at catchment outlet. Peak discharge at outlet for 10Y, 25Y, 50Y and 100Y return period events are 247.44 m^3, 345.12 m^3, 417.52 m^3 and 485.48 m^3 respectively. 100Y return period event peak discharge at catchment has increased by factor of 1.962 compared to 10Y return period event.

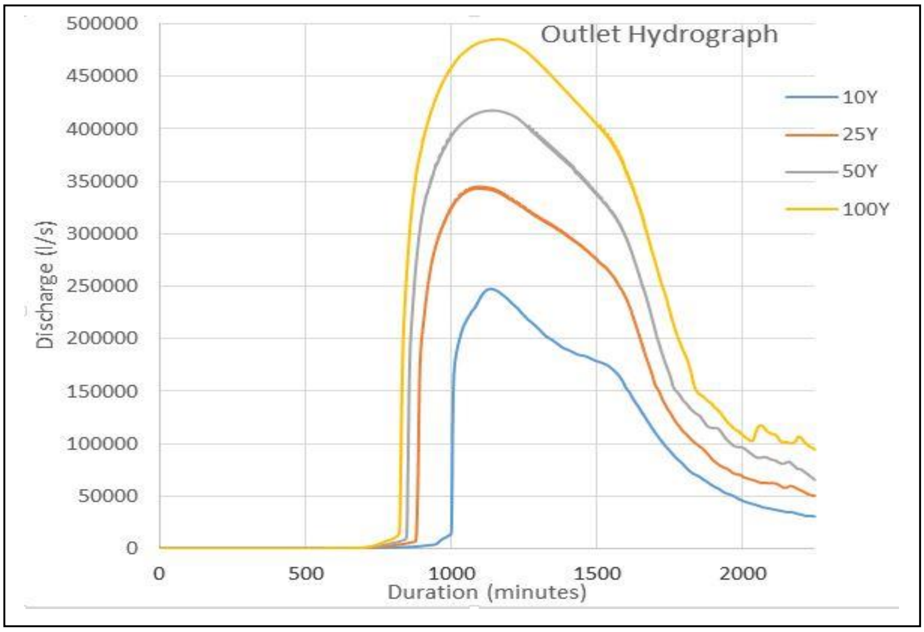

Figure 6-11: Outlet hydrograph for design storms of 10Y, 25Y, 50Y and 100Y return period events 2016

6.5.2. Surface runoff generation and flood behaviour on 1990 LCLU map

1990 LCLU map and NDVI map are introduced to 2016 data base for generation of base maps.As first step, 174 mm real rainfall event on 14 and 15 August 2016 is simulated on 1990 LCLU map. It is done to see response of 1990 LCLU on surface runoff generation and flood occurrence. Then design storms for return period 10, 25, 50 and 100 are considered for simulations. Objective of this simulations is to observe catchment's response on different return period rainfall events as per 1990 LCLU. Comparison of 1990 simulations results with 2016 results might provide effect of LCLU change on surface runoff generation and flood occurrence.

174 mm rainfall event results in total discharge of 20326845 $m^{3.}$ 18507632 m^3 and 19881900 m^2 are maximum level flood volume and maximum level flood area respectively. Peak discharge and time for peak discharge at outlet are 476228.4 l/s and 1473.5minutes correspondingly. Peak discharge and time for peak discharge at outpoint are 255376.2 l/s and 1290 minutes correspondingly. Flood has occurred at low lying areas. It is clear that paddy fields along stream network effected by flooding. Instead of that valley bottoms associated with stream network at upper catchment is also flooded at few locations. Figure 6-12 maximum flood level values and highest flood level is 7.78 m in this incident. Highest flood levels which is more than 3 m can be observed at certain locations along stream network.

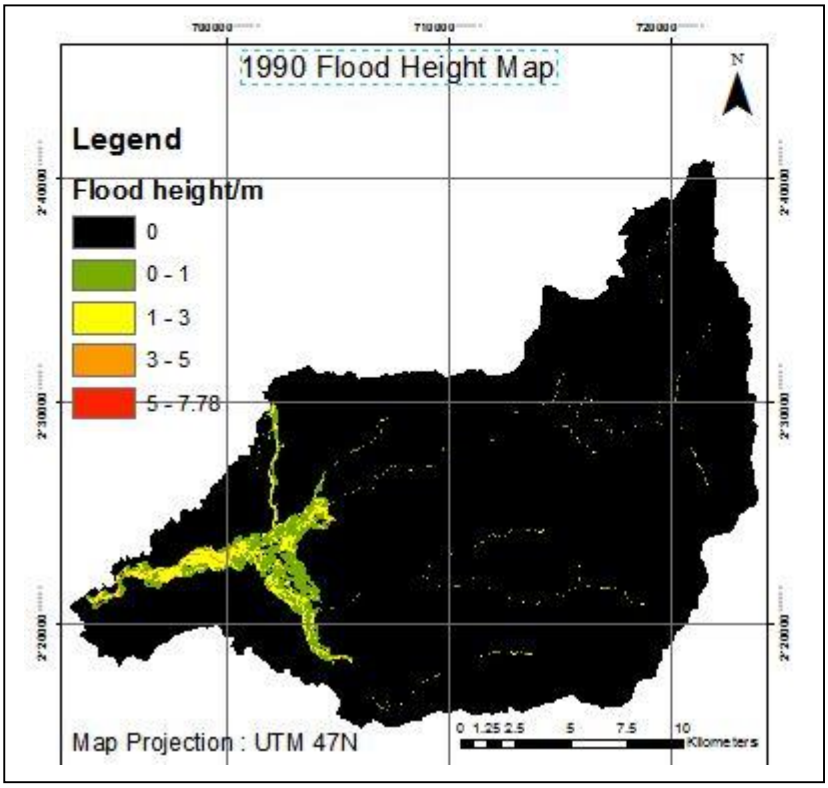

Figure 6-12: 1990 max. Flood level map for 174mm rainfall event

Figure 6-13 shows flood duration map. Highest flood duration is 3689 minutes (61 hours and 29 minutes) in this incident. Low lying areas in lower catchment has flood duration range from 12 to 62 hours. Valley bottoms at upper catchment also have higher flood duration time range from 48 to 62 hours.

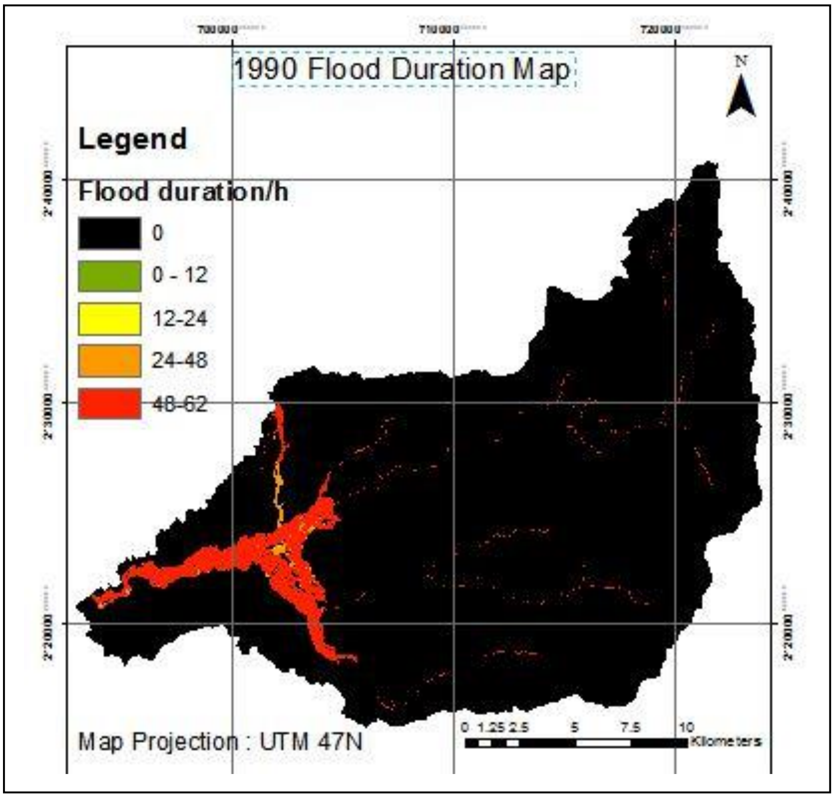

Figure 6-13: 1990 Flood duration map for 174mm rainfall event

Forest cover shows highest infiltration values range from 75 to 112 mm. It means that forest cover generates lower surface runoff. Paddy fields also shows higher infiltration range from 75 to 100 mm. This is an artificial values caused by assignment of very higher k_{sat} values for paddies. Corn cultivation and degraded forest shows least infiltration values range from 19 to 25 mm. In other words, corn cultivation and degraded forest generates highest surface runoff. Figure 6-14 shows infiltration map for 174 mm rainfall event.

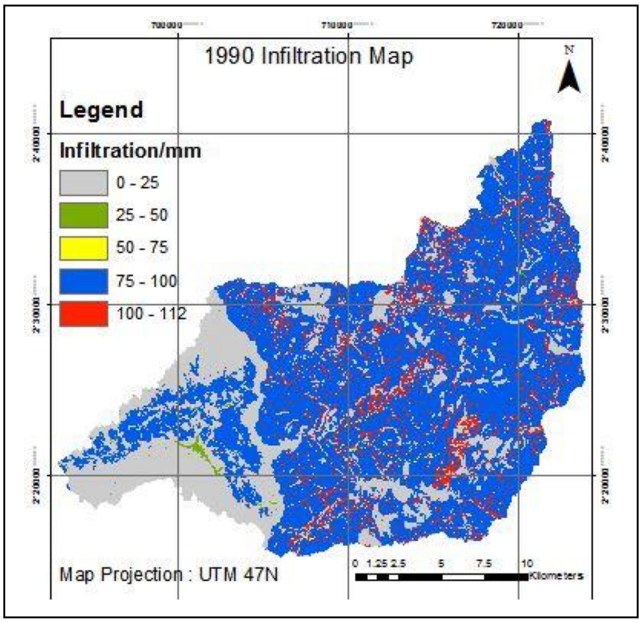

Figure 6-14: 1990 Infiltration map for 174mm rainfall event

Simulation results of few related parameters for 174 mm event and design storms of 10, 25, 50 and 100 years return periods show correlation with rainfall depth. Table 6-4 shows simulation results for these events.

Table 6-4: Simulation results for few hydrological parameters in 174 mm and different return period events for 1990.

Event	Tot dis./ mm	Tot infil. /mm	Wat. in Overland flow/mm	Water in chan. /mm	Tot. dis./m^3	Peak dis./ precip. %	Max. flood vol./m^3	Max flood area /m^2
174 mm	50.23	111.95	6.251	0.8596	20326845	28.87	18507632	19881900
10 Year 151.5 mm	29.84	110.05	3.665	1.8708	12074718	19.84	3804590	7544700
25 Year 178.5 mm	46.19	112.84	10.682	2.1752	18690595	26.04	11243450	16875900
50 Year 199 mm	57.37	114.77	16.066	2.5895	23212834	29.07	16609370	19935000
100 Year 219.5 mm	69.19	117.17	23.590	2.8824	27998953	31.66	22795035	23193000

All parameters: total discharge, total infiltration, water in overland flow, water in channel flow, maximum flood volume and maximum flood area have increasing trend with return period increment. Total infiltration increases in slightly. Infiltration increases with rainfall depth and intensity as a result of surface ponding (Dunne et al., 1991). 100 year return period infiltration has increased by factor of 1.0647 compared to 10 year return period event. Water in overland flow has increased by factor of 6.346 by 100 year return period event. Total discharge, maximum flood volume and maximum flood area have increased by factors of 2.319, 5.991 and 3.074 by 100 year return period event respectively. Figure 6-15 given blow shows flood level and flood duration maps of rainfall events of 10 year and 100 year return periods.

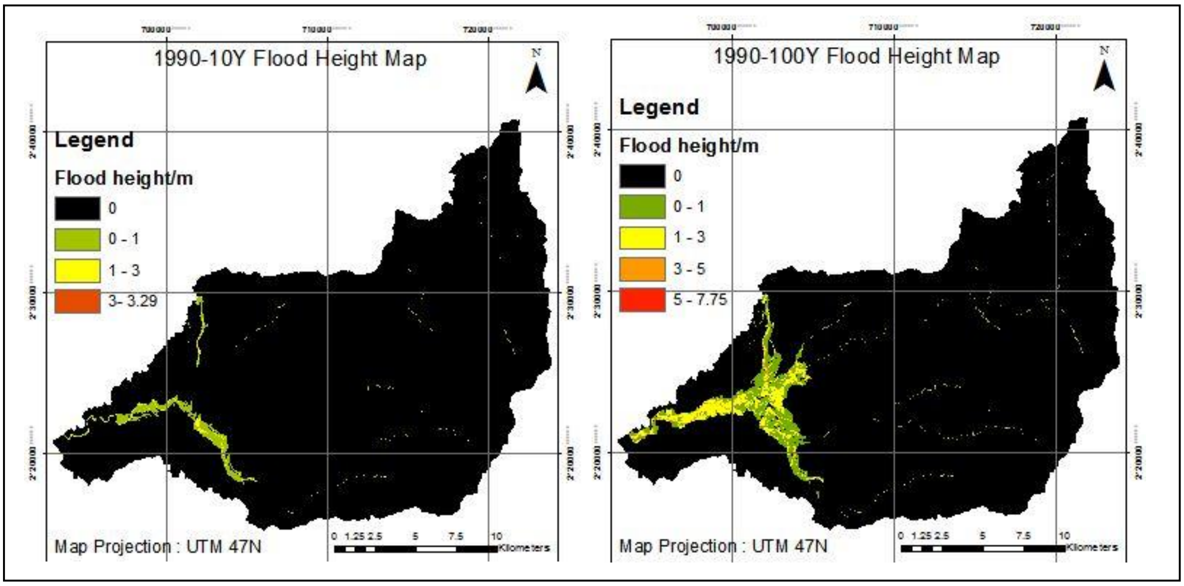

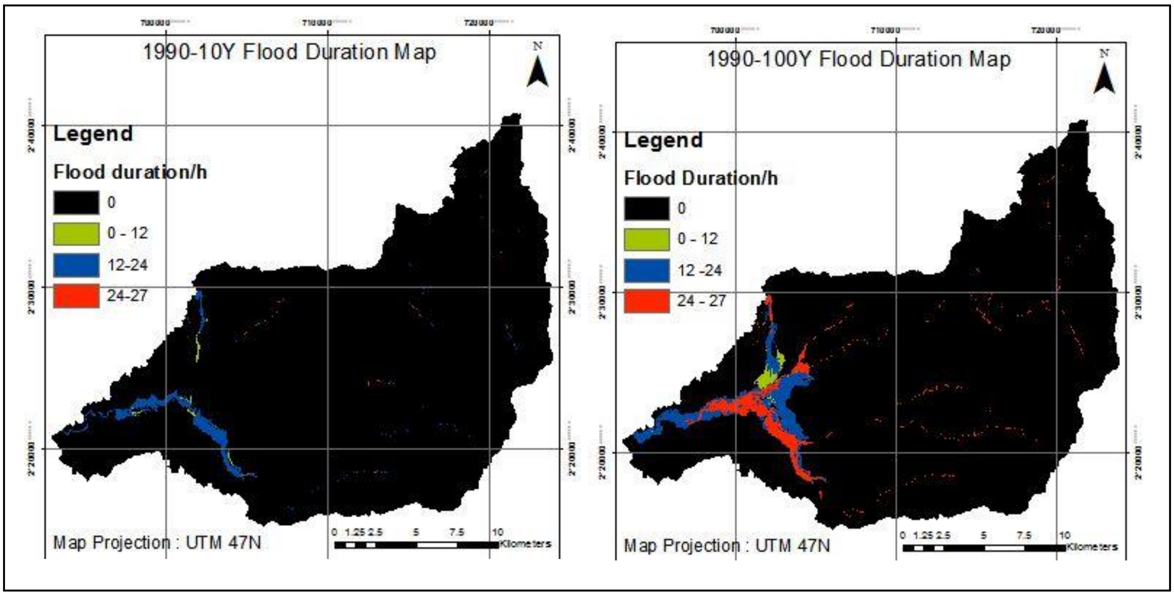

Figure 6-15: Flood height and flood duration maps for 10Y and 100Y return period events for 1990

Figure 6-16 given below shows that hydrograph at catchment outlet. Peak discharge at outlet for 10Y, 25Y, 50Y and 100Y return period events are 260.92 m^3, 375.76 m^3, 444.31 m^3 and 501.57 m^3 respectively. 100Y return period event peak discharge at catchment has increased by factor of 1.922 compared to 10Y return period event.

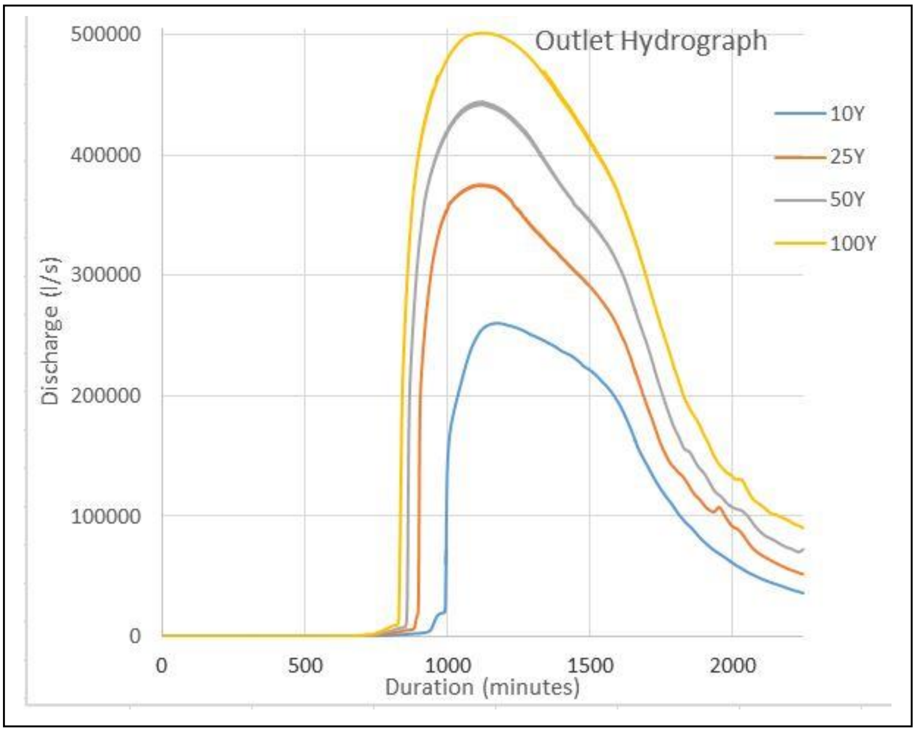

Figure 6-16: Outlet hydrograph for design storms of 10Y, 25Y, 50Y and 100Y return period events 1990

6.5.3. Effect of LCLU change in runoff generation and flood occurrence in 1990 and 2016

Effect of LCLU change on surface runoff generation and flood occurrence is done based on 2016 and 1990 LCLU maps.174 mm rainfall event is selected since it is a natural event. Table 6-5 shows values of relevant hydrological parameters to evaluate effect of LCLU change.

Table 6-5: Simulation results for 2016 and 1990 for 174 mm rainfall event.

Parameter	1990	2016
Total discharge (mm)	50.23	45.28
Total interception (mm)	1.8553	1.8452
Total house interception (mm)	0.0021	0.0109
Total infiltration (mm)	111.95	116.23
Surface storage (mm)	0.1657	0.1510
Water in overland flow (mm)	6.2508	6.9260
Water in channel flow (mm)	0.8596	0.8707
Total discharge (m3)	20326845	18322439
Peak discharge/Precipitation (%)	28.87	26.02
Flood volume (max level) (m3)	18507632	16650558
Flood area (max level) (m2)	19881900	20960100

Even there has been significant loss of forest cover (86.20 km^2) and significant expansion of corn cultivation (74.5 km^2) in hill slopes form 1990 to 2016, surface runoff generation and flood occurrence has reduced by 2016 compared to 1990. Total interception has reduced by factor of 0.99 by 2016. This might be resulted from reduction of forest cover as well as degraded forest cover by 2016. Increment of total house interception by factor of 5.19 by 2016 reflects expansion of built up/residential area within the catchment. Total infiltration has increased by factor of 1.03 by 2016. Average ksat values for different LCLU types (forest-109.94 mm/h, paddy-9.32 mm/h but assigned to 100000, corn-78.11 mm/h, degraded forest-80.48 mm/h and built up/residential area-48.85 mm/h) do not have significant variation. This might be reason for increment of infiltration even forest cover has decreased. Overland flow has increased by factor of 1.11 by 2016. Channel flow has also increased by factor of 1.01 by 2016. This slight increment in overland flow/surface runoff is capable of increasing flood extend by factor of 1.05. But it has decreased flood volume by factor of 0.9 by 2016. Total discharge has decreased by factor of 0.9 by 2016. Increment of overland does not reflect effect of forest cover reduction. Previous studies has shown that clearance of forest cover causes in increasing runoff significantly (Siriwardena et al., 2006). Effect of LCLU change on surface runoff generation and flood occurrence might be hindered by higher and relatively close k_{sat} values of different LCLU types. LCLU changes on hilltops and upper slopes would not affect stream significantly. Previous studies show that runoff generation at hilltops and upper slopes may not reach to streams. It is controlled by slope length and topography of area. Place where LCLU changes have taken place is important fact for flood occurrence. Reduction of forest cover and expansion of corn cultivation at hilltops and upper slope areas in the catchment would not have significant effect on flood occurrence. Hydrograph shows that peak discharge at outlet has increased and time to peak discharge has decreased by 2016. Figure 6-17 behaviour of discharge at outlet on 1990 and 2016 LCLU.

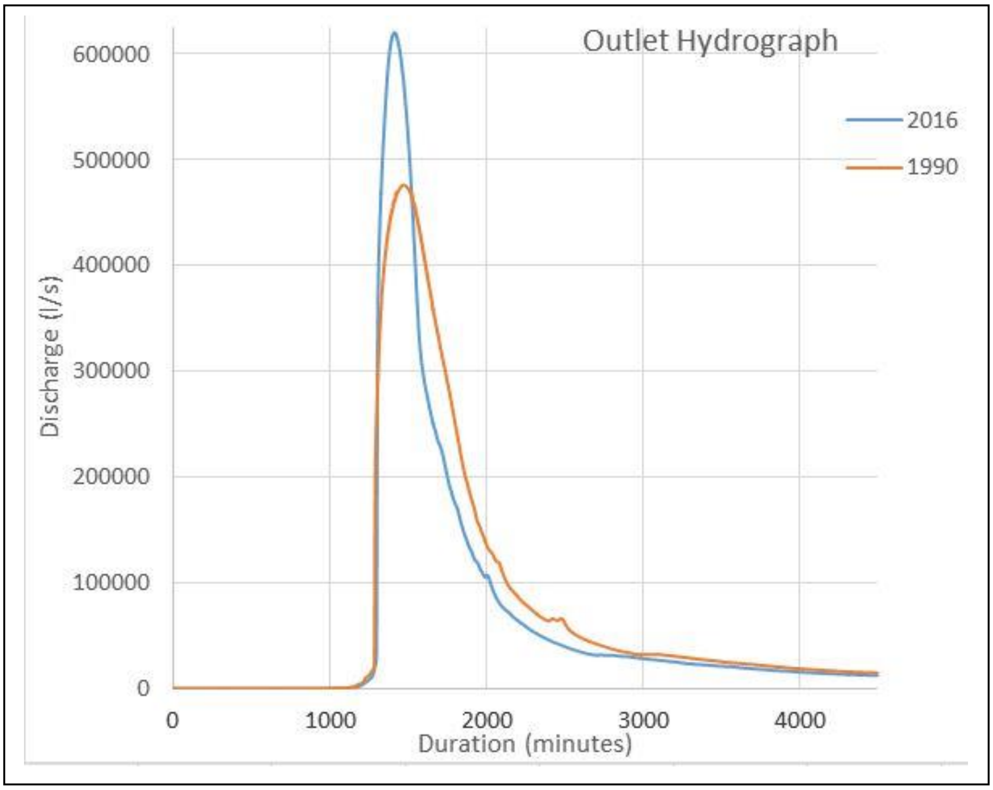

Figure 6-17: 174 mm event outlet hydrograph for 1990 and 2016 LCLU.

6.5.4. Runoff generation and flood occurrence on 2000 and 2010 LCLU for design storms

Surface runoff and flood simulations for 2000 and 2010 is done on design storms of 10, 25, 50 and 100 year return periods. Due to time constraint, 174 mm event could not be simulated. Simulated results could not be analysed in detail. Simulated hydrograph of 2000 shows that peak discharge and time to peak discharge is increased with return periods. 2010 hydrograph also has same trend. 100Y return period in 2000 has slightly higher peak discharge compared to 2010. Figure 6-18 shows simulated hydrograph for 2000 and 2010 for design storms of return period 10Y, 25Y, 50Y and 100Y.

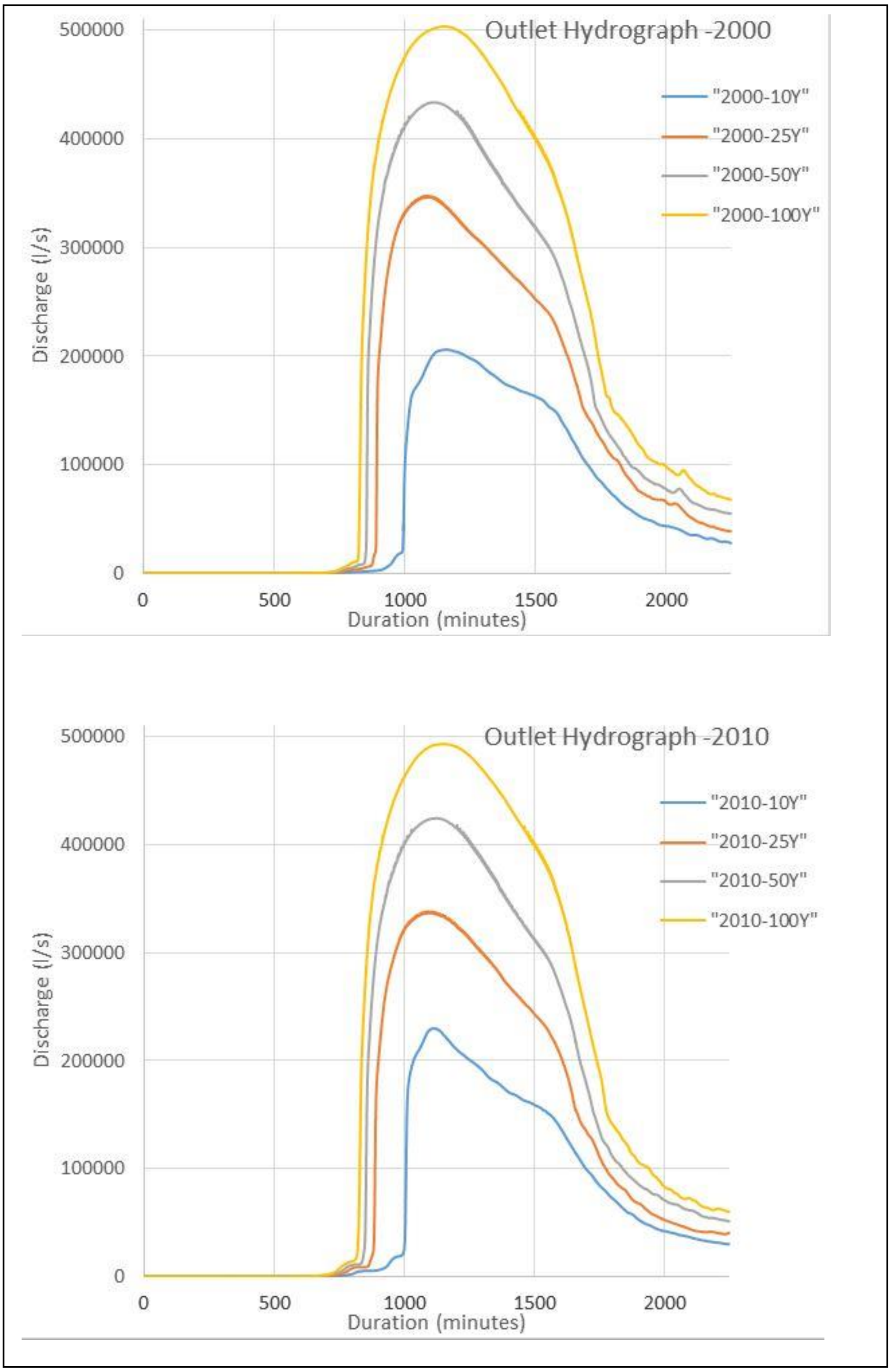

Figure 6-18: simulated hydrograph for 2000 and 2010 for design storms of return period 10Y, 25Y, 50Y and 100Y

7. CONCLUSION AND RECOMMENDATION

7.1. Conclusion

Dense forest cover in Pua watershed has gradually decreased from 1990 to 2016. Corn cultivation has also increased throughout the time period gradually. Build up/residential area has same trend in time period. Paddy cover and degraded forest cover have increased by time period of 1990 to 2016. Dense forest and corn cultivation have changed significantly. This is due to government and non-government organisations support and guidance for commercial intensive agriculture, expansion of transport media good market for agricultural products.

Forest cover has highest infiltration among other LCLU types. It means that forest cover generates low surface runoff. On the other hand corn and degraded forest have how infiltration values and as a consequence those LCLU types generates higher surface runoff.

Simulation results does not reflects expected outcome of LCLU changes. This might be resulted from higher k_{sat} values of LCLU types and relatively close k_{sat} values for different LCLU types. Spatial location of forest cover reduction and corn cultivation expansion might be another reason to have low flood values.

Initial catchment conditions are critical in runoff generation and flood generation. Original data base gives very low discharge at outpoint compared to measured discharge. But 2 times initial soil moisture content is capable of providing comparable simulations for discharge. Initial soil moisture content controls amount of rainfall infiltrated. Higher initial soil moisture content decreases infiltration. As a consequence surface runoff increases.

Detail soil map with required physical parameters might have considerable influence on simulation results.

The model OpenLISEM is highly sensitive to k_{sat} in this study area. Model is relatively less sensitive to initial soil moisture content.

The model OpenLISEM's simulation results for short time durations are more realistic compared to long time simulations. Further studies is necessary for evaluate the effect of simulation time on results.

OpenLISEM's efficiency in simulation of runoff generation and flood occurrence in large catchment is quite low due to higher computation time. It has issues in model calibration due to spatial variability of k_{sat} within large catchments (Baartman et al., 2012).

7.2. Recommendation

Based on results of this study following recommendations can be made.

- Protection and conservation of forest cover would have effect on control of generation of runoff and occurrence of flood at low lying area. Since forest cover is decreased gradually, necessary actions should be taken to protect and to conserve forest cover.

- Steep slopes in upper catchment should be prevented from corn cultivation and agricultural use with a view to reduce runoff generation and to improve soil properties.
- Further studies with full data base (litter interception, fraction of compacted surface, hard surface, rain water storage, surface crust, detail soil map and channel base flow) is recommended to further understand of runoff generation and flood behaviour.
- Spatial distribution of LCLU should be taken into account for get an complete view on flood occurrence in Pua watershed.

7.3. Limitations

- High spatial resolution DEM could not be used due to large catchment size.
- Orographic effect (upper catchment consists with elevated steep slopes) of rainfall could not be incorporated in to simulations due to lack of rainfall data.
- Due to practical matters soil samples and training samples could not be collected covering whole catchment.
- Stream water level data could not be used to model validation and calibration due to unavailability of base flow data

LIST OF REFERENCES

ALJAZEERA. (2017). Flash floods kill 18 in southern Thailand | Thailand News | Al Jazeera. Retrieved January 28, 2017, from http://www.aljazeera.com/news/2017/01/floods-kill-12-southern-provinces-170107070104231.html

Asfaha, T. G., Frankl, A., Haile, M., Zenebe, A., & Nyssen, J. (2015). Determinants of peak discharge in steep mountain catchments – Case of the Rift Valley escarpment of Northern Ethiopia. *Journal of Hydrology*, *529*, 1725–1739. http://doi.org/10.1016/j.jhydrol.2015.08.013

Azmeri, Hadihardaja, I. K., & Vadiya, R. (2016). Identification of flash flood hazard zones in mountainous small watershed of Aceh Besar Regency, Aceh Province, Indonesia. *The Egyptian Journal of Remote Sensing and Space Science*, *19*(1), 143–160. http://doi.org/10.1016/j.ejrs.2015.11.001

Baartman, J. E. M., Jetten, V. G., Ritsema, C. J., & de Vente, J. (2012). Exploring effects of rainfall intensity and duration on soil erosion at the catchment scale using openLISEM: Prado catchment, SE Spain. *Hydrological Processes*, *26*(7), 1034–1049. http://doi.org/10.1002/hyp.8196

Badreldin, N., & Goossens, R. (2014). Monitoring land use/land cover change using multi-temporal Landsat satellite images in an arid environment: a case study of El-Arish, Egypt. *Arabian Journal of Geosciences*, *7*(5), 1671–1681. http://doi.org/10.1007/s12517-013-0916-3

Beilicci, E., & Beilicci, R. (2015). FLASH FLOODS - CAUSES, EFFECTS, POSSIBILITIES OF MODELLING WITH HYDROINFORMATIC TOOLS. *WATER RESOURCES, FOREST, MARINE AND OCEAN ECOSYSTEMS*, *I*, 309–316. http://doi.org/978-619-7105-36-0

Beven, K. (2012a). *Rainfall-Runoff Modelling. Rainfall-Runoff Modelling: The Primer: Second Edition* (2nd ed.). Chichester, UK: John Wiley & Sons, Ltd. http://doi.org/10.1002/9781119951001

Beven, K. (2012b). Rainfall-Runoff Modelling The Primer SECOND EDITION Library of Congress Cataloging-in-Publication Data.

Billi, P., Alemu, Y. T., & Ciampalini, R. (2014). Increased frequency of flash floods in Dire Dawa, Ethiopia: Change in rainfall intensity or human impact? *Natural Hazards*, *76*(2), 1373–1394. http://doi.org/10.1007/s11069-014-1554-0

Blöschl, G., Gaál, L., Hall, J., Kiss, A., Komma, J., Nester, T., … Viglione, A. (2015). Increasing river floods: fiction or reality? *Wiley Interdisciplinary Reviews: Water*, *2*(4), 329–344. http://doi.org/10.1002/wat2.1079

Bryndal, T. (2014). A METHOD FOR IDENTIFICATION OF SMALL CARPATHIAN CATCHMENTS MORE PRONE TO FLASH FLOOD GENERATION . BASED ON THE EXAMPLE OF SOUTH - EASTERN PART OF THE POLISH CARPATHIANS. *Carpathian Journal of Earth and Environmental Sciences*, *9*(3), 109–122.

Caballero, R., Cantón, Y., Chamizo, S., Afana, A., & Albert, S. S. (2012). Effects of biological soil crusts on surface roughness and implications for runoff and erosion. *Geomorphology*, *145–146*, 81–89. http://doi.org/10.1016/j.geomorph.2011.12.042

Cantón, Y., Solé-Benet, A., & Lázaro, R. (2003). Soil–geomorphology relations in gypsiferous materials of the Tabernas Desert (Almería, SE Spain). *Geoderma*, *115*(3–4), 193–222. http://doi.org/10.1016/S0016-7061(03)00012-0

Canty, J. M. (2014). *Image Analysis, Classification and Change Detection in Remote Sensing: With ... - Morton J. Canty - Google Books* (3rd ed.). CRC Press. Retrieved from https://books.google.nl/books?hl=en&lr=&id=fGDOBQAAQBAJ&oi=fnd&pg=PP1&dq=majority+filtering&ots=xvMKgkIcB4&sig=3FYZL5fRMVaj-RAmd-ViGn_OIsc#v=onepage&q=majority filtering&f=false

Carter, M. R., & Gregorich, E. G. (2014). *Soil Sampling and Methods of Analysis* (2nd ed.). Retrieved from https://books.google.nl/books?hl=en&lr=&id=ZTJsbXsikagC&oi=fnd&pg=PA1&dq=purposive+sampling+method+for+soil+samples&ots=VeHAtP0YN2&sig=s3nC-1EUT5_k2ESwGLRNdcEyUnA#v=onepage&q&f=false

CGIAR. (2012). Thailand - Ricepedia. Retrieved May 11, 2017, from http://ricepedia.org/thailand

Chaudhari, P. R., Ahire, D. V., Ahire, V. D., Chkravarty, M., & Maity, S. (2013). Soil Bulk Density as related to Soil Texture, Organic Matter Content and available total Nutrients of Coimbatore Soil. *International Journal of Scientific and Research Publications*, *3*(1), 2250–3153. Retrieved from www.ijsrp.org

Chow. (1959). Manning's n Values. Retrieved from file:///C:/DeskTop1216/Manning's n Values.html
Chow, V., Maidment, D., & Mays, L. (1988). *Design storms. Applied Hydrology, vol. 14*. Retrieved from https://scholar.google.com/scholar?hl=en&q=V.T.+Chow%2C+D.R.+Maidment%2C+L.W.+Mays++Design+storms.+Applied+HydrologyMcGraw-Hill%2C+New+York+%281988%29+%28chap.+14%2C+pp.+444–492%29&btnG=&as_sdt=1%2C5&as_sdtp=
Chow, V. Te, Maidment, D. R., & Mays, L. W. (1988). *Applied hydrology. McGraw-Hill Series in Water Resources and Environmental Engineering*. McGraw-Hill. Retrieved from http://documentatiecentrum.watlab.be/imis.php?module=ref&refid=127685&basketaction=add
Chuenchooklin, S. (2012). Streamflow Modeling for a Small Watershed using Limited Hydrological Data. *International Journal of Environmental,Chemical,Ecological, and Geophysical Engineering*, *6*(10), 868–872.
Chuenchooklin, S., & Pangnakorn, U. (2015). Flood Management Tool for Small Catchment in the Nan River Basin, Thailand. *Journal of Applied Sciences Research*, *11*(21), 1–6.
Chuenchooklin, S., Taweepong, S., & Pangnakorn, U. (2015). Rainfall-Runoff Models and Flood Mapping in a Catchment of the Upper Nan Basin,Thailand. *Journal of Water Resource and Hydraulic Engineering*, *4*(3), 293–302. http://doi.org/10.5963/JWRHE0403012
Climatological Center. (2011). *Natural Disasters 2011*.
Damen, M., & Krol, B. (2015). Geomorphic Image Analysis Selected qualitative and (semi)quantitative methods. Retrieved from https://blackboard.utwente.nl/bbcswebdav/pid-903622-dt-content-rid-1873662_2/courses/M15-AES-117/aes2015_Reader_Geomorphic Image Analysis.pdf
Davies R. (2016). Fitch Ratings Estimate German Flood Claims at €1 Billion - FloodList. Retrieved January 28, 2017, from http://floodlist.com/europe/fitch-ratings-estimate-german-flood-claims-e1-billion
De Roo, A. P. ., & Jetten, V. . (1999). Calibrating and validating the LISEM model for two data sets from the Netherlands and South Africa. *CATENA*, *37*(3), 477–493. http://doi.org/10.1016/S0341-8162(99)00034-X
Deasy, C., Titman, A., & Quinton, J. N. (2014). Measurement of flood peak effects as a result of soil and land management, with focus on experimental issues and scale. *Journal of Environmental Management*, *132*, 304–312. http://doi.org/10.1016/j.jenvman.2013.11.027
Dehotin, J., Breil, P., Braud, I., de Lavenne, A., Lagouy, M., & Sarrazin, B. (2015). Detecting surface runoff location in a small catchment using distributed and simple observation method. *Journal of Hydrology*, *525*, 113–129. http://doi.org/10.1016/j.jhydrol.2015.02.051
Department of Mineral Resources. (2016). geology of Thailand. Retrieved January 13, 2017, from http://www.dmr.go.th/main.php?filename=GeoThai_En
Deursen, W. van. (1995). Geographical Information Systems and Dynamic Models Development and application of a prototype spatial modelling language WPA van Deursen. Retrieved January 8, 2017, from http://pcraster.geo.uu.nl/wp-content/uploads/2011/03/thesisWvanDeursen.pdf
Dodrico, P., & Porporato, A. (2006). *Dryland Ecohydrology - Google Boeken*. Springer. Retrieved from https://books.google.nl/books?id=OIK1siSsBpMC&pg=PA35&lpg=PA35&dq=saturation+excess+runoff&source=bl&ots=6Iz8ulgbBG&sig=muZvfZhY94ZmMR4TaJvVHdir9WE&hl=nl&sa=X&ved=0ahUKEwjGgv77yejRAhWGPRoKHW5qC1sQ6AEIVDAF#v=onepage&q=saturation excess runoff&f=false
Dunne, T., Zhang, W., & Aubry, B. F. (1991). Effects of Rainfall, Vegetation, and Microtopography on Infiltration and Runoff. *Water Resources Research*, *27*(9), 2271–2285. http://doi.org/10.1029/91WR01585
El-Hattab, M. M. (2016). Applying post classification change detection technique to monitor an Egyptian coastal zone (Abu Qir Bay). *The Egyptian Journal of Remote Sensing and Space Science*, *19*(1), 23–36. http://doi.org/10.1016/j.ejrs.2016.02.002
El Kateb, H., Zhang, H., Zhang, P., & Mosandl, R. (2013). Soil erosion and surface runoff on different vegetation covers and slope gradients: A field experiment in Southern Shaanxi Province, China. *CATENA*, *105*, 1–10. http://doi.org/10.1016/j.catena.2012.12.012
Esri. (2016). Resampling Method (Environment setting)—Help | ArcGIS for Desktop. Retrieved April 20, 2017, from http://desktop.arcgis.com/en/arcmap/10.3/tools/environments/resampling-method.htm
Fang, N.-F., Shi, Z.-H., Li, L., Guo, Z.-L., Liu, Q.-J., & Ai, L. (2012). The effects of rainfall regimes and

land use changes on runoff and soil loss in a small mountainous watershed. *CATENA*, *99*, 1–8. http://doi.org/10.1016/j.catena.2012.07.004

Flood Archives. (2007). 2006 Global Register of Major Flood Events. Retrieved December 25, 2016, from http://www.dartmouth.edu/~floods/Archives/2006sum.htm

Gale, E. L., & Saunders, M. A. (2013). The 2011 Thailand flood: Climate causes and return periods. *Weather*, *68*(9), 233–237. http://doi.org/10.1002/wea.2133

Genxu, W., Guangsheng, L., & Chunjie, L. (2012). Effects of changes in alpine grassland vegetation cover on hillslope hydrological processes in a permafrost watershed. *Journal of Hydrology*, *444–445*, 22–33. http://doi.org/10.1016/j.jhydrol.2012.03.033

Ghebrezgabher, M. G., Yang, T., Yang, X., Wang, X., & Khan, M. (2016). Extracting and analyzing forest and woodland cover change in Eritrea based on landsat data using supervised classification. *The Egyptian Journal of Remote Sensing and Space Science*, *19*(1), 37–47. http://doi.org/10.1016/j.ejrs.2015.09.002

Ghimire, C. P., Bruijnzeel, L. A., Bonell, M., Coles, N., Lubczynski, M. W., & Gilmour, D. A. (2014). The effects of sustained forest use on hillslope soil hydraulic conductivity in the Middle Mountains of Central Nepal. *Ecohydrology*, *7*(2), 478–495. http://doi.org/10.1002/eco.1367

GISDA. (2011). 2011 Thailand Flood Execute Summary.

Gong, P., Wang, J., Yu, L., Zhao, Y., Zhao, Y., Liang, L., … Chen, J. (2013). Finer resolution observation and monitoring of global land cover: first mapping results with Landsat TM and ETM+ data. *International Journal of Remote Sensing*, *34*(7), 2607–2654. http://doi.org/10.1080/01431161.2012.748992

Grimm, A. M., Pal, J. S., Giorgi, F., Grimm, A. M., Pal, J. S., & Giorgi, F. (2007). Connection between Spring Conditions and Peak Summer Monsoon Rainfall in South America: Role of Soil Moisture, Surface Temperature, and Topography in Eastern Brazil. *Journal of Climate*, *20*(24), 5929–5945. http://doi.org/10.1175/2007JCLI1684.1

Hauser, S. (2014). Corn or maize, essential crop for millions of Thai farmers. Retrieved May 11, 2017, from http://www.sjonhauser.nl/corn-or-maize-essential-crop-for-millions-of-thai-farmers.html

Hemwan, P. (2013). Agricultural Land Use of Highland Communities in Doi Phu Kha National Park Area, Thailand: Cases of Huai Win, Pang Yang and Maneepluek 1. *Regional Views*, *23*, 1.

Hessel, R. (2005). Effects of grid cell size and time step length on simulation results of the Limburg soil erosion model (LISEM). *Hydrological Processes*, *19*(15), 3037–3049. http://doi.org/10.1002/hyp.5815

Hessel, R., Messing, I., Liding, C., Ritsema, C., & Stolte, J. (2003). Soil erosion simulations of land use scenarios for a small Loess Plateau catchment. *CATENA*, *54*(1), 289–302. http://doi.org/10.1016/S0341-8162(03)00070-5

Hilgert, S., Wagner, A., & Fuchs, S. (2015). Future changes in flash flood frequency and intensity of the Tha Di River (Thailand) based on rainfall–runoff modeling and advanced delta change scaling. Retrieved May 30, 2016, from http://www.hydrol-earth-syst-sci-discuss.net/12/7327/2015/hessd-12-7327-2015.pdf

Hillel, D. (1980). *Applications of Soil Physics - Daniel Hillel - Google Books*. ACADEMIC PRESS. Retrieved from https://books.google.nl/books?hl=en&lr=&id=kdJnylDEtV0C&oi=fnd&pg=PP1&dq=soil+properties+affects+on+surface+runoff&ots=BD2gMB3rji&sig=8IdcUibx_BqxqDU-MeUzCts2lko#v=onepage&q=soil properties affects on surface runoff&f=false

Hillel, D. (1998). *Environmental Soil Physics:* Retrieved from https://books.google.nl/books?hl=en&lr=&id=tP__y5xRd0oC&oi=fnd&pg=PP1&dq=Envirenmental+soil+physics&ots=8715FTonvl&sig=OFL7_DBYQ5tG5OZWyBtGxqPpuuU#v=onepage&q=Envirenmental soil physics&f=false

Hillel, D., Warrick, A. W., Baker, R. S., & Rosenzweig, C. (1998). *Environmental soil physics*. Academic Press. Retrieved from https://books.google.nl/books?hl=en&lr=&id=tP__y5xRd0oC&oi=fnd&pg=PP1&dq=hillel+1998+environmental+soil+physics&ots=8723ILqmrk&sig=55byH7ya3Tx7lUQPcnZGH2Scwio&redir_esc=y#v=onepage&q=hillel 1998 environmental soil physics&f=false

Hossain, M. . S., Sidik, B. J., & Harah, Z. M. (2015). Landsat image enhancement techniques for subtidal and intertidal seagrass detection and distribution mapping in the coastal waters of Sungai Pulai estuary, Malaysia. *Coastal Marine Science*, *38*(1), 27–41.

Hsu, M. ., Chen, S. ., & Chang, T. . (2000). Inundation simulation for urban drainage basin with storm sewer system. *Journal of Hydrology*, *234*(1), 21–37. http://doi.org/10.1016/S0022-1694(00)00237-7
Huang, J., Zhao, X., & Wu, P. (2013). Surface runoff volumes from vegetated slopes during simulated rainfall events. *Journal of Soil and Water Conservation*, *68*(4), 283–295. http://doi.org/10.2489/jswc.68.4.283
Huang, P., Li, Z., Yao, C., Li, Q., & Yan, M. (2016). Spatial Combination Modeling Framework of Saturation-Excess and Infiltration-Excess Runoff for Semihumid Watersheds. *Advances in Meteorology*, *2016*, 1–15. http://doi.org/10.1155/2016/5173984
Hümann, M., Schüler, G., Müller, C., Schneider, R., Johst, M., & Caspari, T. (2011). Identification of runoff processes – The impact of different forest types and soil properties on runoff formation and floods. *Journal of Hydrology*, *409*(3–4), 637–649. http://doi.org/10.1016/j.jhydrol.2011.08.067
Jetten, V. (2013). Basic theory | openLISEM – a spatial model for runoff, floods and erosion. Retrieved April 16, 2017, from http://blogs.itc.nl/lisem/basic-theory/
Johnson, M. S., Coon, W. F., Mehta, V. K., Steenhuis, T. S., Brooks, E. S., & Boll, J. (2003). Application of two hydrologic models with different runoff mechanisms to a hillslope dominated watershed in the northeastern US: a comparison of HSPF and SMR. *Journal of Hydrology*, *284*, 57–76. http://doi.org/10.1016/j.jhydrol.2003.07.005
Kabeja, C. (2016). *Assessing structural and ecosystem based measures to reduce surface runoff ; A comparative study in Mpazi and Byabagabo Jabana sub- Assessing structural and ecosystem based measures to reduce surface runoff ; A comparative study in Mpazi and Byabagabo Jab*.
Kim, J. K., Onda, Y., Kim, M. S., & Yang, D. Y. (2014). Plot-scale study of surface runoff on well-covered forest floors under different canopy species. *Quaternary International*, *344*, 75–85. http://doi.org/10.1016/j.quaint.2014.07.036
Konrad II, C. E. (1996). RELATIONSHIPS BETWEEN PRECIPITATION EVENT TYPES AND TOPOGRAPHY IN THE SOUTHERN BLUE RIDGE MOUNTAINS OF THE SOUTHEASTERN USA. *International Journal of Climatology*, *16*(1), 49–62. http://doi.org/10.1002/(SICI)1097-0088(199601)16:1<49::AID-JOC993>3.0.CO;2-D
Laurens M. B., Ryan P. Crompton, Eberhard F., P. H. R. A. P. (2007, November). Confronting Disster Loses. *AAAS*. http://doi.org/10.1126/science.1149628
Lillesand, T. M., Kiefer, R. W., & Chipman, J. W. (2008). *Remote sensing and image interpretation*. Retrieved from https://books.google.nl/books?hl=en&lr=&id=AFHDCAAAQBAJ&oi=fnd&pg=PA1&dq=visual+image+interpretation&ots=0Bwmc3dzat&sig=ZJigjnJmW09Nam-IqkZ2-2WuQkA&redir_esc=y#v=onepage&q=visual image interpretation&f=false
Limsakul, A., & Singhruck, P. (2016). Long-term trends and variability of total and extreme precipitation in Thailand. *Atmospheric Research*, *169*, 301–317. http://doi.org/10.1016/j.atmosres.2015.10.015
Liu, H., Lei, T. W., Zhao, J., Yuan, C. P., Fan, Y. T., & Qu, L. Q. (2011). Effects of rainfall intensity and antecedent soil water content on soil infiltrability under rainfall conditions using the run off-on-out method. *Journal of Hydrology*, *396*(1), 24–32. http://doi.org/10.1016/j.jhydrol.2010.10.028
Liu, Y.-J., Hu, J.-M., Wang, T.-W., Cai, C.-F., Li, Z.-X., & Zhang, Y. (2016). Effects of vegetation cover and road-concentrated flow on hillslope erosion in rainfall and scouring simulation tests in the Three Gorges Reservoir Area, China. *CATENA*, *136*, 108–117. http://doi.org/10.1016/j.catena.2015.06.006
Liu, Y.-J., Yang, J., Hu, J.-M., Tang, C.-J., & Zheng, H.-J. (2016). Characteristics of the surface–subsurface flow generation and sediment yield to the rainfall regime and land-cover by long-term in-situ observation in the red soil region, Southern China. *Journal of Hydrology*, *539*, 457–467. http://doi.org/10.1016/j.jhydrol.2016.05.058
Lu, D., Mausel, P., Brondízio, E., & Moran, E. (2004). Change detection techniques. *International Journal of Remote Sensing*, *25*(12), 2365–2401. http://doi.org/10.1080/0143116031000139863
Lull, H. ., & Sopper, W. E. (1986). *HYDROLOGIC EFFECTS from URBANIZATION of forested watersheds in the northeast*.
Mahmood, S., Khan, A.-H., & Mayo, S. M. (2016). Exploring underlying causes and assessing damages of 2010 flash flood in the upper zone of Panjkora River. *Natural Hazards*, *83*(2), 1213–1227. http://doi.org/10.1007/s11069-016-2386-x
Marshall, M. R., Ballard, C. E., Frogbrook, Z. L., Solloway, I., McIntyre, N., Reynolds, B., & Wheater, H.

S. (2014). The impact of rural land management changes on soil hydraulic properties and runoff processes: results from experimental plots in upland UK. *Hydrological Processes*, *28*(4), 2617–2629. http://doi.org/10.1002/hyp.9826
Mas, J.-F. (1999). Monitoring land-cover changes: A comparison of change detection techniques. *International Journal of Remote Sensing*, *20*(1), 139–152. http://doi.org/10.1080/014311699213659
Masters, J., & Henson, B. (2016). China's $22 Billion Flood. Retrieved January 27, 2017, from https://www.wunderground.com/blog/JeffMasters/comment.html?entrynum=3355
Mei, A., Manzo, C., Fontinovo, G., Bassani, C., Allegrini, A., & Petracchini, F. (2016). Assessment of land cover changes in Lampedusa Island (Italy) using Landsat TM and OLI data. *Journal of African Earth Sciences*, *122*, 15–24. http://doi.org/10.1016/j.jafrearsci.2015.05.014
Miao, Q., Yang, D., Yang, H., & Li, Z. (2016). Establishing a rainfall threshold for flash flood warnings in China's mountainous areas based on a distributed hydrological model. *Journal of Hydrology*. http://doi.org/10.1016/j.jhydrol.2016.04.054
Miller, J. E. (1984). *Basic Concepts of Kinematic-Wave Models*.
Miyata, S., Kosugi, K., Nishi, Y., Gomi, T., Sidle, R. C., & Mizuyama, T. (2010). Spatial pattern of infiltration rate and its effect on hydrologycal processes in a small headwater catchment. *Hydrological Processes*, *24*(5), 535–549. http://doi.org/10.1002/hyp
Mujumdar, P. P. (2001). Flood Wave Propagation. *RESONANCE*, 66–73.
Neris, J., Jiménez, C., Fuentes, J., Morillas, G., & Tejedor, M. (2012). Vegetation and land-use effects on soil properties and water infiltration of Andisols in Tenerife (Canary Islands, Spain). *CATENA*, *98*, 55–62. http://doi.org/10.1016/j.catena.2012.06.006
NOAA. (2016). Flood Types. Retrieved December 25, 2016, from http://www.nssl.noaa.gov/education/svrwx101/floods/types/
Nunes, A. N., de Almeida, A. C., & Coelho, C. O. A. (2011). Impacts of land use and cover type on runoff and soil erosion in a marginal area of Portugal. *Applied Geography*, *31*(2), 687–699. http://doi.org/10.1016/j.apgeog.2010.12.006
Olang, L. O., & Fürst, J. (2011). Effects of land cover change on flood peak discharges and runoff volumes: model estimates for the Nyando River Basin, Kenya. *Hydrological Processes*, *25*(1), 80–89. http://doi.org/10.1002/hyp.7821
Ongprasert, P. (2014). *FOREST MANAGEMENT IN THAILAND International Forestry Cooperation Office Royal Forest Department Ministry of Natural Resources and Environment*. Retrieved from http://www.forest.go.th/foreign/images/stories/FOREST MANAGEMENT IN THAILAND.pdf
Palmer, R. C., & Smith, R. P. (2013). Soil structural degradation in SW England and its impact on surface-water runoff generation. *Soil Use and Management*, *29*(4), 567–575. http://doi.org/10.1111/sum.12068
Pearce, A. J., Stewart, M. K., & Sklash, M. G. (1986). Storm Runoff Generation in Humid Headwater Catchments: 1. Where Does the Water Come From? *Water Resources Research*, *22*(8), 1263–1272. http://doi.org/10.1029/WR022i008p01263
Peng, T., & Wang, S. (2012). Effects of land use, land cover and rainfall regimes on the surface runoff and soil loss on karst slopes in southwest China. *CATENA*, *90*, 53–62. http://doi.org/10.1016/j.catena.2011.11.001
Pfeffer, K. (2003). *Integrating spatio-temporal environmental models for planning ski runs*. *Nederlandse Geografische Studies*. University of Utrech.
Pleijsier, L. K. (1986). ISRIC 1986 Proceedings of an international workshop on laboratory methods. In *International workshop on laboratory methods* (pp. 123–124). International Soil Reference and Information center.
Population statistics 2015. (2016). Retrieved January 10, 2017, from http://stat.dopa.go.th/stat/statnew/statTDD/views/showDistrictData.php?statType=1&year=58&rcode=55
Qin, J., Ding, Y., Wu, J., Gao, M., Yi, S., Zhao, C., … Wang, S. (2013). Understanding the impact of mountain landscapes on water balance in the upper Heihe River watershed in northwestern China. *Journal of Arid Land*, *5*(3), 366–383. http://doi.org/10.1007/s40333-013-0162-2
Rawat, J. S., Biswas, V., & Kumar, M. (2013). Changes in land use/cover using geospatial techniques: A case study of Ramnagar town area, district Nainital, Uttarakhand, India. *The Egyptian Journal of Remote Sensing and Space Science*, *16*(1), 111–117. http://doi.org/10.1016/j.ejrs.2013.04.002
Reli, S. N., Yusoff, I. M., Lateh, H., & Ujang, M. U. (2016). A Review of Infiltration Excess Overland

Flow (IEOF): Terms , Models and Environmental Impact Academic Discipline And Sub-Disciplines Subsurface water in Hydrology. *Journal of Advances in Humanities*, *4*(October), 490–502.

reliefweb. (2009). Thailand: Flashflood hits Pua district of Nan. Retrieved January 28, 2017, from http://reliefweb.int/report/thailand/thailand-flashflood-hits-pua-district-nan

Renard, K. G., Foster, G. R., Weesies, G. A., Mccool, D. K., & Yoder, D. C. (1997). *Predicting Soil Erosion By Water : a Guide To Conservation Planning With the Revised Universal Soil Loss Equation (Rusle)*.

Rientjes, T. H. maria. (2004). *Inverse modelling of the rainfall-runoff relation: A multi objective model calibration approach*. University of Delft. Retrieved from file:///C:/Users/user/Downloads/ceg_rientjes_20040510.PDF

Rugai, D. S. (2008). *Combined Hydrological and Hydrodynamic modelling for Flood hazard assessment ; A case study of upper Kaluganga Catchment , Ratnapura , Sri Lanka Combined Hydrological and Hydrodynamic modelling for Flood hazard assessment ; A Case study of Kaluganga Catch*.

Rumynin, V. G. (2015). Rainfall-Induced Runoff and Subsurface Stormflow at the Hillslope Scale (pp. 51–81). Springer International Publishing. http://doi.org/10.1007/978-3-319-21801-4_2

Safari, A., Kavian, A., Parsakhoo, A., Saleh, I., & Jordán, A. (2016). Impact of different parts of skid trails on runoff and soil erosion in the Hyrcanian forest (northern Iran). *Geoderma*, *263*, 161–167. http://doi.org/10.1016/j.geoderma.2015.09.010

Sajikumar, N., & Remya, R. S. (2015). Impact of land cover and land use change on runoff characteristics. *Journal of Environmental Management*, *161*, 460–468. http://doi.org/10.1016/j.jenvman.2014.12.041

Seng, V., Craswell, E., Fukai, S., Fischer, K., & Penh, P. (2004). *Water in agriculture edited Water in Agriculture Proceedings of a CARDI International Conference on Research on Water in Agricultural Production in Asia for the 21st Century*. Retrieved from http://researchrepository.murdoch.edu.au/id/eprint/11189/1/Rainfed_lowland_rice-growing.pdf

Sharma, R. D., Sarkar, R., & Dutta, S. (2013). Run-off generation from fields with different land use and land covers under extreme storm events. *CURRENT SCIENCE*, *104*(8), 1046–1053. Retrieved from http://ezproxy.utwente.nl:2062/full_record.do?product=WOS&search_mode=GeneralSearch&qid=40&SID=W1bN6MQxo8TH3JPw2Xs&page=6&doc=56

Shih, P. T.-Y. (2014). Evaluating Information Loss of SRTM DEM Data with Different Grid Sizes. *Journal of Surveying Engineering*, *140*(4), 4014010. http://doi.org/10.1061/(ASCE)SU.1943-5428.0000132

Shrestha, D., & Jetten, V. (2016). ANALYSIS OF RAINFALL DATA. Retrieved from https://blackboard.utwente.nl/bbcswebdav/pid-908768-dt-content-rid-1903424_2/courses/M16-AES-103/Analysis of Rainfall data_D Shrestha%281%29.pdf

Singh, V. P. (1996). *Kinematic Wave Modeling in Water Resources, Surface-Water Hydrology*. JHON WILEY & SONS. Retrieved from https://books.google.nl/books?hl=en&lr=&id=-O9nEOnZYUwC&oi=fnd&pg=PR15&dq=applications+of+Kinematic+wave&ots=rJ-EBXyc7D&sig=FYJnfPS8MeTSSRjkoc8pHQX73A0#v=onepage&q=applications of Kinematic wave&f=false

Siriwardena, L., Finlayson, B. L., & McMahon, T. A. (2006). The impact of land use change on catchment hydrology in large catchments: The Comet River, Central Queensland, Australia. *Journal of Hydrology*, *326*(1), 199–214. http://doi.org/10.1016/j.jhydrol.2005.10.030

Sisodia, P. S., Tiwari, V., & Kumar, A. (2014). A comparative analysis of remote sensing image classification techniques. In *2014 International Conference on Advances in Computing, Communications and Informatics (ICACCI)* (pp. 1418–1421). IEEE. http://doi.org/10.1109/ICACCI.2014.6968245

Solín, Ľ., Feranec, J., & Nováček, J. (2011). Land cover changes in small catchments in Slovakia during 1990–2006 and their effects on frequency of flood events. *Natural Hazards*, *56*(1), 195–214. http://doi.org/10.1007/s11069-010-9562-1

Solomon, H. (2005). *GIS-Based Surface Runoff Modeling and Analysis of Contributing Factors ; A Case Study of the Nam Chun Watershed , Thailand A GIS based Surface Runoff Modelling and Analysis of Contributing Factors ; A Case Study of the Nam Chun Watershed Thailand*. University of Twente.

Tarboton, D. G. (2003). *Rainfall-Runoff Models*. Utah State University.

Terranova, O. G., & Gariano, S. L. (2014). Rainstorms able to induce flash floods in a Mediterranean-climate region (Calabria, southern Italy). *Natural Hazards and Earth System Science*, *14*(9), 2423–2434. http://doi.org/10.5194/nhess-14-2423-2014

The Weather Channel. (2016). Retrieved January 27, 2017, from

https://weather.com/news/weather/news/historic-august-louisiana-flooding-billion-dollar-disaster
Tsui, C.-C., Chen, Z.-S., & Hsieh, C.-F. (2004). Relationships between soil properties and slope position in a lowland rain forest of southern Taiwan. *Geoderma*, *123*(1), 131–142. http://doi.org/10.1016/j.geoderma.2004.01.031
UN. (2016). flood-disaster-figures-1995-2015. Retrieved December 25, 2016, from http://floodlist.com/dealing-with-floods/flood-disaster-figures-1995-2015
UNSIDR. (2016). Flash Floods are a Major Global Threat says UN. Retrieved May 31, 2016, from http://floodlist.com/america/unisdr-flash-floods-major-global-threat
US Army Corps Of Engineers. (1993). Introduction and Application of Kinematic Wave Routing Techniques Using HEC-1 (pp. 1–4). Retrieved from http://www.hec.usace.army.mil/publications/TrainingDocuments/TD-10.pdf
USDA. (1986). *Urban Hydrology for Small. Soil Conservation*. Retrieved from http://scholar.google.com/scholar?hl=en&btnG=Search&q=intitle:Urban+Hydrology+for+Small+watersheds#1
USGS. (2015). Landsat 8 OLI/TIRS Collection 1 Data Dictionary | The Long Term Archive. Retrieved May 11, 2017, from https://lta.cr.usgs.gov/Landsat_8_C1.html#image_quality_landsat_8
USGS. (2016). Runoff (Surface water runoff), USGS Water Science School. Retrieved December 29, 2016, from http://water.usgs.gov/edu/runoff.html
Van Reeuwijk, L. P. (2002). *PROCEDUERS FOR SOIL ANALYSIS* (Sixth).
Vieux, B. E. (1993). DEM Aggregation and Smoothing Effects on Surface Runoff Modeling. *Journal of Computing in Civil Engineering*, *7*(3), 310–338. http://doi.org/10.1061/(ASCE)0887-3801(1993)7:3(310)
Wang, G., Yang, H., Wang, L., Xu, Z., & Xue, B. (2014). Using the SWAT model to assess impacts of land use changes on runoff generation in headwaters. *Hydrological Processes*, *28*(3), 1032–1042. http://doi.org/10.1002/hyp.9645
Wangpimool, W., Pongput, K., Sukvibool, C., Sombatpanit, S., & Gassman, P. W. (2013). The effect of reforestation on stream flow in Upper Nan river basin using Soil and Water Assessment Tool (SWAT) model. *International Soil and Water Conservation Research*, *1*(2), 53–63. http://doi.org/10.1016/S2095-6339(15)30039-3
Welcher, P. (2017). *Rice Market and Policy Changes over the Past Decade*. Retrieved from https://gain.fas.usda.gov/Recent GAIN Publications/Rice Market and Policy Changes Over the Past Decade_Bangkok_Thailand_1-18-2017.pdf
Westen, C., & Jetten, V. (2015). *CHARIM Caribbean Handbook on Risk Information Management Report on methodologies for hazard mapping in the Caribbean Suggested methods for analysis at various scales Version 3*.
Westra, S., Fowler, H. J., Evans, J. P., Alexander, L. V., Berg, P., Johnson, F., … Roberts, N. M. (2014). Future changes to the intensity and frequency of short-duration extreme rainfall. *Reviews of Geophysics*, *52*(3), 522–555. http://doi.org/10.1002/2014RG000464
Wikipedia. (2016). List of deadliest floods. Retrieved January 27, 2017, from http://www.dallasnews.com/sharedcontent/dws/news/world/stories/DN-pakfloods_05int.ART.State.Edition1.359c7c2.html
Xu, Q. X., Wang, T. W., Cai, C. F., Li, Z. X., Shi, Z. H., & Fang, R. J. (2013). Responses of Runoff and Soil Erosion to Vegetation Removal and Tillage on Steep Lands. *PEDOSPHERE*, *23*(4), 532–541. Retrieved from http://ezproxy.utwente.nl:2062/full_record.do?product=WOS&search_mode=GeneralSearch&qid=19&SID=W1bN6MQxo8TH3JPw2Xs&page=8&doc=79
Yu, X., Li, B., Sha, L., Zhou, L., Duan, H. (2015). LAND COVER CHANGE DETECTION OF EZHOU HUARONG DISTRICT BASED ON MULTI-TEMPORAL ZY-3 SATELLITE IMAGES. In *2015 23RD INTERNATIONAL CONFERENCE ON GEOINFORMATICS*. Retrieved from http://ezproxy.utwente.nl:2062/full_record.do?product=WOS&search_mode=GeneralSearch&qid=2&SID=V2UFiiFDMN1k3vWK1FA&page=2&doc=20
Zevenbergen, C., van Herk, S., Rijke, J., Kabat, P., Bloemen, P., Ashley, R., … Veerbeek, W. (2013). Taming global flood disasters. Lessons learned from Dutch experience. *Natural Hazards*, *65*(3), 1217–1225. http://doi.org/10.1007/s11069-012-0439-3
Zhang, M., Wei, X., Sun, P., & Liu, S. (2012). The effect of forest harvesting and climatic variability on

runoff in a large watershed: The case study in the Upper Minjiang River of Yangtze River basin. *Journal of Hydrology*, *464*, 1–11. http://doi.org/10.1016/j.jhydrol.2012.05.050

Zhiwei, Z., Zhangxiong, Z., Yan, W., Wali, F., & Wen, Z. (2010). Soil infiltration capacity and its influencing factors of different land use types in Karst slope. *Transactions of the Chinese Society of Agricultural Engineering*, *26*(6), 71–76.

Ziadat, F. M., & Taimeh, A. Y. (2013). EFFECT OF RAINFALL INTENSITY, SLOPE, LAND USE AND ANTECEDENT SOIL MOISTURE ON SOIL EROSION IN AN ARID ENVIRONMENT. *Land Degradation & Development*, *24*(6), 582–590. http://doi.org/10.1002/ldr.2239

Zimmermann, B., Elsenbeer, H., & De Moraes, J. M. (2006). The influence of land-use changes on soil hydraulic properties: Implications for runoff generation. *Forest Ecology and Management*, *222*(1), 29–38. http://doi.org/10.1016/j.foreco.2005.10.070

Zinke, P. J. (1962). The Pattern of Influence of Individual Forest Trees on Soil Properties. *Ecology*, *43*(1), 130–133. http://doi.org/10.2307/1932049

APPENDIX

Appendix1: Accuracy assessment reports for Landsat image classifications

CLASSIFICATION ACCURACY ASSESSMENT REPORT OF 1990 Landsat Image

----

Image File : c:/ls5-90-4-12-130-47.img

User Name : user

Date : Mon Mar 27 22:59:47 2017

ERROR MATRIX

Reference Data

Classified Data	Unclassifi	F12	P12	C9
Unclassified	0	0	0	0
F12	0	5	0	0
P12	0	1	6	0
C9	0	1	0	5
PF10	0	3	2	2
R7	0	0	0	0
Column Total	0	10	8	7

Reference Data

Classified Data	PF10	R7	Row Total
Unclassified	0	0	0
F12	0	0	5
P12	0	2	9
C9	0	0	6
PF10	11	1	19
R7	0	2	2
Column Total	11	5	41

----- End of Error Matrix -----

ACCURACY TOTALS

Class Name	Reference Totals	Classified Totals	Number Correct	Producers Accuracy	Users Accuracy
----------	----------	----------	-------	---------	-----
Unclassified	0	0	0	---	---
F12	10	5	5	50.00%	100.00%
P12	8	9	6	75.00%	66.67%
C9	7	6	5	71.43%	83.33%
PF10	11	19	11	100.00%	57.89%
R7	5	2	2	40.00%	100.00%
Totals	41	41	29		

Overall Classification Accuracy = 70.73%

----- End of Accuracy Totals -----

KAPPA (K^) STATISTICS

Overall Kappa Statistics = 0.6210

Conditional Kappa for each Category.

Class Name	Kappa
----------	-----
Unclassified	0.0000
F12	1.0000
P12	0.5859
C9	0.7990
PF10	0.4246
R7	1.0000

----- End of Kappa Statistics -----

CLASSIFICATION ACCURACY ASSESSMENT REPORT OF 2000 Landsat Image

Image File : c:/ls5-00-3-6-130-47.img
User Name : user
Date : Sat Jan 25 21:22:51 2017

ERROR MATRIX

Reference Data

Classified Data	Unclassifi	f16	p10	c10
Unclassified	0	0	0	0
f16	0	6	0	2
p10	0	0	5	0
c10	0	2	1	4
pf8	0	2	1	1
res7	0	0	1	0
Column Total	0	10	8	7

Reference Data

Classified Data	pf8	res7	Row Total
Unclassified	0	0	0
f16	0	0	8
p10	0	0	5
c10	0	0	7
pf8	11	2	17
res7	0	5	6
Column Total	11	7	43

----- End of Error Matrix -----

ACCURACY TOTALS

Class Name	Reference Totals	Classified Totals	Number Correct	Producers Accuracy	Users Accuracy
----------	----------	----------	-------	---------	-----
Unclassified	0	0	0	---	---
f16	10	8	6	60.00%	75.00%
p10	8	5	5	62.50%	100.00%
c10	7	7	4	57.14%	57.14%
pf8	11	17	11	100.00%	64.71%
res7	7	6	5	71.43%	83.33%
Totals	43	43	31		

Overall Classification Accuracy = 72.09%

----- End of Accuracy Totals -----

KAPPA (K^) STATISTICS

Overall Kappa Statistics = 0.6444

Conditional Kappa for each Category.

Class Name	Kappa
----------	-----
Unclassified	0.0000
f16	0.6742
p10	1.0000
c10	0.4881
pf8	0.5257
res7	0.8009

----- End of Kappa Statistics -----

CLASSIFICATION ACCURACY ASSESSMENT REPORT OF 2010 Landsat Image
----

Image File : c:/ls45-10-5-5-130-47.img
User Name : user
Date : Mon Jan 02 17:44:29 2017

ERROR MATRIX

Reference Data

Classified Data	Unclassified	F27	P21	C32	PF32	R16	Row Total
Unclassified	0	0	0	0	0	0	0
F27	0	7	0	1	0	0	8
P21	0	0	7	1	0	1	9
C32	0	1	0	5	2	0	8
PF32	0	2	1	1	5	1	10
R16	0	0	0	0	0	4	4
Column Total	0	10	8	8	7	6	39

Reference Data

Classified Data	PF32	R16	Row Total
Unclassified	0	0	0
F27	0	0	8
P21	0	1	9
C32	2	0	8
PF32	5	1	10
R16	0	4	4
Column Total	7	6	39

----- End of Error Matrix -----

ACCURACY TOTALS

Class Name	Reference Totals	Classified Totals	Number Correct	Producers Accuracy	Users Accuracy
----------	----------	----------	-------	---------	-----
Unclassified	0	0	0	---	---
F27	10	8	7	70.00%	87.50%
P21	8	9	7	87.50%	77.78%
C32	8	8	5	62.50%	62.50%
PF32	7	10	5	71.43%	50.00%
R16	6	4	4	66.67%	100.00%
Totals	39	39	28		

Overall Classification Accuracy = 71.79%

----- End of Accuracy Totals -----

KAPPA (K^) STATISTICS

Overall Kappa Statistics = 0.6457

Conditional Kappa for each Category.

Class Name	Kappa
----------	-----
Unclassified	0.0000
F27	0.8319
P21	0.7204
C32	0.5282
PF32	0.3906
R16	1.0000

----- End of Kappa Statistics -----

CLASSIFICATION ACCURACY ASSESSMENT REPORT OF 2016 Landsat Image

Image File : c:/jan19/lc16_111.img
User Name : user
Date : Thu Jan 19 22:39:26 2017

ERROR MATRIX

Reference Data

Classified Data	Background	Class 1	Class 2	Class 3
Background	0	0	0	0
Class 1	0	6	0	1
Class 2	0	0	5	0
Class 3	0	0	0	4
Class 4	0	2	1	1
Class 5	0	0	0	0
Column Total	0	8	6	6

Reference Data

Classified Data	Class 4	Class 5	Row Total
Background	0	0	0
Class 1	1	0	8
Class 2	0	1	6
Class 3	0	0	4
Class 4	6	1	11
Class 5	1	3	4
Column Total	8	5	33

----- End of Error Matrix -----

ACCURACY TOTALS

Class Name	Reference Totals	Classified Totals	Number Correct	Producers Accuracy	Users Accuracy
----------	----------	----------	-------	---------	-----
Class 0	0	0	0	---	---
Class 1	8	8	6	75.00%	75.00%
Class 2	6	6	5	83.33%	83.33%
Class 3	6	4	4	66.67%	100.00%
Class 4	8	11	6	75.00%	54.55%
Class 5	5	4	3	60.00%	75.00%
Totals	33	33	24		

Overall Classification Accuracy = 72.73%

----- End of Accuracy Totals -----

KAPPA (K^) STATISTICS

Overall Kappa Statistics = 0.6534

Conditional Kappa for each Category.

Class Name	Kappa
----------	-----
Class 0	0.0000
Class 1	0.6700
Class 2	0.7963
Class 3	1.0000
Class 4	0.4000
Class 5	0.7054

----- End of Kappa Statistics -----

Appendix2: Rainfall depth, intensity data and IDF curve for 24 hours storms at A. Muang rain gauge

Frequency Analysis of Maximum Rainfall for Each Period at **A.Muang C.Nan**

(1964-1983,1986-1993)

Time	Rainfall Amount (mm)								
(hr)	2 yr	5 yr	10 yr	25 yr	50 yr	100 yr	200 yr	500 yr	1000 yr
0.25	24.3	29.9	33.6	38.2	41.7	45.2	48.6	53.1	56.5
0.5	35.3	44.6	50.7	58.4	64.1	69.8	75.5	82.9	88.6
0.75	44.8	59.7	69.5	82.0	91.2	100.4	109.5	121.6	130.7
1	45.4	56.4	63.8	73.0	79.9	86.7	93.5	102.4	109.2
2	51.0	64.3	73.0	84.1	92.3	100.4	108.6	119.3	127.4
3	56.0	69.3	78.1	89.2	97.4	105.6	113.8	124.6	132.7
6	64.5	80.6	91.3	107.7	114.7	124.6	134.5	147.5	157.4
12	72.8	96.1	111.4	130.9	145.3	159.6	173.9	192.7	206.9
24	83.4	115.6	136.8	163.7	183.6	203.4	223.2	249.2	268.8

Time	Rainfall intensity (mm/hr)								
(hr)	2 yr	5 yr	10 yr	25 yr	50 yr	100 yr	200 yr	500 yr	1000 yr
0.25	97.1	119.4	134.2	153.0	166.8	180.6	194.4	212.4	226.2
0.5	70.6	89.1	101.3	116.8	128.2	139.6	150.9	165.9	177.2
0.75	59.7	79.6	92.7	109.3	121.6	133.9	146.1	162.1	174.3
1	45.4	56.4	63.8	73.0	79.9	86.7	93.5	102.4	109.2
2	25.5	32.1	36.5	42.0	46.1	50.2	54.3	59.6	63.7
3	18.7	23.1	26.0	29.7	32.5	35.2	37.9	41.5	44.2
6	10.8	13.4	15.2	18.0	19.1	20.8	22.4	24.6	26.2
12	6.1	8.0	9.3	10.9	12.1	13.3	14.5	16.1	17.2
24	3.5	4.8	5.7	6.8	7.7	8.5	9.3	10.4	11.2

Rainfall Intensity-Duration-Frequency Curve at **A.Muang C.Nan**

(1964-1983,1986-1993)

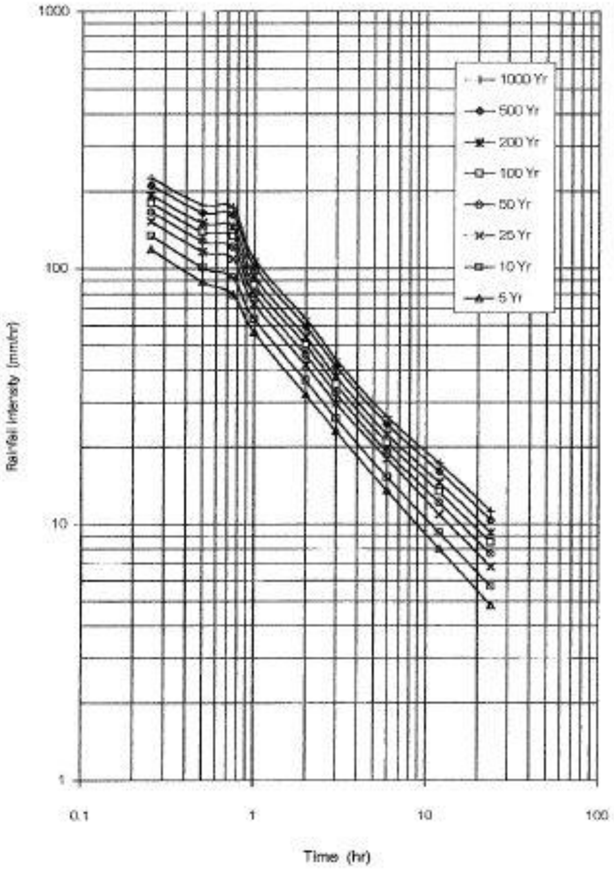

Appendix3: PCRaster script used to generate OpenLISEM input maps

```
! --matrixtable --lddin
################################################################
##############
# PCRASTER script for the generation of an openLISEM input database      #
# 1 dec 2013, Victor Jetten                                   #
################################################################
##############


binding

#####################
### input maps   ###
#####################

   Dem =  dem30mfill.map;           # digital elevation model
   fields =  landunit50m.map;    # land use based units
   texture =  soil50.map;        # soil based units, usualyy texture classes
   chanmask =  stream.map;  # user defined channel
   mainout = outlet.map;     # user defined true outlet (1 =voutlet, 0 is rest)
   mask = mask50m.map;          # user defined catchment mask
   roads = rw50.map;            # user defined roads
   barriers50 = barriers50m.map;
# tables with soil physical properties and land use properties
   lutbl = landuse.tbl;
   soiltbl = soil.tbl;

# units (1=forest, 2=paddyfield, 3=corn, 4=degforest, 5=built up/residential area)

########################
### input constants ###
########################

   Soildepth = soildepth.map;   # soil depth in mm
   Chancoh = 8;        # channel cohesion kPa
   Chanman = 0.05;     # channel manning's n
   Chanside = 0;       # chanside angle, leave at 0
   Chanksat = 1;       # channel staurated hydraulic conductivity in mm/h
   ChanWidthScaling = 100;  # with caling parameter from source to outket
   MinSlope = 0.002;   # minimum slope cannot be 0

######################
### output maps   ###
######################

  # basic topography related maps
```

```
  Ldd =  ldd.map;           # Local Drain Direction
  grad =  grad.map;         # sine of slope (not tangent)
  id =  id.map;             # pluviograph influence zones (1,2, ...n)
                            # if there are more classes the rainfall file needs more columns
  outlet =  outlet.map;     # location of main outlet
  outpoint = outpoints.map;  # location of additional information points, 1 (outlet) 2-n

 # vegetation/crop maps
  lu = landunit.map;   # for output stats
  coverc= per.map;     # vegetation cover fraction
  lai= lai.map;        # leaf area index (m2/m2) for interception storage
  cropheight= ch.map;  # vegetation/crop height for splash detachment energy
  smax = smax.map; # interception canopy strorage mm

 # soil maps, "1" stands for layer 1
  ksat= ksat1.map;       # Saturated hydraulic conductivity (mm/s)
  psi= psi1.map;         # matrix suction at the wetting front (cm)
  pore= thetas1.map;     # porosity (-)
  thetai= thetai1.map;   # initial moisture content (-)
  soildepth= soildepth.map; # soil depth in mm

 # surface maps
  rr = rr.map;  # random roughness (cm) for surface storge and witdh of flow
  mann = n.map; # mannings n, overland flow resistance
  roadwidth = roadwidt.map;

 # channel maps
  lddchan =  lddchan.map;    # channel network
  chanwidth =  chanwidt.map; # width (m)
  changrad =  changrad.map;  # sine gradient of channel/river bed
  chanman =  chanman.map;    # flow resistance
  chanside = chanside.map;   # tangent side wall angle, 0 = rechtangular, 1 is 45 degrees
  chancoh =  chancoh.map;    # cohesion (kPa)
  chanksat =  chanksat.map;  # Ksat of channel (mm/h)
  chandepth = chandepth.map; # depth (m) only for flooding
  barriers = barriers.map;   # additional elemants, elevations, dikes, taluts to be added to the DEM (m)

 # housing maps
  house = housecover.map;    # structure cover fraction
  roof = roofstore.map;      # roof interception storage in mm

areamap

 # MASK
  Dem;

initial
```

```
#######################
### BASE MAPS      ###
#######################

# mask=scalar(Dem/Dem); # make a mask if user defined is not good

# confine all input to mask
fields *=mask;
texture *= mask;
Dem *= mask;
chanmask *= mask;
mainout *= mask;

out = if(mainout eq 1,mainout,0);

# make ldd and ensure it flows to channel and to the main outlet
report ldd.map = lddcreate(Dem-chanmask*2-out*10+barriers50*2,1e20,1e20,1e20,1e20);
#  report ldd.map = lddcreate(Dem-mainout*10,1e20,1e20,1e20,1e20);

report outpoint = outpoint;
report outlet = out;

# maps for user, not used in lisem
report ws.map=catchment(ldd.map,nominal(out));  # sub watersheds
report ups.map=accuflux(ldd.map,1);       # accumulated channel map

# sine gradient (-), make sure slope > 0
report grad = max(sin(atan(slope(Dem))),MinSlope);

###########################################
### MAPS WITH RAINFALL INFLUENCE ZONE ###
###########################################

report id = nominal(mask);

########################
### CROP MAPS       ###
########################

report lu = fields; # copy the landuse to a landunit.map for stats output

# fraction soil cover (including residue), from col 5 of land use table
report coverc = 1 - exp(-2*NDVI1.map)/(1.5-NDVI1.map);

# LAI (m2/m2) from cover fraction
report lai = ln(1-coverc)/-0.4;
#  grass = 0*mask
```

```
 ###############################################################
 ### INFILTRATION MAPS for option one layer GREEN & AMPT ###
 ###############################################################

  report ksat = lookupscalar(lutbl, 5,fields);
#  report ksat = lookupscalar(soiltbl, 7, texture);
  report pore = lookupscalar(lutbl, 6, fields);
  report thetai = lookupscalar(lutbl, 7, fields); #80% drier
  report psi =  lookupscalar(soiltbl, 5, texture)* mask;

  report soildepth = scalar(Soildepth);
  #report textunit.map = nominal( lookupscalar(soiltbl, 9, texture)* mask);

 ###############################
 ### SOIL SURFACE MAPS     ###
 ###############################

  # micro relief, random roughness (=std dev in cm)
  report rr = lookupscalar(lutbl, 3, fields);
  # Manning's n (-)
  report mann = lookupscalar(lutbl, 4, fields);
  report roadwidth = roads*mask;


 #######################
 ### CHANNEL MAPS   ###
 #######################

  chanmask = chanmask/chanmask;
  # channel is 1 and rest missing value

  report lddchan = lddcreate(Dem*chanmask-mainout*10,1e20,1e20,1e20,1e20);

  report changrad = max(MinSlope,sin(atan(slope(chanmask*Dem))));
  report chancoh = chanmask*scalar(Chancoh);
  report chanman = chanmask*scalar(Chanman);
  report chanside = chanmask*scalar(Chanside);
  # width empirical scaled up from 1 to 15 meter

  report chanksat = chanmask*scalar(0);

# chanwidth = max(2.0, min(celllength()*0.95, accuflux(lddchan, celllength()/$5)); #cellarea())/$5));
 #relation by Allen and Pavelski (2015)
 report   chanwidth = max(2.0, min(celllength()*0.95, accuflux(lddchan, cellarea()/3.22e4)**(1.18)));
#cellarea())/$5));
 report   chandepth = sqrt(chanwidth)*0.6;

 #######################
```

```
### house MAPS   ###
#######################

 report house = if(fields eq 5, uniform(1)*0.7+0.3, 0) * mask;
 # random housecover from 0 to 1 in unit 9 settlement.
 # Note that 9 has compacted soil physical values
 report roof = if(fields eq 5,1,0)*mask;

smax = mask*0;
smax  = if(fields == 3 or fields == 2, 0.935+0.498*lai-0.00575*(lai * lai), smax);
 report smax  = if(fields == 1 or fields == 4, 0.7856 * lai, smax);
```

Appendix4: Locations of soil samples

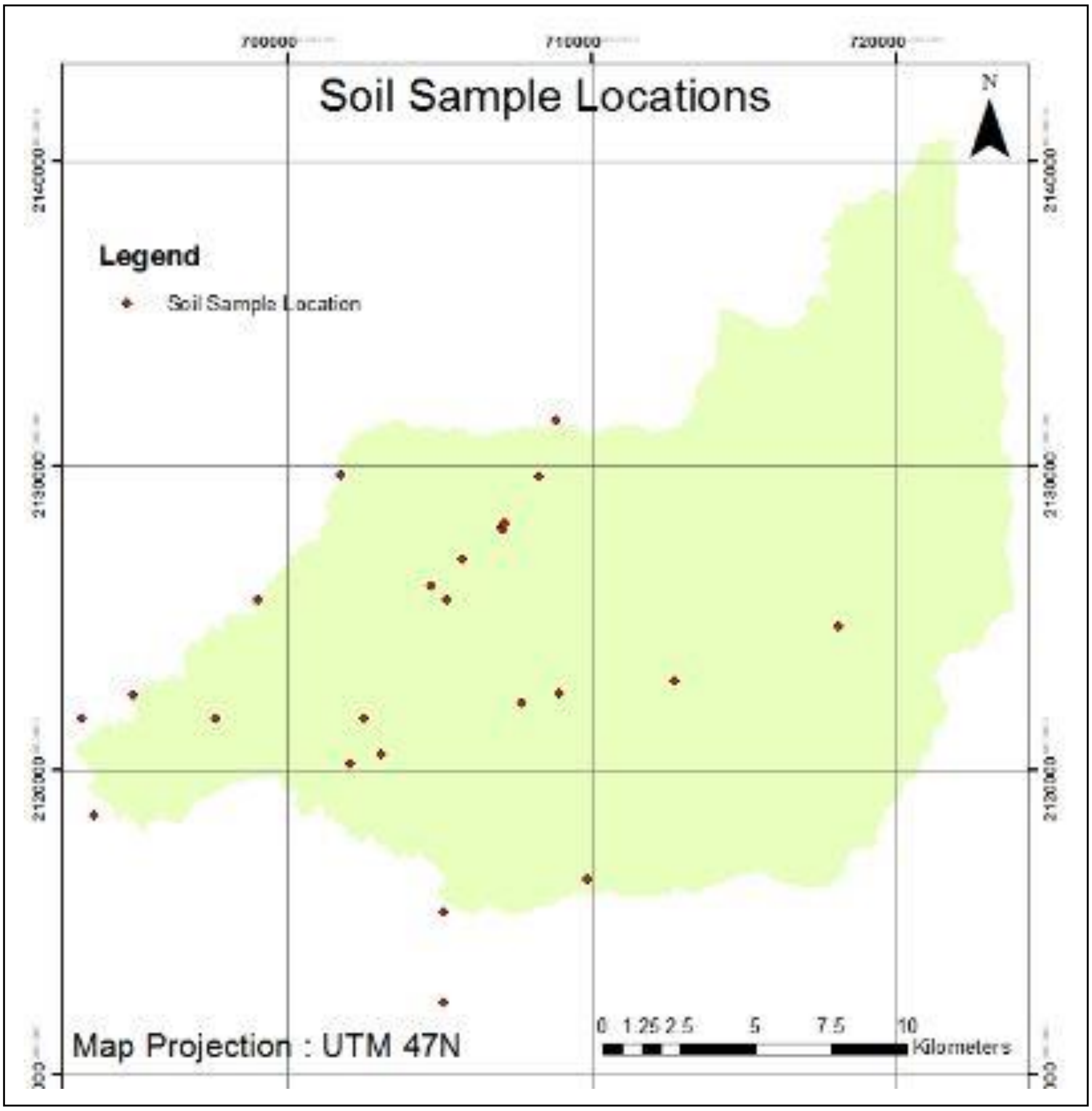

Appendix5: Random roughness and Manning's n values for LCLU types

Table A: Random roughness and Manning's n values for LCLU types in study area

LCLU type	Random roughness	Manning's n
Forest	1.5	0.1
Paddy fields	0.5	0.2
Corn	1.8	0.03
Degraded forest	1.5	0.1
Built up/residential area	0.7	0.02

Table B: Channel parameter values assigned for study area

Parameter	Value
Channel cohesion	8 kPa
Channel Manning;s n	0.05
Channel side angle	0^0
Channel k_{sat}	1 mm/h

Appendix6: Model sensitivity analysis results for k_{sat}, thetai and thetas

Table 5-1: Sensitivity analysis results for k_{sat}, thetai and thetas

Parameter	k_{sat}	thetai	thetas	Total discharge /(l/s)	Flood volume (max)/m³	Flood area (max)/m²	Discharge change %
Original	1	1	1	362376	21	9900	-
k_{sat}	0.8	1	1	379664	28	9900	+4.8
k_{sat}	0.9	1	1	369253	24	9900	+1.9
k_{sat}	1.1	1	1	357282	20	9900	-1.4
k_{sat}	1.2	1	1	353393	19	9900	-2.5
thetai	1	0.8	1	359589	21	9900	-0.8
thetai	1	0.9	1	360959	21	9900	-0.4
thetai	1	1.1	1	364715	21	9900	0.6
thetai	1	1.2	1	367267	21	9900	+1.3
thetas	1	1	0.9	542366	1240	39600	+50
thetas	1	1	1.1	151743	0	0	-58

Appendix7: Model calibration data

Table C: Simulation and measured discharge and water level data

Parameter	Measurement						Simulations					
	Discharge m^3/s			Water level/m			Discharge m^3/s			Water level/m		
	Aug 15	Aug 16	Aug 17	Aug 15	Aug 16	Aug 17	Aug 15	Aug 16	Aug 17	Aug 15	Aug 16	Aug 17
Original	96.61	15.58	11.51	4.6	3.95	3.9	2.67	2.13	0.61	0.15	0.13	0.06
Thetai*2	96.61	15.58	11.51	4.6	3.95	3.9	98.49	4.50	1.12	1.36	0.21	0.09

Table D: Differences between measurements and simulations

Parameter	Difference						Difference %					
	Discharge			Water level			Discharge			Water level		
	Aug 15	Aug 16	Aug 17	Aug 15	Aug 16	Aug 17	Aug 15	Aug 16	Aug 17	Aug 15	Aug 16	Aug 17
Original	-93.94	-13.45	-10.9	-4.45	-3.82	-3.84	-97.24	-84.86	-94.7	-96.7	-96.7	-98.5
Thetai*2	1.88	-11.08	-10.39	-3.24	-3.74	-3.81	1.95	-71.12	-90.27	-70.44	-94.68	-97.69

Appendix8: Model validation data

Table E: Results of model validation

Event	Simulation		Measurements		Difference		Difference %	
	Discharge /(m^3/s)	Water level/m	Discharge /(l/s)	Water level/m	Discharge /m^3	Water level/m	Discharge	Water level
2014.08.29 rainfall event under 2016 calibrated database	15.76	0.44	18.40	3.97	-2.64	-3.53	-14.35	-88.92

Appendix9: Change matrix for LCLU classification of 1990, 2000, 2010 and 2016 Landsat images

	Change Matrix 1990-2000							
					2000 LCLU/km2			
		Forest	Paddy	Corn	Degrade	Built up/F	Total Are	Loss
	Forest	234.93	0.6	46.08	11.63	0.04	293.28	58.35
	Paddy	1.04	30.11	1.81	4	0.14	37.1	6.99
1990 LCL	Corn	12.46	0.1	20.58	0.94	0.01	34.09	13.51
	Degrade	5.44	2.87	4.18	24.95	0.51	37.95	13
	Built up/F	0.01	0.12	0.03	0.15	1.07	1.38	0.31
	Total Are	253.88	33.8	72.68	41.67	1.77		
	Gain	18.95	3.69	52.1	16.72	0.7		

	Change Matrix 2000-2010							
					2010 LCLU/km2			
		Forest	Paddy	Corn	Degrade	Built up/F	Total Are	Loss
	Forest	196.11	0.67	51.72	4.82	0.08	253.4	57.29
	Paddy	1.38	22.83	2.47	6.54	0.47	33.69	10.86
2000 LCL	Corn	38.93	1.52	27.85	4.08	0.1	72.48	44.63
	Degrade	15.29	4.66	3.52	17.43	0.52	41.42	23.99
	Built up/F	0.11	0.2	0.04	0.3	1.35	2	0.65
	Total Are	251.82	29.88	85.6	33.17	2.52		
	Gain	55.71	7.05	57.75	15.74	1.17		

	Change Matrix 2010-2016							
					2016 LCLU/km2			
		Forest	Paddy	Corn	Degrade	Built up/F	Total Are	Loss
	Forest	181.94	1.56	50.57	17.84	0.22	252.13	57.29
	Paddy	0.01	25.36	0.14	3.89	0.51	29.91	10.86
2010 LCL	Corn	23.31	2.99	54.41	4.98	0.04	85.73	44.63
	Degrade	1.66	6.65	3.35	20.51	1.03	33.2	23.99
	Built up/F	0	0.37	0.01	0.34	1.81	2.53	0.65
	Total Are	206.92	36.93	108.48	47.56	3.61		
	Gain	24.98	11.57	54.07	27.05	1.8		

Appendix10: Tot result file for simulation of 174 mm event for 2016

LISEM run with:,C:/March23/runs/luse50m.run	
LISEM results at time (min):, 4499.000000000	
Catchment area (ha):	44199.3802
Total Precipitation (mm):	174
Total discharge (mm):	45.2807382
Total interception (mm):	1.84516067
Total House interception (mm):	0.010884839
Total infiltration (mm):	116.2251406
Surface storage (mm):	0.151022995
Water in overland flow (mm):	6.926034622
Water in channels (mm):	0.870659988
Total outflow (mm):	45.2807382
Total baseflow (mm):	0
Total discharge (m3):	18322438.66
Total Tile discharge (m3):	0
Peak time precipitation (min):	1020.5
Peak discharge/Precipitation (%):	26.02341276
Flood volume (max level) (m3):	16650557.52
Flood area (max level) (m2):	20960100
Splash detachment (land) (ton):	0
Flow detachment (land) (ton):	0
Deposition (land) (ton):	0
Suspended Sediment (land) (ton):	0
Flow detachment (channels) (ton):	0
Deposition (channels) (ton):	0
Susp. Sediment (channels) (ton):	0
Flow detachment (flood) (ton):	0
Deposition (flood) (ton):	0
Susp. Sediment (flood) (ton):	0
Total soil loss (ton):	0
Average soil loss (kg/ha):	0
Peak discharge for outlet 0 (l/s):	444003.8132
Peak discharge for outlet 1 (l/s):	441485.9887
Peak discharge for outlet 2 (l/s):	235441.9212
Peak time discharge for outlet 0 (min):	1463.5
Peak time discharge for outlet 1 (min):	1462.5
Peak time discharge for outlet 2 (min):	1304